SOLAR NEUTRINOS:
BEYOND STANDARD SOLAR MODELS

V. CASTELLANI[a,b,c], S. DEGL'INNOCENTI[d,e], G. FIORENTINI[e,f],
M. LISSIA[g,h], B. RICCI[e]

[a] Dipartimento di Fisica dell'Università di Pisa, I-56100 Pisa, Italy
[b] Osservatorio Astronomico di Collurania, I-64100 Teramo, Italy
[c] Istituto Nazionale di Fisica Nucleare, LNGS, I-67017 Assergi (l'Aquila), Italy
[d] Max-Planck Institut for Astrophysics, D-85740 Garching bei München, Germany
[e] Istituto Nazionale di Fisica Nucleare, Sezione di Ferrara, via Paradiso 12, I-44100 Ferrara, Italy
[f] Dipartimento di Fisica dell'Università di Ferrara, via Paradiso 12, I-44100 Ferrara, Italy
[g] Istituto Nazionale di Fisica Nucleare, Sezione di Cagliari, via Negri 18, I-09127 Cagliari, Italy
[h] Dipartimento di Fisica dell'Università di Cagliari, via Ospedale 72, I-09124 Cagliari, Italy

Solar neutrinos: beyond standard solar models

V. Castellani[a,b,c,1], S. Degl'Innocenti[d,e,2], G. Fiorentini[e,f,3], M. Lissia[g,h,4], B. Ricci[e,5]

[a] Dipartimento di Fisica dell'Università di Pisa, I-56100 Pisa, Italy
[b] Osservatorio Astronomico di Collurania, I-64100 Teramo, Italy
[c] Istituto Nazionale di Fisica Nucleare, LNGS, I-67017 Assergi (l'Aquila), Italy
[d] Max-Planck Institut for Astrophysics, D-85740 Garching bei München, Germany
[e] Istituto Nazionale di Fisica Nucleare, Sezione di Ferrara, via Paradiso 12, I-44100 Ferrara, Italy
[f] Dipartimento di Fisica dell'Università di Ferrara, via Paradiso 12, I-44100 Ferrara, Italy
[g] Istituto Nazionale di Fisica Nucleare, Sezione di Cagliari, via Negri 18, I-09127 Cagliari, Italy
[h] Dipartimento di Fisica dell'Università di Cagliari, via Ospedale 72, I-09124 Cagliari, Italy

Contents

---

[1] E-mail: vittorio@astrpi.difi.unipi.it.
[2] E-mail: scilla@vaxfe.fe.infn.it.
[3] E-mail: fiorentini@vaxfe.fe.infn.it.
[4] E-mail: lissia@vaxca.ca.infn.it.
[5] E-mail: ricci@vaxfe.fe.infn.it.

Abstract

After a short survey of the physics of solar neutrinos, giving an overview of hydrogen burning reactions, predictions of standard solar models and results of solar neutrino experiments, we discuss the solar-model-independent indications in favour of non-standard neutrino properties. The experimental results appear to be in contradiction with each other, even after disregarding some experiments: unless electron neutrinos disappear in their trip from the sun to the earth, the fluxes of intermediate energy neutrinos (those from ^7Be electron capture and from the CNO cycle) turn out to be unphysically negative, or extremely reduced with respect to standard solar model predictions. Next we review extensively the non-standard solar models built as attempts to solve the solar neutrino puzzle. The dependence of the central solar temperature on chemical composition, opacity, age and on the values of the astrophysical S-factors for hydrogen-burning reactions is carefully investigated. Also, possible modifications of the branching among the various pp-chains in view of nuclear physics uncertainties are examined. Assuming *standard* neutrinos, all solar models examined fail in reconciling theory with experiments, even when the physical and chemical inputs are radically changed with respect to present knowledge and even if some of the experimental results are discarded.

0. Introduction

In a prophetical paper of 1946, Bruno Pontecorvo [1] reviewed the arguments for the existence of neutrinos (at that time based mainly on conservation laws) and stated:

"Direct proof of the existence of the neutrino ... must be based on experiments, the interpretation of which does not require the law of conservation of energy, i.e., on experiments in which some characteristic process produced by free neutrinos ... *is observed."*

Then he pointed out the relevance of inverse beta decay for neutrino detection and outlined the potential of neutrinos from nuclear reactors in physics. He also mentioned solar neutrinos: *"The neutrino flux from the sun is of the order of* 10^{10} *neutrinos/cm²/s. The neutrinos emitted by the sun, however, are not very energetic ..."*. In 1946 Pontecorvo was not optimistic about the detection of solar neutrinos. Since then, solar neutrino physics has made enormous progress, with a significant acceleration during the last decade.

From the seventies to the first half of the eighties the only result was that of the Chlorine experiment [2], essentially implying an observed ^{8}B neutrino flux lower than that predicted by Standard Solar Models (SSMs). Many physicists were not convinced of the existence of a solar neutrino problem, mainly because of the uncertainties in estimating the flux of the rare, high energy ^{8}B neutrinos. In 1989 [3] results from the KAMIOKANDE experiment were presented, confirming the low ^{8}B neutrino flux. However, as observed by Bahcall and Bethe [4], the comparison between KAMIOKANDE and Chlorine data implied an additional puzzle. As the Chlorine experiment is also sensitive to ^{7}Be neutrinos, if one subtracts the ^{8}B contribution from the Cl signal as implied by KAMIOKANDE data (for standard neutrinos), no room is left for ^{7}Be neutrinos. Thus the problem started involving also these less energetic neutrinos, for which the theoretical predictions are much more robust. At the beginning of the nineties, the results of Gallium experiments (GALLEX [5] and SAGE [6]) became available; for these the signal is expected to depend primarily on pp neutrinos, but to a lesser extent also on ^{7}Be neutrinos and on ^{8}B neutrinos. In both Gallium experiments the signals were again significantly smaller than the SSM predictions. The exposure of the Gallium detectors to a ^{51}Cr neutrino source [7, 8] was important for confirming quantitatively the sensitivity of the apparatus for neutrino detection.

By combining the results of the various experiments, it became possible to obtain relevant information on neutrinos independently of solar models. As we shall see, the solar neutrino experiments tell us that the following assumptions are most likely contradictory:

- Neutrino properties are correctly described by the minimal standard model of electroweak interactions (i.e. "standard" neutrinos).
- Solar energy arriving on the earth is produced in the sun by nuclear reactions of the form:

$$4p + 2e^- \rightarrow \,^4He + 2\nu_e \,.$$
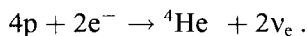
Since there is little doubt that the sun, as many other stars, is powered by the conversion of hydrogen into helium, experiments point towards some non-standard neutrino properties and – as was the case in 1946 – energy conservation becomes again a key tool, albeit an indirect one, for the study of neutrinos.

This paper attempts to answer the following questions:

(i) which information on neutrino properties can be obtained directly from solar neutrino experiments, independently – as much as possible – of solar models?

(ii) how much room – if any – is still open for an astrophysical or nuclear physics solution of the solar neutrino puzzle?

As the SSM has to be abandoned in face of the clear disagreement with all experiments, we shall present a systematic analysis of non-standard solar models (i.e. models where some input parameter is varied beyond its estimated uncertainty), in order to explore the possibility of reconciling theory and experiments.

As we were writing this paper, a generation of solar neutrino experiments has been essentially completed. In preparation for the exciting future experiments (SUPERKAMIOKANDE [9], BOREXINO [10], SNO [11], HELLAZ [12], ...), it is time to summarize what we have learnt so far.

In the minimal standard model of electroweak interactions, neutrinos are massless and consequently there is no mixing among weak flavour states. Also their magnetic moments vanish and they are stable. The experimental hint of non-standard neutrino properties (i.e. masses, mixing, magnetic moments, possible decay schemes, ...) thus seems to indicate some physics beyond the standard model. The present situation looks to us very similar to the one described by Pontecorvo in 1946: just change the word *existence* to *non-standard properties*, in the sense that solar neutrino experiments together with energy conservation strongly point towards non-standard neutrino properties. Much as in 1946, the future of neutrino physics now demands experiments yielding decisive *direct* evidence of non-standard neutrino properties.

0.1. The plan of this paper

In Section 1 we present a short and simple introduction to the field for non-experts, reviewing: (i) hydrogen burning in the sun and neutrino production, (ii) the predictions of Standard Solar Models (SSM) and (iii) the results of solar neutrino experiments.

In the next section we discuss the information on neutrino fluxes which can be derived directly from experiments, almost independently of solar models, assuming standard neutrinos. This is the main part of our review, as it is meant to demonstrate that, *for standard neutrinos*:

- the available experimental results appear to be mutually inconsistent, even dismissing one out of four experiments.
- Even after neglecting these inconsistencies, the flux of intermediate energy neutrinos (Be+CNO) as derived from experiments is significantly smaller than the prediction of SSM's.
- The different reductions of the ^7Be and ^8B neutrino fluxes with respect to the SSM predictions are essentially in contradiction with the fact that both ^7Be and ^8B neutrinos originate from the same parent ^7Be nuclei.

In Section 3 we describe a strategy for building non-standard solar models leading to reduced ^7Be and ^8B neutrino fluxes. There are essentially two ways: (i) producing models with smaller central solar temperatures; (ii) playing with the nuclear cross sections which determine the branches of the fusion chain. In the same section we introduce some algorithms for discussing the non-standard models, to be presented in the subsequent sections: we essentially seek parameterizations of the results (neutrino fluxes and physical quantities characterizing the solar interior, ...) in terms of the input quantity which is being varied.

In Section 4 we examine non-standard solar models with a central temperature T_c different from the SSM prediction. Clearly the central temperature is not a free parameter, its value being fixed by the equations of stellar structure and by the physical inputs one is relying on. We present a systematic analysis for the variations of several physical inputs (S_{pp}, opacity tables, chemical composition, age, ...) affecting T_c. An interesting feature common to a large majority of the models that we examined, is that the radial temperature profiles appear largely unchanged, aside from a scaling factor which can be evaluated, as e.g., the ratio of central temperatures. Thus, the profile is the same for a given value of T_c independently of which parameter is varied in order to obtain that central temperature. This allows one to compare experimental data with the theoretical predictions as a function of just one parameter, namely T_c.

Section 5 is devoted to the rôle of the nuclear cross sections which can influence the branching ratios of the p–p chain. We discuss in detail the rôle of the He+He reactions and we consider possible effects of screening of nuclear charges by the stellar plasma. We also discuss the rôle of the p+^{7}Be reaction.

In Section 6 we compare the non-standard solar models just built with experimental data. We also consider hybrid models, where both T_c and nuclear cross sections are varied simultaneously. All our attempts to reconcile theory and experiments having failed, we conclude that

• for standard neutrinos, the present experimental data look in disagreement not only with the standard solar model, but with any solar model that we are able to build.

In Appendix A, we specify our standard solar model in some detail. We concentrate here on our own calculations as we obviously have for these a more detailed knowledge of the physical and chemical inputs and outputs of the code. In fact, several groups have produced in the last few years updated and accurate standard solar model calculations [13,23]. In this paper we shall not give a systematic presentation of these. We also do not describe solar neutrino experiments nor helioseismology. All these matters are excellently covered in other review works, e.g.,

– Bahcall's book [24] and papers in Review of Modern Physics [13–15], all extremely useful, centered around standard solar models.

– The report by Koshiba [25], providing a fascinating journey through the experimental techniques of neutrino astrophysics.

– The review by Turck-Chièze et al. [26], again centered around standard solar models, including a clear discussion of helioseismology in relationship to the solar neutrino problem.

– A recent reprint collection [27], presenting most of the significant papers on solar neutrinos, and an excellent bibliography.

1. Overview

The earlier discovery of the enormous energy stored in nuclei led astrophysicists to speculate that reactions among nuclear species were the source of energy in stars:

"Certain physical investigations in the past year make it probable to my mind that some portion of sub-atomic energy is actually being set free in a star. ... Aston has ... shown ... that the mass of the helium atom is less than the sum of the masses of the four hydrogen atoms which enter into it. ... Now mass cannot be annihilated, and the deficit can only represent the energy set free in the transmutation. ... If five per cent of a star's mass consists initially of hydrogen atoms, which

*are gradually being combined to form more complex elements, the total heat liberated will more
than suffice for our demands, and we need look no further for the source of a star's energy ...*
(Eddington, 1920) [28].[6]

After the discovery of the tunnel effect in 1928 [29, 30], Atkinson and Houtermans presented the
first qualitative theoretical approach to the problem [31]. From the nuclear data available to them
and the already known fact that hydrogen is the most abundant element in the sun and the universe,
they concluded that the energy-producing mechanism involved primarily hydrogen, as suggested by
Eddington. As a matter of fact, the fusion of hydrogen nuclei to form helium is still the only known
process that can supply the required power for the long solar life.

Hydrogen burning can be represented symbolically by the "fusion" reaction:

$$4p + 2e^- \rightarrow {}^4He + 2\nu_e \,. \tag{1}$$

The total energy released in Eq. (1) is $Q = 26.73$ MeV and only a small part of it (about 0.6 MeV)
is carried away by the two neutrinos.

From the solar radiative flux at the earth, called the solar constant $K_\odot = 8.533(1 \pm 0.004) \cdot 10^{11}$ MeV cm^{-2} s^{-1} [15], one immediately derives the total flux Φ_{tot} of electron neutrinos arriv-
ing on the earth, if they are not lost en route (by neglecting the small fraction of energy carried by
neutrinos):

$$\Phi_{tot} \approx 2K_\odot/Q \approx 7 \times 10^{10} \text{ cm}^{-2} \text{ s}^{-1} \,. \tag{2}$$

The definite proof of nuclear energy production in the solar core lies in the detection of solar
neutrinos. Since the cross sections for neutrino detection depend strongly on neutrino energy, the
energy spectrum of solar neutrinos has to be known and that requires a detailed knowledge of the
reactions summarized by Eq. (1).

1.1. Hydrogen burning reactions

In stellar interiors, nuclear interactions between charged particles (nuclei) occur at collision ener-
gies E well below the height of the Coulomb barrier and are only possible due to the tunnel effect,
with a characteristic probability [29]:

$$P \approx \exp\left[-Z_i Z_j e^2 2\pi/\hbar \sqrt{\mu_{ij}/2E}\right] \,, \tag{3}$$

where $Z_{i,j}$ are the atomic numbers of the colliding nuclei and μ_{ij} their reduced masses. The lightest
elements thus react most easily and the conversion of H into He is the first chain of nuclear reactions
which can halt the contraction of a new-born stellar structure and settle stars in the so-called Main
Sequence phase.

The mechanisms for hydrogen burning were first elucidated in the late 1930s independently by von
Weizsäcker and Bethe and Critchfield [32–34]; from their works it became clear that two different
sets of reactions could convert sufficient hydrogen into helium to provide the energy needed for a

---

[6] In the same paper, a few line ahead, one reads: *"If indeed the sub-atomic energy in the stars is being freely used to
maintain their great furnaces, it seems to bring a little nearer to fulfilment our dream of controlling this latent power
for the well-being of the human race – or for its suicide."*
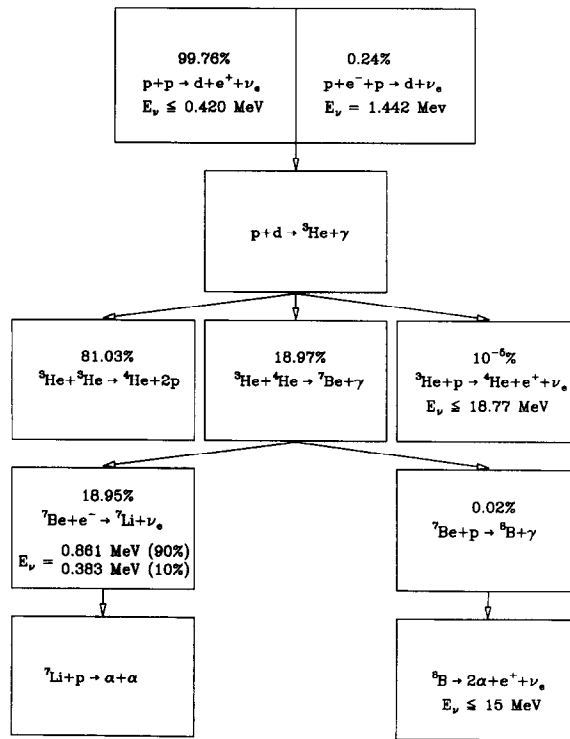
Fig. 1. The pp chain. The probability of the different branches are from the reference solar model [15]. The neutrino energies E_ν are also indicated.

star's luminosity, namely the proton–proton (p–p) chain and the CNO bi-cycle, which we are going to review briefly (see [35] for a more extended presentation).

At the temperature and density characteristic of the solar interior, hydrogen burns with the largest probability (98%) through the pp chain. This develops through the nuclear reactions presented in Fig. 1, where we show the different possible branches.

The chain starts with a weak interaction process, either the pp or the pep reaction. The mechanisms for these two reactions are very similar and hence the ratio of pep to pp reaction probabilities is fixed almost independently of the details of the solar model; at the densities of the solar interior ($\rho \lesssim 150\,\mathrm{g\,cm^{-3}}$) the three body process has a smaller probability. The deuterons produced quickly burn into ^{3}He as a consequence of the much larger cross section of the electromagnetic process d+p→^{3}He +γ.

After ^{3}He production, several branches occur. The hep reaction turns out to have a negligible rate and will not be discussed further. Even if the ^{3}He abundance remains a factor 10^4 lower than that of ^{4}He in the energy production region, the ^{3}He+^{3}He→^{4}He +2p reaction is favoured with respect to ^{3}He+^{4}He→^{7}Be+γ, because the probability of the reaction mediated by strong interaction is four orders of magnitude larger than that of the electromagnetic process and because the tunnelling probability through the Coulomb barrier for the case of the lighter ^{3}He nuclei is a factor ten larger.

With the ^{3}He+^{3}He reaction the chain reaches one of the possible terminations (pp-I chain). On the other hand, after the ^{3}He+^{4}He reaction, the chain branches again at the ^{7}Be level, due to the

Fig. 2. The CNO cycle.

competition between electron and proton capture. Note that, at the temperatures of the solar interior, the electron capture (although it is a weak process) dominates over the electromagnetic reaction since it has no Coulomb barrier. The chain passing through the $^7Be+e^-$ reaction is called pp-II chain, and the one involving the ^7Be+p reaction is called pp-III chain.
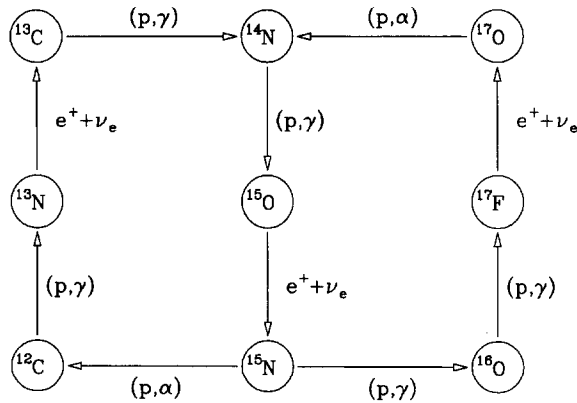
To conclude this overview of the pp chain we remark that the basic process in any case is the aggregation of four protons to form a ^4He nucleus, the isotopes $^2H, ^3He, ^7Be, ^7Li$ and ^8B being intermediate products which are created and destroyed along the chain, their number densities staying constant (and small) when the chain reaches equilibrium.

Regarding the neutrino production we note that:

(i) in the pp-I chain only pp or pep neutrinos are produced, the latter with a small probability (0.2% in the standard solar model).

(ii) In the pp-II chain one pp (or pep) and one ^7Be neutrino are emitted.

(iii) In the pp-III chain one pp (or pep) and one ^8B neutrino are emitted.

Fig. 2 shows the main reactions in the CN and NO cycles which become efficient at rather high temperatures. The overall conversion of four protons to form a ^4He nucleus is achieved with the aid of C, N and O nuclei. The total energy release is clearly the same as in the pp chain. The ratio of the astrophysical S-factors[7] for the two reactions ^{15}N $(p,^4He)^{12}C$ and ^{15}N $(p,\gamma)^{16}O$ being about a factor 1000, the rôle of NO cycle is generally marginal. In the sun essentially only the CN cycle (left-hand side of Fig. 2) is contributing to the energy production.

For each fusion of four protons into ^4He via the CN cycle one neutrino from the decay of ^{13}N and another from that of ^{15}O are produced. Note that the efficiency of the process is determined by the reaction with the smallest cross section, which clearly is $p+^{14}N \rightarrow ^{15}O +\gamma$, an electromagnetic process with the largest Coulomb repulsion.

1.2. Stellar structures and standard solar models

According to the theory of stellar structure and evolution, the condition for hydrostatic equilibrium jointly with the conservation of energy and the mechanism for energy transport determine the physical

---

[7] We denote as σ_{ij} the cross section for the reaction between nuclei with atomic mass numbers i and j, v_{ij} is the relative velocity, E is the collision energy and the astrophysical S-factor is: $S_{i,j} = \sigma_{ij} \exp[2\pi Z_i Z_j e^2/(\hbar v_{ij})]E$.

structure of a star and its evolution from four main inputs, namely:

(i) The initial chemical composition.

(ii) The equation of state for stellar matter.

(iii) The radiative opacity, κ, as a function of density ρ, temperature T and chemical composition.

(iv) The energy production per unit mass and time ε, again as a function of ρ, T and chemical composition.

For the equation of state (EOS) one has to evaluate the ionization degree and the population of excited states for all nuclear species. In addition, one has to take into account several physical effects of the stellar plasma (like Coulomb interaction and/or electron degeneracy) which introduce deviations from the "perfect gas law" prediction. The study of EOS has improved over the years and accurate tabulations are available (see [36] for a recent discussion).

The radiative opacity κ is directly connected with the photon mean free path, $\lambda = 1/\kappa\rho$. All throughout the internal radiative region κ governs the temperature gradient through the well known relation [37]:

$$\frac{dT}{dr} = -\frac{3}{4ac}\frac{\rho\kappa}{T^3}F , \qquad (4)$$

where F is the electromagnetic energy flux. The evaluation of κ as a function of the composition of the gas and of its physical conditions requires a detailed knowledge of all the processes important for radiative flow (elastic and inelastic scattering, absorption and emission, inverse bremsstrahlung, ...) and in turn a detailed evaluation of the atomic levels in the solar interior. As a consequence, the evaluation of κ is a rather complex task, but the results have been continuously improving over the years. At present one relies mainly on the calculations of the OPAL group at the Lawrence Livermore National Laboratories (see, e.g. Refs. [38–40]).

Expressions for (the nuclear contribution) to ε are derived essentially from the tables of nuclear reaction rates, originally compiled and continuously updated by Fowler, until his death (see Ref. [41] and references therein).

According to Stix [42], "*The standard model of the sun could be defined as the model which is based on the most plausible assumptions.*" This means that physical and chemical inputs are chosen at the central values of experimental/observational/theoretical results. We prefer to call such a model the reference solar model (RSM); throughout this review we use as such the "best model with diffusion" of Bahcall and Pinsonneault [15] denoted as BP95. More generally, let us *define a standard solar model* (SSM) *as one which reproduces, within uncertainties, the observed properties of the sun, by adopting a set of physical and chemical inputs chosen within the range of their uncertainties.*

The actual sun has a mass $M_\odot = (1.98892 \pm 0.00025) \times 10^{33}$ g [43] and a radius $R_\odot = (6.9598 \pm 0.0007) \times 10^{10}$ cm [44]. Denoting by X, Y and Z the relative mass abundances of H, He and heavier elements respectively $(X + Y + Z = 1)$, the present ratio of heavy elements (metallicity) to hydrogen in the photosphere is $(Z/X)_{photo} = 0.0245(1 \pm 0.061)$ [45, 15]. At the age $t_\odot = (4.57 \pm 0.01)$ Gyr [15], the sun is producing a luminosity $L_\odot = 3.844(1 \pm 0.001) \times 10^{33}$ erg s^{-1} [15].

If a complete information about the (initial) photospheric composition was available and if the theory of stellar models was capable to predict stellar radii firmly, then there would be no free parameter. The theoretical model should account for the solar luminosity and radius at the solar age, without tuning any parameters.

The photospheric helium abundance is however not strongly constrained by direct observations, since no helium line exists at the photospheric depth, see Ref. [46] for a critical discussion (helioseismology can however provide some indirect information, see later). Furthermore, the present observed photospheric composition is different from the initial one due to diffusion and gravitational settling. Moreover, the radii (but only the radii) of stars with convective envelopes (e.g. the sun) depend on the assumption made about the convective transport, as we shall discuss later on. As a consequence, one has the freedom of adjusting some parameters in the course of the calculation.

In order to produce a standard solar model, one studies the evolution of an initially homogeneous solar mass up to the sun age. To obtain $L_\odot$, $R_\odot$ and $(Z/X)_{\text{photo}}$ at $t_\odot$, one can tune three parameters: the initial helium abundance Y, the metal abundance Z and a third quantity related to the efficiency of convection (see below).

The effects of these parameters can be understood simply. The luminosity of the sun (more generally of any star in the main sequence) depends in a rather sensitive way on the initial helium content Y; increasing it, the initial sun is brighter and a given luminosity is reached in a shorter time. Since the ratio Z/X is constrained by observational data, Y and Z cannot be chosen independently: if Y increases, Z must decrease.

To get the proper radius $R_\odot$, one adjusts the efficiency of the external convection, which dominates the energy transport in the outer layers of the sun (about the outer 30% of the solar radius). The precise description of the convection in the external part of the sun is an essentially unsolved problem, and the process is commonly described in terms of a phenomenological model, the so-called "mixing length theory", see e.g. Ref. [37]. Following this approach, we define the mixing length l as the distance over which a moving unit of gas can be identified before it mixes appreciably. This length is related to the pressure scale height $H_p = 1/(d \ln P/dr)$ through

$$l = \alpha H_p \,, \tag{5}$$

where α is assumed to be independent of the radial coordinate and it is used as free parameter. By varying α, one varies the mixing length and thus the convection efficiency, which determines the solar radius. Thus if α is increased, convection becomes more efficient, the temperature gradient smaller and the surface temperature higher. Since the solar luminosity is fixed, the radius has to decrease.

In the last few years, one of the principal improvements of SSMs was the treatment of element diffusion [14–16, 21–23, 47–52]. Noerdlinger [47] first included the effects of He diffusion on the evolution of the sun, while Cox et al. [48] were the first to take into account the settling of heavy elements. The stronger pull of gravity on helium and heavier elements causes them to diffuse slowly downward, relative to hydrogen. As a result, if diffusion is taken into account, helium and heavier elements in the solar photosphere are depleted with respect to their abundance in the original mixture.

We remark that, as a strong simplification, the sun is taken as spherically symmetric, i.e. all physical quantities vary only radially. This relies on the assumption that the internal rotation is sufficiently slow [53] and the internal magnetic fields are sufficiently weak so that the corresponding forces are negligible.

All in all, it looks that a solar model has three (essentially) free parameters, α, Y, and $(Z/X)_{\text{in}}$, and produces three numbers which can be directly measured: the present radius, luminosity and heavy element content of the photosphere. This may not look as a big accomplishment. At this stage, one's confidence in the SSMs actually rests on the success of stellar evolution theory to describe many, and more complex, evolutionary phases in good agreement with observational data.
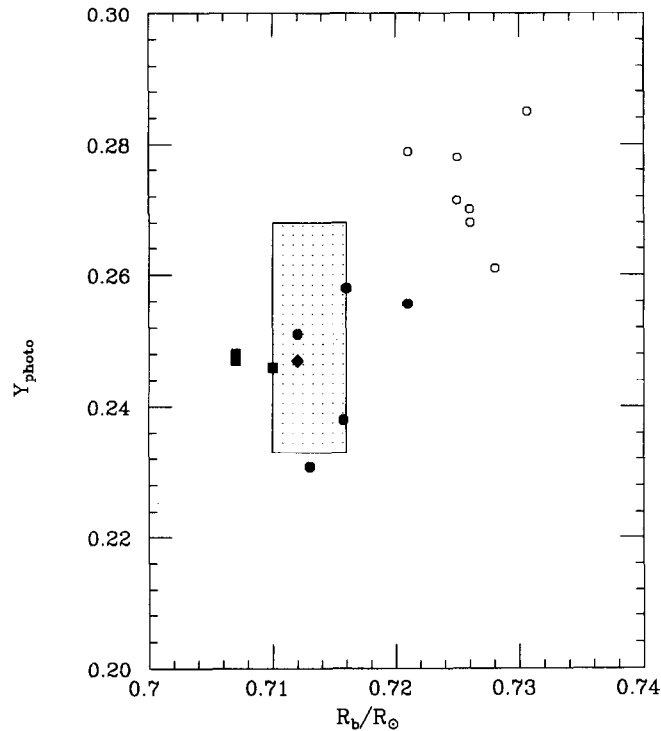
Fig. 3. The photospheric helium mass fraction Y_{photo} and the depth of the convective zone $(R_b/R_\odot)$: (a) as constrained by helioseismology (the dotted rectangle), see Section 1.2; (b) as predicted by solar models without diffusion, open circles from top to bottom correspond to [23,21,22,17,16,15,56]; (c) as predicted by solar model with helium diffusion, full squares from top to bottom correspond to [21,14,16]); (d) as predicted by solar model with helium and heavy elements diffusion: the full circles, from top to bottom correspond to [22,48,16,56,23]) and the full diamond indicates the RSM [15].

In recent years, however, helioseismology has added important data on the solar structure, which provide severe constraints and tests of standard solar model calculations. Helioseismology can accurately determine the depth of the convective zone and the speed of sound c_b at the transition radius R_b between convective and radiative transport [54]:

$$R_b/R_\odot = 0.710\text{–}0.716\,, \tag{6}$$

$$c_b = (0.221\text{–}0.225)\,\text{Mm s}^{-1}\,.$$

The indicated range for R_b has been confirmed recently [22].

Actually, within the present uncertainties, the information on R_b and on c_b are not independent, since to the per cent level, c_b and R_b are related through [54]:

$$c_b^2 \simeq \frac{2}{3}\frac{GM_\odot}{R_\odot}\left(\frac{R_\odot}{R_b} - 1\right). \tag{7}$$

Several determinations of the helium photospheric abundances have been derived from inversion (deconvolution) of helioseismological data (see Fig. 3), yielding (see Table 4):

$$Y_{photo} = 0.233\text{–}0.268\,. \tag{8}$$

One should note that the small errors often quoted generally reflect the observational frequency errors only. The results actually depend on the method of inversion and on the starting physical inputs, e.g. the EOS. Such a dependence has been recently studied in Ref. [22].

With these additional constraints, Eqs. (6) and (8), there are essentially no free parameters for SSM builders.

1.3. Results of standard solar models

Table 1 shows the main results of recent solar models produced by various authors: *all of them include microscopic diffusion of helium and heavy elements*, using (slightly) different physical and chemical inputs, which are summarized in Table 2.

By varying Y and α, and adjusting $(Z/X)_{in}$ within the observed range, all models are able to reproduce $L_\odot$, $R_\odot$ and $(Z/X)_{photo}$ at the solar age.

The comparison with helioseismological measurements, which provide additional constraints, is interesting, see Fig. 3 from [55]. Only some of the recent solar models with microscopic diffusion are in agreement with the helioseismological constraints. With the notation of Table 1, they are P94 [16], RVCD96 [22], BP95 [15] and FRANEC96 [56]. On the other hand, all models without diffusion fail. The importance of diffusion for achieving agreement with helioseismological data is discussed in Appendix A.

Table 1
Comparison among several solar models, all calculated including diffusion of helium and heavy elements

	CGK89 Ref. [48]	P94 Ref. [16]	DS96 Ref. [23]	RVCD96 Ref. [22]	RSM Ref. [15]	FRANEC96
$t_\odot$ (Gyr)	4.54	4.60	4.57	4.60	4.57	4.57
$L_\odot (10^{33}$ erg/cm^{-2} s^{-1})	3.828	3.846	3.844	3.851	3.844	3.844
$R_\odot (10^{10}$ cm)	6.9599	6.9599	6.960	6.959	6.9599	6.960
$(Z/X)_{photo}$	0.02464	0.02694	0.02263	0.0263	0.02446	0.0245
X_{in}	0.691	0.6984	0.7295	0.7012	0.70247	0.711
Y_{in}	0.289	0.2803	0.2509	0.2793	0.27753	0.269
Z_{in}	0.02	0.02127	0.01833	0.0195	0.02	0.0198
X_{photo}	0.7265	0.7290	0.7512	0.7226	0.73507	0.744
Y_{photo}	0.2556	0.2514	0.2308	0.2584	0.24695	0.238
Z_{photo}	0.0179	0.01964	0.0170	0.0190	0.01798	0.0182
$R_b/R_\odot$	0.721	0.7115	0.7130	0.716	0.712	0.716
$T_b (10^6$ K)	2.142		2.105	2.175	2.204	2.17
$c_b (10^7$ cm s^{-1})	2.21[a]		2.21[a]	2.22[a]	2.25[a]	2.22
$T_c (10^7$ K)	1.573	1.581	1.561	1.567	1.5843	1.569
$\rho_c (100$ g cm^{-3})	1.633	1.559	1.554	1.545	1.562	1.518
Helioseismology	No	Yes	No	Yes	Yes	Yes

Note: The "best model with diffusion" of [15] will be used as the reference solar model (RSM) in this paper. FRANEC96 indicates our best model with diffusion, model (e) of Appendix A. The last row indicates the consistency with helioseismology, see Section 1.2.
[a] Values of c_b calculated by us, assuming fully ionized perfect gas EOS.

Table 2

Physical and chemical inputs of the solar models in Table 1. The correspondence between acronyms and references is as follows: C&S70=[156], MHD = [157], CEFF = [158] with the Coulomb correction added (see [159]), EFF = [158], BP92 = [14], G&N93 = [45], G91 = [76], F75 = [134], C&F88 = [41]. Note that RVCD96 also includes rotational mixing

	CGK89 Ref. [48]	P94 Ref. [16]	DS96 Ref. [52]	RVCD96 Ref. [22]	RSM Ref. [15]	FRANEC96
Opacity	C&S70	OPAL	OPAL	OPAL	OPAL	OPAL
EOS	MHD	CEFF	DS96	MHD	BP92	OPAL
Mixture	G&N93	G91	G&N93	G91	G&N93	G&N93
Cross sections	F75	BP92	DS96	C&F88	Table 28	Table 28

Table 3

Comparison among the neutrino fluxes of the solar models of Table 1. All of them, except for DS96, are SSMs according to our definition

	P94 Ref. [16]	DS96 Ref. [23]	RVCD96 Ref. [22]	RSM Ref. [15]	FRANEC96
Φ_{pp} (10^9 cm^{-2} s^{-1})	59.1	61.0	59.4	59.1	59.92
Φ_{pep}(10^9 cm^{-2} s^{-1})	0.139	0.143	0.138	0.140	0.14
Φ_{Be} (10^9 cm^{-2} s^{-1})	5.18	3.71	4.8	5.15	4.49
Φ_{N} (10^9 cm^{-2} s^{-1})	0.64	0.382	0.559	0.618	0.53
Φ_{O} (10^9 cm^{-2} s^{-1})	0.557	0.374	0.481	0.545	0.45
Φ_{B} (10^6 cm^{-2} s^{-1})	6.48	2.49	6.33	6.62	5.16
S_{Ga}[SNU]	136.9	115	132.77	137.0	128
S_{Cl}[SNU]	9.02	4.1	8.49	9.3	7.4

We shall consider as SSMs *only those models which pass the helioseismological tests.* We recall that, among these, *we shall refer to* BP95 "*best model with diffusion*" [15] *as to the reference solar model* (*RSM*).

From Table 1 one sees that calculated central temperatures are in agreement at the per cent level.

As a matter of fact, this shows that building up a stellar model is by now a well-established and reliable procedure, the small differences being essentially the result of small variations in the assumed physics input. At the same time, this agreement indicates the consensus about the treatment of the rather sophisticated physics needed to account for the behaviour of stellar structures.

Concerning neutrinos, the solar model determines the internal distribution of temperature, density and H abundance and, thus, the efficiency of the various chains. In this way, one gets the fluxes at earth of the different neutrino components ($\Phi_{pp}, \Phi_{pep}, \Phi_{Be}, \ldots$). From Table 3 one notes that:

(i) the fluxes of pp neutrinos are stable to a few percent. As they are the most abundant ($\Phi_{pp} \approx \Phi_{tot}$) by far, their flux is directly related to the solar luminosity.

(ii) The ratio

$$\xi = \Phi_{pep}/(\Phi_{pep} + \Phi_{pp}) \tag{9}$$

is almost independent of solar models, as it is weakly sensitive to the solar temperature and density.

(iii) After the pp, the ^{7}Be neutrinos are the most abundant, their flux accounting for about 8% of the total, and again the prediction is rather stable among the different calculations with the exception of DS96.

Table 4
Helioseismological determinations of the present surface He abundance, Y_{photo}. In RVCD96 uncertainties depending on the inversion method and on the EOS are included

Reference	Y_{photo}
Dappen (1988) [160]	$Y = 0.233 \pm 0.003$
Dappen (1991) [161]	$Y = 0.268 \pm 0.002$
Dziembowski (1991) [155]	$Y = 0.234 \pm 0.005$
Vorontsov (1991) [162]	$Y = 0.250 \pm 0.010$
Dziembowski (1994) [163]	$Y = 0.24295 \pm 0.0005$
Hernandez (1994) [164]	$Y = 0.242 \pm 0.003$
RVCD96 [22]	$Y = 0.250 \pm 0.005$

(iv) The spread of the calculated ^{8}B neutrino fluxes is much larger showing the larger sensitivity to the different physical inputs used in different solar models.

(v) Concerning neutrinos from the CN cycle, again their prediction is somehow model-dependent. [8] For a full CN cycle one should clearly have the same number of ^{13}N and ^{15}O neutrinos. Actually, the reaction ^{14}N $(p,\gamma)^{15}$O is too slow in the solar region below 10^7 K and the chain has not reached equilibrium, still favouring the transformation of ^{12}C into ^{14}N . This is why ^{13}N neutrinos are slightly more abundant than the ^{15}O neutrinos, i.e., if one defines

$$\eta = \Phi_N/(\Phi_N + \Phi_O), \tag{10}$$

one finds η slightly larger than 0.5. Note that $\eta = 0.53$ in most calculations. Table 3 does not include results on ^{17}F neutrinos, which are two orders of magnitude less abundant than ^{13}N or ^{15}O neutrinos. [9]

Helioseismological determinations of the present surface He abundance are listed in Table 4.

We find it useful to group some neutrinos according to their origin, putting pp and pep neutrinos in the same group

$$\Phi_p = \Phi_{pp} + \Phi_{pep} , \tag{11}$$

and into another the neutrinos from the CN cycle:

$$\Phi_{CNO} = \Phi_N + \Phi_O . \tag{12}$$

Following the common terminology, we call these latter the "CNO neutrinos", although they are neutrinos just from the CN cycle.

Fig. 5 shows the production region in the sun for the main neutrino components. Because of the strong temperature dependence, ^{8}B neutrino production is peaked at a very small distance from the solar center ($R \approx 0.04R_\odot$). The same holds for ^{13}N and ^{15}O neutrinos, which are produced with equal rate up to $R \approx 0.14R_\odot$. The secondary peak at $R \approx 0.16R_\odot$ is due to ^{13}N neutrinos only, in a region where the CN cycle is marginally active, C and N have not reached their equilibrium values

---

[8] In [52] Shaviv presented values of Φ_N and Φ_O an order of magnitude smaller than those of all other calculations. This feature is no more present in the more recent calculation by the same author [23].

[9] The reader will note that the model DS96 [23] is the one yielding the smallest prediction on ^{7}Be, CNO and ^{8}B neutrino fluxes (Table 3) and the smallest central temperature. We remark that this model does not satisfy the helioseismological constraints. In addition the astrophysical S-factors used in [23] seem to us not acceptable, see Sections 4.2 and 5.

Table 5

For each component of the neutrino flux, we show the average neutrino energy $\langle E_v \rangle$ and the averaged neutrino capture cross sections (10^{-9} SNU cm^2 s = 10^{-45} cm^2) for chlorine and gallium, with errors at 1σ level . When averaging the pp and pep components to get p, we use the relative weights of the RSM; similarly for ^{13}N and ^{15}O to get CNO. All data from [24] but for $\sigma_{Cl,B}$ from [165]

	$\langle E_v \rangle_i$ (MeV)	$\sigma_{Cl,i}$ (10^{-9} SNU cm^2 s)	$\sigma_{Ga,i}$ (10^{-9} SNU cm^2 s)
pp	0.265	0	1.18(1 ± 0.02)
pep	1.442	1.6 (1 ± 0.02)	21.5 (1 ± 0.07)
p = pp+pep	0.268	0.0038(1 ± 0.02)	1.23(1 ± 0.02)
^{7}Be	0.814	0.24 (1 ± 0.02)	7.32(1 ± 0.03)
^{13}N	0.707	0.17 (1 ± 0.02)	6.18(1 ± 0.03)
^{15}O	0.996	0.68 (1 ± 0.02)	11.6 (1 ± 0.06)
CNO = ^{13}N + ^{15}O	0.842	0.41 (1 ± 0.02)	8.72(1 ± 0.05)
^{8}B	6.71	1110 (1 ± 0.03)	2430 (1 ± 0.25)

and nuclear reactions are transforming the more abundant ^{12}C into ^{14}N. The ^{7}Be neutrino production peaks at $R \approx 0.06 R_\odot$, whereas for pp+pep neutrinos it peaks at $R \approx 0.1 R_\odot$ and extends over a large portion of the solar core.

1.4. Solar neutrino spectrum and the predicted neutrino signals

The energy spectrum of each component (pp, pep, ^{7}Be, ^{8}B, ...) *is determined by kinematics and/or nuclear physics and it is* (*essentially*) *independent of solar physics.*

The pp neutrinos have a continuous energy spectrum extending up to $E_v = 0.42$ MeV [13]. For a pep neutrino, its momentum has to match that of the produced deuteron and consequently its energy is uniquely determined by kinematics, giving $E_v = 1.442$ MeV. The energy of ^{7}Be neutrino depends on the state of ^{7}Li produced in the electron capture reaction. One has $E_v = 0.861$ MeV with 90% probability (^{7}Li ground state), and $E_v = 0.383$ MeV with 10% probability (first excited state). The energy spectrum of ^{8}B neutrinos extends up to $E_v = 15$ MeV [13, 57]. Except for the very rare hep neutrinos, ^{8}B neutrinos are thus the most energetic ones. In the CN cycle, the neutrinos from β^+ decay of ^{13}N and ^{15}O have end points at 1.20 and 1.73 MeV, respectively.

In Table 5 we give the average energy for each neutrino component. The average energies for the p and CNO neutrinos have been calculated by taking the values of η and ξ as in the RSM.

The solar neutrino spectrum predicted by standard solar models is shown in Fig. 4 (from Ref. [24]). Note that the pp neutrinos, which are the most abundant and the most reliably predicted ones, are also those with the lowest energy and thus are most difficult to detect, since neutrino cross sections increase with neutrino energy. On the other hand, ^{8}B neutrinos, which are rare and delicate to predict, are those with the highest energy so that their detection is comparatively "easy".

The solar neutrino signal in radiochemical experiments is expressed as the reaction rate per target atom. A suitable unit is the solar neutrino unit (SNU), defined as one reaction per second per 10^{36} atoms. A 1 SNU signal means that in a target containing 10^{31} atoms (of the order of several hundred tons) there is about one reaction per day; this already gives an idea of the low counting rate of these radiochemical experiments. The signal S is expressed in terms of the neutrino interaction cross
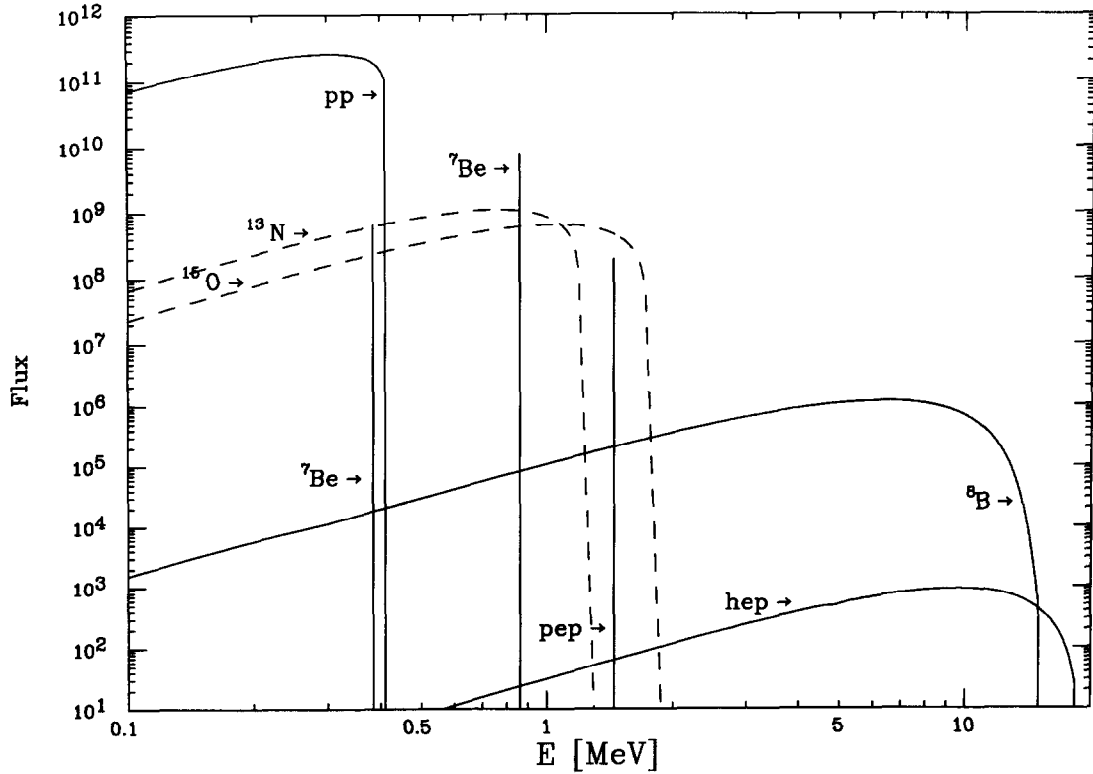
Fig. 4. The solar neutrino spectrum, from [24]. For continuous sources, the differential flux is in $cm^{-2} s^{-1} MeV^{-1}$. For the lines, the total flux is in $cm^{-2} s^{-1}$.

section $\tilde{\sigma}(E_\nu)$ and the differential neutrino flux $d\Phi/dE_\nu$:

$$S = \int_{E_{th}} dE_\nu \, \tilde{\sigma}(E_\nu) \, d\Phi/dE_\nu \,, \tag{13}$$

where E_{th} is the energy threshold for the detection. In the case of standard neutrinos, the spectrum can be written for each component as

$$d\Phi_i/dE_\nu = \Phi_i \, df/dE_\nu \,, \tag{14}$$

where df/dE_ν is normalized to unity and it is fully determined from nuclear physics and kinematics, see Fig. 5. The signal can thus be expressed as the sum of contributions arising from each neutrino component

$$S = \sum_i \sigma_i \Phi_i \,, \tag{15}$$

where

$$\sigma_i = \int dE_\nu \, \tilde{\sigma}(E_\nu) \, df/dE_\nu \tag{16}$$
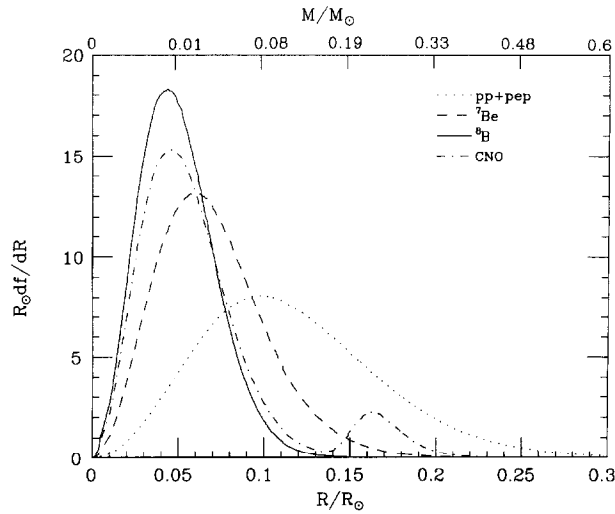
Fig. 5. For the indicated components, df is the fraction of neutrinos produced inside the sun within dR. On the bottom (top) scale the radial (mass) coordinate is indicated.

is the detection cross section averaged over the spectrum of the ith neutrino component, and is again determined purely from nuclear physics.

In summary, nuclear physics is responsible for σ_i, whereas solar physics determines Φ_i.

Of course σ_i depends on the reaction which one is considering and we present in Table 5 the quantities relevant for the two reactions so far used in the experiments

$$\nu_e + {}^{37}\text{Cl} \rightarrow e^- + {}^{37}\text{Ar} \quad (E_{th} = 0.814\,\text{MeV}) \tag{17}$$

and

$$\nu_e + {}^{71}\text{Ga} \rightarrow e^- + {}^{71}\text{Ge} \quad (E_{th} = 0.233\,\text{MeV}), \tag{18}$$
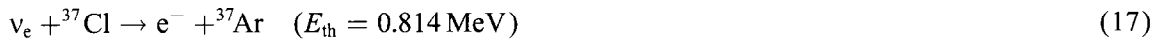
where the threshold energies are indicated in parenthesis.[10]

The cross sections increase with the neutrino energy. This is a general feature of weak interaction cross sections at energies well below the Fermi energy scale. In addition, this trend is more evident at low energies due to the presence of reaction thresholds, so that only neutrinos with high enough energy can induce the process. Note that the ${}^8\text{B}$ neutrinos, which are the most energetic ones, have cross sections three order of magnitude larger than the others, and this compensates for their significantly smaller flux.

The contributions $(\sigma_i \Phi_i)$ to the signal in the chlorine and gallium experiments from each component of the neutrino flux are shown in Table 7, as predicted by the RSM. For chlorine most of the signal comes from ${}^8\text{B}$ neutrinos, whereas for gallium the largest contribution is from pp neutrinos. This is a consequence of the quite different energy thresholds for the two reactions.

---

[10] Note that ν_μ and ν_τ cannot induce reactions (17) and (18) as the corresponding charged lepton (μ or τ) would require neutrino energies orders of magnitude larger than those appropriate for the sun.

Table 3 shows the total signals in the chlorine and gallium detectors,

$$S_{Ga} = \sum_i \sigma_{Ga,i} \Phi_i , \qquad S_{Cl} = \sum_i \sigma_{Cl,i} \Phi_i , \qquad (19)$$

as predicted by the different SSMs.

For the chlorine signal the predicted values vary among the SSM within 20%, mainly due to the variations of the ^{8}B flux. The spread of predictions for the gallium experiments is smaller, reflecting the rather stable estimates on pp and ^{7}Be neutrino fluxes.

Radiochemical experiments are not the only way to detect neutrinos. As an alternative approach one can use the neutrino–electron elastic scattering

$$\nu + e^- \rightarrow \nu + e^- , \qquad (20)$$

detecting the scattered electron.

Whereas for neutrino interactions with nuclei the cross section depends on nuclear physics and it is thus subject to some uncertainties, the cross section for scattering on electrons is well known from elementary particle physics. Both charged and neutral current interactions occur for electron neutrinos. For ν_μ and ν_τ *only* the neutral current interaction contributes and this results in a reduced cross section, e.g. for KAMIOKANDE $\sigma_{\nu_\mu} \approx (1/7)\sigma_{\nu_e}$. If one detects electrons with energy E_e larger than some minimal value E_0, the signal is

$$S(E_e > E_0) = \int_{E_0} dE_e \, dE_\nu \frac{d\sigma(E_\nu, E_e)}{dE_e} \frac{d\Phi(E_\nu)}{dE_\nu} , \qquad (21)$$

where $d\sigma/dE_e$ is the differential neutrino–electron elastic cross section, which depends on the energy of the scattered electron E_e. Because of background limitations, E_0 is generally larger than a few MeV, so that only ^{8}B neutrinos are detected.

Assuming standard neutrinos, the signal can thus be translated into an effective (energy integrated) ^{8}B neutrino flux, and data are generally presented in that form. Note, however, that this "experimental flux" can be taken as the true ^{8}B neutrino flux only for standard neutrinos: should ν_e transform into ν_μ, the detection cross section would be different.

1.5. A look at experimental results

So far we have results from four solar neutrino experiments; see Table 6 for a summary and Refs. [24, 25] for detailed reviews.

The KAMIOKANDE experiment [3], located in the Japanese Alps, detects the Cerenkov light emitted by electrons that are scattered in the *forward* direction by solar neutrinos, through the reaction (20).

This experiment, being sensitive to the neutrino direction, is the prototype of neutrino telescopes and is the only real-time experiment so far.

The experiment is only sensitive to the high energy neutrinos ($E_\nu \geq 7$ Mev) from ^{8}B decay. The solar neutrino spectrum deduced from KAMIOKANDE is in agreement (within large uncertainties) with that of neutrinos from ^{8}B decay in the laboratory [3]. Assuming that the spectra are the same (i.e. standard ν_e), one gets for the ^{8}B neutrino flux the result shown in Table 6. This corresponds to about 500 neutrino events collected in a 5.4 yr data-taking period. Although there is no really

Table 6
The main characteristic of each neutrino experiment: type, detection reaction, energy threshold E_{th}, experimental results with statistical and systematical errors. In the last column the reference solar model [15] predictions are presented. Errors are at 1σ level

Experiment	Type	E_{th}[a]	Result[b]	BP95[b]
Homestake	Radiochemical $\nu + {}^{37}Cl \rightarrow e^- + {}^{37}Ar$	0.814	$2.55 \pm 0.17 \pm 0.18$	$9.3^{+1.2}_{-1.4}$
KAMIOKANDE	Scattering $\nu + e^- \rightarrow \nu + e^-$	7	$(2.73 \pm 0.17 \pm 0.34)$	$6.62(1.00^{+0.14}_{-0.17})$
GALLEX	Radiochemical $\nu + {}^{71}Ga \rightarrow e^- + {}^{71}Ge$	0.233	$77.1 \pm 8.5^{+4.4}_{-5.4}$	137^{+8}_{-7}
SAGE	Radiochemical $\nu + {}^{71}Ga \rightarrow e^- + {}^{71}Ge$	0.233	$69 \pm 10^{+5}_{-7}$	137^{+8}_{-7}

[a] Energy in Mev.
[b] In SNU for radiochemical experiments; in $10^6\,cm^{-2}\,s^{-1}$ for KAMIOKANDE.

sound way of combining statistical and systematical errors, we use the usual recipe and combine them quadratically (see next section); here and in the following, we take

$$\Phi_{KA} = (2.73 \pm 0.38) \times 10^6\,cm^{-2}\,s^{-1} \,. \tag{22}$$

This value is less than one half that predicted by the RSM.

All other experiments use radiochemical techniques. The ${}^{37}Cl$ experiment of Davis and collaborators [2] has been the first operating solar neutrino detector. The reaction used for neutrino detection is the one proposed by Pontecorvo in 1946 [1]:

$$\nu_e + {}^{37}Cl \rightarrow e^- + {}^{37}Ar \,. \tag{23}$$

The energy threshold being 0.814 MeV, the experiment is sensitive mainly to ${}^8B$ neutrinos, but also to ${}^7Be$ neutrinos. The target, containing 10^5 gallons of perchloroethylene, is located in the Homestake gold mine in South Dakota. Every few months a small sample of ${}^{37}Ar$ (typically some fifteen atoms!) is extracted from the tank and these radioactive atoms are counted in low background proportional counters. The result, averaged over more than 20 years of operation, is [2]

$$S_{Cl} = 2.55 \pm 0.25\,SNU \,. \tag{24}$$

The theoretical expectation is higher by a factor three. For almost 20 years this discrepancy has been known as the "Solar Neutrino Problem". *About 75% of the total theoretical rate is due to ${}^8B$ neutrinos*, see Table 7, and hence it was for a long time believed that the discrepancy was due to the difficulty in predicting this rare source.

Two radiochemical solar neutrino experiments using ${}^{71}Ga$ are operating: GALLEX, located at the Gran Sasso laboratory in Italy and using 30 tons of gallium in an aqueous solution, and SAGE, in the Baksan valley in Russia, which uses 60 tons of gallium metal. The neutrino absorption reaction is

$$\nu_e + {}^{71}Ga \rightarrow e^- + {}^{71}Ge \,. \tag{25}$$

Table 7
Contribution from the main components of neutrino flux to the signals (SNU) in ^{71}Ga and ^{37}Cl detectors according to the RSM, from 15

	^{71}Ga	^{37}Cl
pp	69.7	0.0
pep	3.0	0.22
^{7}Be	37.7	1.24
^{13}N	3.8	0.11
^{15}O	6.3	0.37
^{8}B	16.1	7.36
Total	136.6	9.30

The energy threshold is $E = 0.233$ MeV, and most of the signal arises from pp neutrinos with a significant contribution from ^{7}Be neutrinos as well (see Table 7). In each experiment, the rate of neutrino interactions in the gallium tank is about 0.5 event per day. The germanium atoms are removed chemically from the gallium and the radioactive decays of ^{71}Ge (half-life = 11.4 days) are detected in small proportional counters. The results of the two experiments, see Table 6, can be combined (see next section) to give

$$S_{\text{Ga}} = 74 \pm 8 \text{ SNU}, \tag{26}$$

which we shall use as the representative value of the gallium signal. Again the value is almost a factor two below the theoretical prediction.

An overall efficiency test of the GALLEX detector has been performed by using an intense ^{51}Cr neutrino source, (61.9 ± 1.2) PBq [7].[11] The source, produced via neutron irradiation of about 36 kg of chromium enriched in ^{50}Cr, primarily emits 756 keV neutrinos. It was placed for a period of a few months inside the GALLEX tank, to expose the gallium chloride target to a known neutrino flux. The number of observed neutrino events agrees with expectation to the 10% level. This result "(a) *provides an overall check of GALLEX, indicating that there are no significant experimental artifacts or unknown errors at the* 10% *level that are comparable to the* 40% *deficit of observed solar neutrino signal;* (b) *directly demonstrates for the first time, using a man-made neutrino source the validity of the basic principles of radiochemical methods used to detect rare events...*" [7]. And last but not least: "*because of the close similarity in neutrino energy spectra from* ^{51}Cr *and from the solar* ^{7}Be *branch, this source experiment also shows that the gallium detector is sensitive to* ^{7}Be *neutrinos with full efficiency.*" [7].

1.6. A remark on errors

Because of the subtleties of the experiments, of the difficulty in estimating errors of theoretical evaluations and in face of the persistent discrepancy between experimental results and standard theory (standard solar models and standard neutrinos), the discussion about the meaning of errors is lively at almost every conference on solar neutrinos. In this section we intend to define the errors we

---

[11] The preliminary results on ^{51}Cr neutrino source measurements by SAGE collaboration have been presented recently in [8].

adopt, describe what we want to do with these errors, provide some justification to our choice and outline its limits.

Concerning experimental errors, we add in quadrature statistical and systematical errors. We tentatively use this global error as an indicator of the distance between the true and the measured values of a physical quantity, according to the rules of Gaussian statistics.

Essentially we are assuming that the systematical uncertainty is a variable which can fluctuate according to statistical rules, so that we consider statistical and systematical errors as independent of each other and on the same footing. This choice seems to be crazy (and actually it would be in many cases), however it has some justification in the present context.

As an example, consider measuring the period of a pendulum using a watch. This watch is guaranteed to measure time better than one second per day: one does not know if it is fast or slow, but it does not gain or loose more than $1\,\mathrm{s\,d^{-1}}$. This systematical error cannot be traced to a single origin (otherwise it would be eliminated), but arises from many different sources, essentially the mechanical tolerances on each of the many components of the watch. Each of these sources gives a small contribution, positive as well as negative, to the final error. Also each contribution is statistically independent from the others. Under these conditions one can reasonably suppose that, if one produces a large number of watches of the same kind, the systematical errors are distributed according to a gaussian with null average, i.e. the distribution is the same as for statistical fluctuations.

Clearly, one does not gain any accuracy by repeating the measurements over several oscillations, in exactly the same conditions with the same watch. On the other hand, if one is using N different watches of the same kind (each one with its systematical error $\varepsilon_0 = \pm 1\,\mathrm{s\,d^{-1}}$) and combine the results, accuracy is improved, as the chance of having a fast and a slow watch are equal. In other words, in this example systematical errors can be treated similarly to statistical fluctuations.

The situation, at least in radiochemical experiments, is somehow similar. For instance the 33 runs of GALLEX are actually 33 independent experiments: after each run, the ^{71}Ge atoms are extracted in specific conditions, which are independent of the run number, and placed in a new counter. The radon content of the atmosphere, where extraction occurs, fluctuates around some mean value, within some systematical uncertainty. All counters have approximately the same efficiency, again within some systematical uncertainty, but one is better and another is worse than the estimated mean efficiency. Thus the systematical error of the full experiment is significantly reduced with respect to that pertaining to each individual run and, it can approximately be determined by statistical considerations.

The same procedure used to combine different runs can be used in principle to combine two different experiments like SAGE and GALLEX. The resulting systematical error is

$$1/\varepsilon^2(\mathrm{syst}) = 1/\varepsilon^2_{\mathrm{GALLEX}}(\mathrm{syst}) + 1/\varepsilon^2_{\mathrm{SAGE}}(\mathrm{syst})\,, \tag{27}$$

in analogy to the statistical one

$$1/\varepsilon^2(\mathrm{stat}) = 1/\varepsilon^2_{\mathrm{GALLEX}}(\mathrm{stat}) + 1/\varepsilon^2_{\mathrm{SAGE}}(\mathrm{stat})\,; \tag{28}$$

and the global error on Gallium result becomes

$$\varepsilon^2 = \varepsilon^2(\mathrm{syst}) + \varepsilon^2(\mathrm{stat})\,. \tag{29}$$

This is how Eq. (26) has been obtained.

The situation is more complex when considering errors of theoretical results. When these errors correspond to uncertainties on some measured quantities which are used as input in the theoretical calculations, we are back to the previous case. Often, however, additional uncertainty is added due to extrapolations of experimental data, e.g. when estimating nuclear cross sections at energies of astrophysical interest. In other cases (e.g. opacity tables) the only information comes from theoretical calculations. In these cases one can only resort to a comparison among different calculations. A total theoretical range ε_{TTR} is defined by Bahcall as "*the range in values of published state-of-the-art calculations*" [24,13], and this might be considered as the equivalent of an experimental three sigma error, i.e. the probability of being outside this range is about 0.3%. This looks plausible, how many sigmas being clearly a matter of taste. We generally adhere to Bahcall's choice. For consistency of notations, as we always show experimental 1σ errors, we shall add to the theoretical quantities an error

$$\varepsilon_{\text{theo}} = \tfrac{1}{3}\varepsilon_{TTR} \, . \tag{30}$$

All this clearly means that *treating errors given by equations of the form (29) or (30) as if they were indicators of statistical (Gaussian) fluctuations is just a rough approximation, or even an undue simplification.*

The confidence levels obtained in this way are thus to be taken *cum grano salis*, or much more.

2. Neutrino fluxes almost independently of solar models

All experiments give signals significantly smaller than those predicted by the RSM and by other SSMs, for standard neutrinos. Is this a problem of SSMs or is there anything deeper? Insight on this question can be gained by looking at properties of neutrino fluxes which are largely independent of solar models. In essence, one is asking if experimental data are in agreement with the following assumptions:

(A) the solar luminosity is supported by H burning reactions;
(B) electron neutrinos do not disappear in their travel from sun to earth (i.e. standard neutrinos).

The first assumption looks rather innocent, the second one being really the hypothesis to be tested. We shall follow this approach by discussing: a lower bound on the gallium signal for standard neutrinos (Section 2.2); the relationship between KAMIOKANDE and chlorine signals (Section 2.3); the information on intermediate energy neutrinos derived by using the full set (or any subset) of the data (Section 2.4).

We shall show that the experimental results look mutually inconsistent if the above two assumptions hold true. The point is that the flux of intermediate energy neutrinos ($E_v \approx 0.5$–$2\,\text{MeV}$):

$$\Phi_{\text{int}} = \Phi_{\text{Be}} + \Phi_{\text{CNO}} + \Phi_{\text{pep}} \tag{31}$$

would have to be negative!

We shall see that the same occurs if we disregard any of the experiments. Actually *we do not know of any sound argument to doubt the experimental results, but we shall entertain this possibility, just as a working hypothesis,* to test the consistency of the assertion: neutrinos are standard and (some) experiments are correct. We would like to make this point as clear as possible: when saying

"disregard one experiment" or "assume it is wrong" we are advocating some hypothetical, large, unknown systematic error, just for the sake of saving/testing the hypothesis of standard neutrinos. This is clearly a desperate hypothesis, at least for ^{51}Cr-calibrated gallium detectors.

The inconsistencies will be derived by treating the different components of the neutrino flux as essentially free parameters. Additional information can be gained from the physical relationships among the neutrino components, as imposed by the development of the fusion chains. For example, pep neutrinos accompany pp neutrinos, with a proportion which has to be essentially the same in any solar model. Also, if the CN cycle is efficient, there will be about as many ^{13}N as ^{15}O neutrinos. By using these additional, however weak, assumptions one gets more severe hints against the hypothesis of standard neutrinos and/or tighter constraints on ^{7}Be and CNO neutrino fluxes (see Sections 2.5 and 2.6). Quantitative statements about the chances of standard neutrinos and upper bounds on intermediate energy neutrino fluxes are presented in Section 2.7. These bounds appear in conflict with the results of SSM, particularly for ^{7}Be neutrino flux (Section 2.8).

Furthermore, since ^{7}Be and ^{8}B neutrinos both originate from ^{7}Be nuclei, there is a relationship between them which looks again in contradiction with the experimental data, for standard neutrinos (Section 2.9).

All these (essentially) solar model independent arguments point towards some non-standard neutrino properties, the main ingredient being the luminosity constraint A). In Section 2.10 we relax even this hypothesis, still finding indications towards non-standard neutrinos. On the same grounds, we discuss in Section 2.11 the case of universal neutrino oscillations in the framework of a solar model independent approach.

Before presenting the discussion let us give an advance warning. We regard this section as the most relevant one of the present review and we therefore tried to be as detailed as possible. For a first reading we recommend Sections 2.1 and 2.2, where the basic ideas are explained, and Sections 2.5 and 2.6, which contain the main results, and the concluding remarks at the end of this section.

2.1. The solar luminosity constraint

The solar luminosity constraint, essentially given in Eq. (2), will be a major ingredient of this section, so that it is important to express it more precisely and to discuss its accuracy.

Assuming that all solar energy originates from nuclear reactions, and that all these reach completion, i.e.:

$$4p + 2e^- \rightarrow {}^4He + 2\nu_e , \tag{32}$$

one immediately gets the following constraint for the neutrino fluxex Φ_i:

$$K_\odot = \sum_i \left(\frac{Q}{2} - \langle E_\nu \rangle_i \right) \Phi_i , \tag{33}$$

where $Q = 26.73$ MeV and $\langle E_\nu \rangle_i$ is the average energy carried by ith neutrino. The coefficients

$$Q_i = \frac{Q}{2} - \langle E_\nu \rangle_i \tag{34}$$

represent the average electromagnetic energy released per emitted neutrino, and can be calculated from Table 5. Except for the rare ^{8}B neutrinos, $\langle E_v \rangle_i$ is of the order of half MeV, so that Eq. (2) – corresponding to Eq. (33) when $\langle E_v \rangle_i$ is neglected – is accurate to the 5% level.

Concerning the accuracy of Eq. (33), the following comments are in order, see [58]: [12]

(i) gravitational energy generation is neglected. According to standard solar model calculations, this causes an error of about 3×10^{-4} [13], negligible in comparison with the uncertainty on $K_\odot$.

(ii) The abundance of ^{3}He nuclei is assumed to be in equilibrium, which is not strictly correct. In the outer region of the solar core ^{3}He is continually produced, but the temperature is too low to burn ^{3}He at the equilibrium rate. Thus the pp chain is not always completed. Similar considerations hold for the CN cycle. All this gives, according again to standard solar model calculations, corrections to Eq. (33) of the order of 4×10^{-4} [58].

All in all, Eq. (33) should be accurate to better than 1%.

Finally, we remark that one assumes the sun to be at thermal equilibrium when using Eq. (33) to relate the *present* solar constant to the *present* nuclear energy production rate and *present* neutrino fluxes. The assumption of thermal equilibrium (stationary sun) looks quite reasonable to us. For the reader who is willing to abandon it, we have anyhow prepared Section 2.10.

2.2. The minimal gallium signal for standard neutrinos

For standard neutrinos, one can find a lower bound to the gallium signal by the following considerations [59]:

(i) Since the pp neutrinos are the least energetic ones, they have the smallest cross section in gallium detectors, i.e. $\sigma_{Ga,i} \geq \sigma_{Ga,pp}$. Thus from Eq. (19) one derives

$$S_{Ga} \geq \sigma_{Ga,pp} \sum_i \Phi_i = \sigma_{Ga,pp} \Phi_{tot} , \tag{35}$$

i.e. the minimum signal is obtained by assuming that all neutrinos are from the pp reaction.

(ii) The solar luminosity, namely, the electromagnetic energy released per unit time, is obtained with a minimum number of fusions when neutrinos carry away the least energy. The minimum total flux Φ_{min} is thus obtained when all neutrinos are from pp, and it is thus related to the solar constant $K_\odot$:

$$\Phi_{tot} \geq \Phi_{min} = \frac{K_\odot}{Q_{pp}} , \tag{36}$$

where the term in the denominator is the average electromagnetic energy released per emitted pp neutrino. This gives thus:

$$S_{Ga}^{min} = \sigma_{Ga,pp} \frac{K_\odot}{Q_{pp}} . \tag{37}$$

In other words, the minimum gallium signal is obtained when all neutrinos are from the pp-reaction. *Any solar model will give a prediction not smaller than S_{Ga}^{min}, provided only that the present electromagnetic energy production rate in the sun equals the* presently *observed solar luminosity.*

---

[12] In the same paper one derives direct upper bounds on neutrino fluxes by using Eq. (33).

By using the values previously given [15], $K_\odot = (0.853 \pm 0.003) \times 10^{12}\,\mathrm{MeV\,cm^{-2}\,s^{-1}}$ and $\sigma_{\mathrm{Ga,pp}} = (1.18 \pm 0.02) \times 10^{-9}\,\mathrm{SNU\,cm^2\,s}$, one derives:

$$S_{\mathrm{Ga}}^{\mathrm{min}} = 77 \pm 2\,\mathrm{SNU}\,, \tag{38}$$

where the error essentially comes from the uncertainty on $\sigma_{\mathrm{Ga,pp}}$. The central value of this prediction is already 3 SNU above that of the experimental result (74 ± 8 SNU), however the distance between the two values is well within the errors. Gallium results do not violate the lower limit for solar neutrinos.

However, this is far from being a satisfactory result. If pp burning is at work, it appears difficult to switch off the pep reaction. The pep neutrinos being more energetic, the minimal signal clearly increases. In Ref. [59] the value $S_{\mathrm{Ga}}^{\mathrm{min}} = 79\,\mathrm{SNU}$ is obtained under the physically plausible assumption that together with pp neutrinos also pep neutrinos are created, with the ratio $\xi = \Phi_{\mathrm{pep}}/(\Phi_{\mathrm{pp}} + \Phi_{\mathrm{pep}}) \approx 2.5 \times 10^{-3}$ as given by the solar model of the same Ref. [59]. We did not consider pep contribution as we wanted to use minimal assumptions; should we follow the approach of Ref. [59], with the cross sections given in Table 5 and $\xi = 2.36 \times 10^{-3}$ we would find, in place of Eq. (38), $S_{\mathrm{Ga}}^{\mathrm{min}} = 80 \pm 2$ SNU,[13] which is still consistent with the experimental result at 1σ level.

However the situation gets somehow puzzling if one takes into account the other measurements. For example, KAMIOKANDE does observe the energetic ^{8}B neutrinos, implying a ^{8}B contribution to the gallium signal of about 7 ± 2 SNU, for standard neutrinos. All this means that for standard neutrinos the signal in gallium experiments has to exceed 87 ± 3 SNU. The difference between this minimal expectation and the measured gallium signal gets now larger than the error.

By considering the above information, one finds that the contribution of ^{7}Be and CNO neutrinos is

$$S_{\mathrm{Be+CNO}} = (-13 \pm 8.5)\,\mathrm{SNU}\,. \tag{39}$$

Therefore, it should not exceed 13 SNU, if the observed signal has to agree with the minimal estimate to the three sigma level. This is significantly smaller than the predictions of all SSMs (about 50 SNU, including 38 SNU arising from ^{7}Be neutrinos, see Table 7).

In conclusion, gallium results are still consistent with standard neutrinos, essentially implying that the vast majority of them are from the pp reaction and that intermediate energy neutrinos are definitely fewer than in the SSMs.

The recently proposed gallium neutrino observatory GNO [60] which foresees a 100 ton target and improved detection techniques, aims at a measurement of the gallium signal with an accuracy of 5%. This would provide a significant progress in the "minimal gallium signal" test.

2.3. Chlorine and KAMIOKANDE

As soon as the KAMIOKANDE data were available, assuming standard neutrinos, it became clear that they presented a new puzzle, when compared with the chlorine results. Let us divide the chlorine signal in two parts, corresponding to intermediate energy neutrinos and to ^{8}B neutrinos, respectively,

$$S_{\mathrm{Cl}} = S_{\mathrm{Cl},int} + S_{\mathrm{Cl,B}}\,. \tag{40}$$

---

[13] The small difference with respect to the result of Ref. [59] originates from the slightly different, more recent values for $\sigma_{\mathrm{Ga,pp}}$, $\sigma_{\mathrm{Ga,pep}}$ and ξ which we are using.

KAMIOKANDE only detects high energy events ($E_v \geq 7\,\mathrm{MeV}$); assuming standard neutrinos this is enough to tell the energy integrated flux of $^8\mathrm{B}$ neutrinos, and thus their expected contribution to the chlorine signal, $S_{\mathrm{Cl,B}}$, can be calculated, by using the estimated value of $\sigma_{\mathrm{Cl,B}}$ (see Table 5):

$$S_{\mathrm{Cl,B}} = \sigma_{\mathrm{Cl,B}} \Phi_{\mathrm{B}}^{\mathrm{Kam}} = 2.98 \pm 0.41\,\mathrm{SNU}\,, \tag{41}$$

where most of the error comes from uncertainties on the KAMIOKANDE signal. By comparison with the measured chlorine signal $S_{\mathrm{Cl}} = 2.55 \pm 0.25\,\mathrm{SNU}$, one sees that the $^8\mathrm{B}$ neutrinos, as measured by KAMIOKANDE, should produce a signal in chlorine larger than observed. So little space is left for the intermediate energy neutrinos:

$$S_{\mathrm{Cl},int} = -0.48 \pm 0.49\,\mathrm{SNU}\,. \tag{42}$$

Note that the central value is negative, however Eq. (42) is clearly consistent with zero. At "three sigma" level one has $S_{\mathrm{Cl},int} < 1\,\mathrm{SNU}$, this limit being a factor two smaller than the RSM prediction, see Table 7.

Let us remark that the above estimate on $S_{\mathrm{Cl},int}$ is independent of the stationary sun hypothesis A).

The present uncertainty on $S_{\mathrm{Cl},int}$ depends essentially on the systematical error of the KAMIOKANDE result. A better determination of $S_{\mathrm{Cl},int}$ would require a strong reduction of the systematical error in SUPERKAMIOKANDE with respect to KAMIOKANDE. In this case the ultimate uncertainty would be that due to the chlorine experiment, implying $\Delta S_{\mathrm{Cl},int} \approx 0.25\,\mathrm{SNU}$, which would provide significant information on intermediate energy neutrinos.

2.4. The space for intermediate energy neutrinos

An extension of the minimal gallium signal argument of Section 2.2 can elucidate the role of various experiments in providing solar model independent information on neutrino fluxes. We already known that experimental results are smaller than the expectation from SSM and consequently the fluxes of intermediate and high energy neutrinos should be smaller than theoretically predicted. The relevant question is: how large neutrino fluxes are allowed?

We have three equations relating the solar constant, the gallium and chlorine signals with the fluxes Φ_i:

$$K_\odot = \sum_i Q_i \Phi_i\,, \tag{43}$$

$$S_{\mathrm{Ga}} = \sum_i \sigma_{\mathrm{Ga},i} \Phi_i\,, \tag{44}$$

$$S_{\mathrm{Cl}} = \sum_i \sigma_{\mathrm{Cl},i} \Phi_i\,, \tag{45}$$

and the $^8\mathrm{B}$ neutrino flux as measured by KAMIOKANDE

$$\Phi_{\mathrm{B}}^{\mathrm{Kam}} = (2.73 \pm 0.38) \times 10^6\,\mathrm{cm}^{-2}\,\mathrm{s}^{-1}. \tag{46}$$

In order to determine the maximal allowed fluxes of intermediate energy neutrinos let us assume that *only one* flux Φ_k ($k = \mathrm{Be, N, O}$ or pep) is non-vanishing and attribute to Φ_k all the signal in the chlorine and GALLEX experiments pertaining to the intermediate energy neutrinos.

For the chlorine experiment, one has just to subtract from the experimental value the ^{8}B contribution, i.e. the maximal flux Φ_k satisfies

$$S_{Cl} = \sigma_{Cl,k}\Phi_k + \sigma_{Cl,B}\Phi_B \,. \tag{47}$$

For handling the information provided by gallium experiments, we derive Φ_{pp} from the luminosity equation. In terms of the average electromagnetic energy Q_i released per emitted neutrino, see Eq. (34), one has from Eq. (43):

$$\Phi_{pp} = \frac{K_\odot}{Q_{pp}} - \frac{Q_B}{Q_{pp}}\Phi_B - \sum_{int} \Phi_i \frac{Q_i}{Q_{pp}} \tag{48}$$

so that

$$S_{Ga} = \frac{K_\odot}{Q_{pp}}\sigma_{Ga,pp} + \left(\sigma_{Ga,B} - \frac{Q_B}{Q_{pp}}\sigma_{Ga,pp}\right)\Phi_B + \sum_{int} \left(\sigma_{Ga,i} - \frac{Q_i}{Q_{pp}}\sigma_{Ga,pp}\right)\Phi_i \,. \tag{49}$$

All terms in the brackets are of course positive as the minimum signal is obtained when all neutrinos are from pp.

Again isolating the kth component, one obtains the maximal allowed flux from:

$$S_{Ga} = \sigma_{Ga,pp}\frac{K_\odot}{Q_{pp}} + \left(\sigma_{Ga,B} - \frac{Q_B}{Q_{pp}}\sigma_{Ga,pp}\right)\Phi_B + \left(\sigma_{Ga,k} - \frac{Q_k}{Q_{pp}}\sigma_{Ga,pp}\right)\Phi_k \,. \tag{50}$$

The reader recognizes, for the limiting case $\Phi_k = \Phi_B = 0$, the inequality found in the previous section.

Clearly this exercise is most interesting for ^{7}Be neutrinos, as they are predicted to be the second most abundant ones. By using the cross sections in Table 5 and taking $k = Be$, from Eqs. (47) and (50) one gets:

$$S_{Cl} = 0.24\Phi_{Be} + 1.11\Phi_B \tag{51}$$

and

$$S_{Ga} = 77 + 6.19\Phi_{Be} + 2.43\Phi_B \,, \tag{52}$$

where the signals are in SNU, Φ_{Be} in $10^9 \, cm^{-2} \, s^{-1}$ and Φ_B in $10^6 \, cm^{-2} \, s^{-1}$.[14]

In this way the experimental information can be presented in the (Φ_B, Φ_{Be}) plane, see Fig. 6. Dashed lines are obtained by adopting in Eqs. (51) and (52) the central values of experimental results. Full lines correspond to the experimental results $\pm 1\sigma$. Even by allowing for such a spread, still the curves intersect in the unphysical region ($\Phi_{Be} \leq 0$).

In Fig. 6 we also introduce the information from KAMIOKANDE experiment, Eq. (46), and the following conclusions can be drawn:

  (i) the 1σ allowed areas intersect in the unphysical ($\Phi_{Be} < 0$) region. The same holds if one disregards either the chlorine or the KAMIOKANDE experiment. Should one disregard gallium result, still at 1σ one has a very small value $\Phi_{Be} \leq 1.0 \times 10^9 \, cm^{-2} \, s^{-1}$.

  (ii) in order to stay within 2σ from each experimental result the beryllium flux has to be $\Phi_{Be} < 1.5 \times 10^9 \, cm^{-2} \, s^{-1}$, i.e. a factor three at least smaller than the predictions from SSMs.

---

[14] We note that errors on the cross sections are negligible with respect to the uncertainties in the experimental signals.
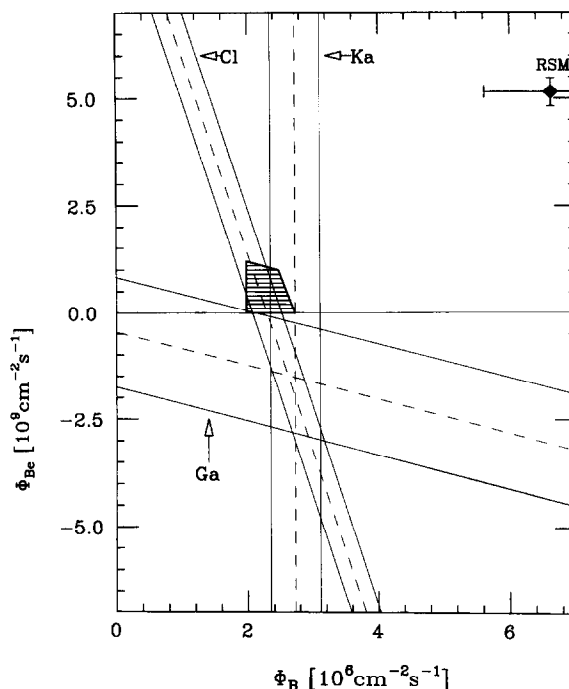
Fig. 6. The ^{8}B and ^{7}Be neutrino fluxes, consistent with the luminosity constraint and experimental results, for standard neutrinos. The dashed (solid) lines correspond to central ($\pm 1\sigma$) experimental values for chlorine (Cl), gallium (Ga) and KAMIOKANDE (Ka), see Eqs. (24), (26) and (22). The hatched area corresponds to the region within 2σ from each experimental result. The diamond represents the prediction of the reference solar model, RSM [15], and the bars its estimated uncertainties.

Similar considerations hold for the other intermediate energy neutrinos, see Table 8. In any case, the best fit point is in the unphysical region and no point can be found in the physical region which is within 1σ from each experiment.

Roughly speaking, the hypothesis of standard neutrinos (which requires positive fluxes) disagrees with each of the three independent experimental results by at least 1σ. The probability for such a situation is at most $(0.32)^3$, i.e. a few percent. Little space seems to be left for intermediate energy neutrinos.

2.5. Four equations and four unknowns

So far the only assumption about the sun was Eq. (43), that connecting neutrino fluxes to the solar constant. Stricter constraints on the intermediate energy neutrinos can be obtained by using some additional, albeit very weak, hypothesis. Theoretically, we know that pep neutrinos must accompany pp neutrinos and also that the CN cycle is (almost) at equilibrium when it is efficient in the sun. The precise values of $\zeta = \Phi_{pep}/(\Phi_{pp} + \Phi_{pep})$ and $\eta = \Phi_N/(\Phi_N + \Phi_O)$ are not important for the following discussion and we shall use $\zeta = 2.36 \times 10^{-3}$ and $\eta = 0.53$, according to the RSM [15].

In this way we reduce our unknowns to just four variables:

$$\Phi_p = \Phi_{pp} + \Phi_{pep}, \qquad \Phi_{CNO} = \Phi_N + \Phi_O, \qquad \Phi_{Be} \quad \text{and} \quad \Phi_B, \tag{53}$$

i.e. as many as the available pieces of information. With the numerical values in Table 5, from Eq. (43) (after dividing both sides by $Q/2$) and Eqs. (44) and (45) one gets

$$63.85 = 0.980\Phi_p + 0.939\Phi_{Be} + 0.937\Phi_{CNO} + 0.498 \times 10^{-3}\Phi_B, \tag{54a}$$

$$S_{Ga} = 1.23\Phi_p + 7.32\Phi_{Be} + 8.72\Phi_{CNO} + 2.43\Phi_B, \tag{54b}$$

$$S_{Cl} = 0.38 \times 10^{-2}\Phi_p + 0.24\Phi_{Be} + 0.41\Phi_{CNO} + 1.11\Phi_B, \tag{54c}$$

$$\Phi_B^{Kam} = \Phi_B, \tag{54d}$$

where all fluxes are in units of $10^9\,\mathrm{cm}^{-2}\,\mathrm{s}^{-1}$ but for the ^8B flux which is in units of $10^6\,\mathrm{cm}^{-2}\,\mathrm{s}^{-1}$ and signals of radiochemical experiments are in SNU. Uncertainties on the numerical coefficients (arising from errors on the estimated neutrino cross sections) have been omitted, since errors on the experimental signals are dominant.

We thus determine the four fluxes:

$$\Phi_p = 1.90S_{Cl} - 0.229S_{Ga} - 1.56\Phi_B^{Kam} + 83.1,$$

$$\Phi_{Be} = -10.6S_{Cl} + 0.57S_{Ga} + 10.4\Phi_B^{Kam} - 43.1,$$

$$\Phi_{CNO} = 8.6S_{Cl} - 0.33S_{Ga} - 8.8\Phi_B^{Kam} + 24.4, \qquad \Phi_B = \Phi_B^{Kam}. \tag{55}$$

inserting the signals given in Table 6, one finds: [15]

$$\Phi_p = (66.7 \pm 2.0) \times 10^9\,\mathrm{cm}^{-2}\,\mathrm{s}^{-1},$$

$$\Phi_{Be} = (0.4 \pm 6.6) \times 10^9\,\mathrm{cm}^{-2}\,\mathrm{s}^{-1},$$

$$\Phi_{CNO} = (-2.0 \pm 4.8) \times 10^9\,\mathrm{cm}^{-2}\,\mathrm{s}^{-1}. \tag{56}$$

It is remarkable that, for *standard neutrinos* and with minimal and quite reasonable assumptions about solar models (i.e. the values of ζ and η), the main components of the solar neutrino flux are fully determined from available experiments. *In other words, a solar neutrino spectroscopy is already at hand and it could be used to study the solar interior, if we know enough about neutrinos.*

We see, for example, from Eq. (56) that the pp+pep flux is determined for standard neutrinos with an accuracy of about 3%. This result might be surprising when considering that all experiments have no more than 10% accuracy. The point is that the total flux is fixed by the luminosity, whereas the cross section depends crucially on neutrino energy, so that approximately ($\sigma_{Ga,Be} \gg \sigma_{Ga,pp}$):

$$\left(\frac{\Delta\Phi_p}{\Phi_p}\right) \approx \left(\frac{\Delta S_{Ga}}{S_{Ga}}\right)\frac{\sigma_{Ga,pp}}{\sigma_{Ga,Be}}. \tag{57}$$

---

[15] When errors on the neutrino cross section are taken into account, the errors quoted in Eq. (56) are slightly enlarged, becoming ± 2.2, ± 7.2 and ± 5.1, respectively.

The result on Φ_{CNO} clearly shows – again for standard neutrinos – that the CN cycle cannot be the main energy source in the sun, otherwise one should have

$$\Phi_{CNO} \approx \frac{2K_\odot}{Q} \approx 60 \times 10^9 \, \mathrm{cm^{-2}\,s^{-1}} \,, \tag{58}$$

in violent contradiction with Eq. (56). If the CN cycle were to dominate solar energy production, then the gallium signal would be

$$S_{Ga} \approx \frac{2K_\odot}{Q} \sigma_{Ga,CNO} \approx 550 \, \mathrm{SNU} \,, \tag{59}$$

an order of magnitude larger than the actual result.

2.6. Where are Be and CNO neutrinos?

One notes that the central value of Φ_{CNO} in Eq. (56) is negative i.e. unphysical. In view of the estimated errors, this does not seem to be a problem. However, there is a strong correlation between Φ_{CNO} and Φ_{Be}, so that *if Φ_{CNO} is forced to be positive, then Φ_{Be} becomes negative, and* vice versa.

In order to understand what is going on, and to clarify the role of each experimental result, let us once more reduce the number of unknowns. We start again from the basic equations (43)–(46) and use the following tricks, similar to those used previously:

(a) we group the neutrino fluxes as in Eq. (53), so that we are left with the four variables $\Phi_p, \Phi_{Be}, \Phi_{CNO}$ and Φ_B.

(b) Since $\langle E_v \rangle_{CNO} \geq \langle E_v \rangle_{Be}$, the corresponding cross section is larger than that of ^7Be neutrinos. Thus the minimal CNO signal is obtained with the replacements

$$\langle E_v \rangle_{CNO} \rightarrow \langle E_v \rangle_{Be} \quad \mathrm{and} \quad \sigma_{CNO} \rightarrow \sigma_{Be} \,. \tag{60}$$

This corresponds to dropping terms containing Φ_{CNO} in Eqs. (54a)–(54d) and replacing Φ_{Be} with $\Phi_{Be} + \Phi_{CNO}$, so that only the combination $\Phi_{Be} + \Phi_{CNO}$ enters. We remark that such a substitution represents also a safe approach, since the theoretical value of $\sigma_{Ga,Be}$ has essentially been verified (to the 10% level) by the GALLEX neutrino source experiment [7], whereas only theoretical predictions exist for $\sigma_{Ga,CNO}$.

One can eliminate Φ_p by using the luminosity equation (54a), and each experiment provides a constraint on Φ_{Be+CNO} and/or Φ_B:

$$S_{Ga} = 80.1 + 6.14\Phi_{Be+CNO} + 2.43\Phi_B \,,$$

$$S_{Cl} = 0.248 + 0.236\Phi_{Be+CNO} + 1.11\Phi_B \,, \qquad \Phi_B^{Kam} = \Phi_B \,. \tag{61}$$

The result of each experiment can be plotted in the (Φ_B, Φ_{Be+CNO}) plane, as shown in Fig. 7.

With respect to the situation of Section 2.4, the intersection moves towards even more negative values of Φ_{Be+CNO}, see Table 8, and the allowed region in the physical part of the plane shrinks. Whichever experiment is discarded there is no point in the physical region within 1σ from the remaining two results. The region at 2σ from each experiment now allows only $\Phi_{Be+CNO} < 1$. This bound is stronger than we found previously, *the main reason being that the small, but*
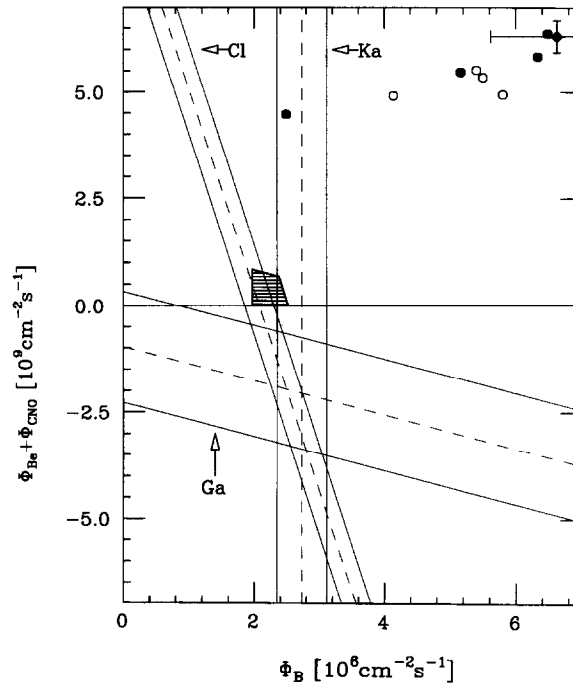
Fig. 7. Same as in Fig. 6, for the ^{8}B and ^{7}Be + CNO neutrino fluxes. The luminosity constraint is supplemented with the estimates for $\Phi_{pep}/(\Phi_{pep} + \Phi_{pp})$ and $\Phi_N/(\Phi_N + \Phi_O)$, from the RSM [15]. The prediction of the RSM model [15] (full diamond) is shown, together with those of other solar models including diffusion of helium and heavy elements (full circles), corresponding from right to left to [16,22,56,23]. Solar model calculations without diffusion are represented by open circles, corresponding to [19,18,20,17], again from right to left.

Table 8
Experimental information on the fluxes of intermediate energy neutrinos (in units of 10^9 cm^{-2} s^{-1}). In (a) only the luminosity constraint is assumed. In (b) we assume also ξ and η as given by the RSM [15], see Section 2.4. The best fit points and upper limits, within 2σ from each experimental results, are presented

	(a)				(b)	
	^{13}N	^{7}Be	^{15}O	pep	^{7}Be+CNO	CNO
Best fit	−2.2	−1.6	−0.8	−0.2	−2.2	−1.7
Upper limit (2σ)	1.8	1.5	0.8	0.5	0.9	0.7

non-negligible, contribution of pep neutrinos to chlorine and gallium signals is included from the beginning.

The bound on the sum clearly holds separately for ^{7}Be and CNO neutrinos. For these latter, however, we can get tighter constraints by putting $\Phi_{Be} = 0$ in Eqs. (54a)–(54d), see again Table 8. In this way one finds that in the area within two standard deviations from each experiment $\Phi_{CNO} \leq 0.7$.

2.7. Probabilities, confidence levels and all that

The intermediate energy neutrino fluxes, which we derive from the experimental signals assuming standard neutrinos, favor negative, i.e. unphysical values. Here we shall discuss the statistical significance of this information. We try to estimate quantitatively the probability of compatibility with standard neutrinos and to determine the significance of upper bounds on neutrino fluxes.

For pedagogical reasons, let us discuss first a kindred situation where only one variable is present, namely the determination of the neutrino mass from β decay experiments.

2.7.1. Neutrino mass and β decay

Measurements of the electron energy spectrum from tritium decay determine a parameter m_{app}^2 (apparent squared mass), which a priori is just a combination of experimental data and theoretical inputs. In principle, m_{app}^2 can be positive as well as negative. This parameter can be identified with the actual ν_e squared mass m^2 only if the interpretation of the experimental data (underlying theory, estimated energy resolution,...) is correct, and in that case it should be positive. Even so $(m_{app}^2 \geq 0)$ experimental results $\hat{m}_{app}^2$ might come out negative due to statistical fluctuations of the physical quantities entering the definition of m_{app}^2.

The latest edition of the Particle Data Book [61] considers four tritium β decay experiments, all giving $\hat{m}_{app}^2 < 0$, and presents the weighted average:

$$\hat{m}_{app}^2 = (-54 \pm 30)\,\text{eV}^2\,. \tag{62}$$

This result prompts the following questions:
- (a) Is the interpretation of the data ("working hypothesis") correct?
- (b) Which upper bounds can be set on the actual neutrino mass?

In the discussion we follow – to some extent – the approach of Ref. [61]. We assume that the experimental results have a Gaussian distribution, centered at an unknown value m_{app}^2, the width being given by the quoted experimental uncertainty $\Delta = 30\,\text{eV}^2$.
- (a) If the theory is correct $(m_{app}^2 = m^2)$ then of course $m_{app}^2 \geq 0$. Evidently, the probability of obtaining a value equal or smaller than $\hat{m}_{app}^2 = -54\,\text{eV}^2$ is maximal when the neutrino mass is zero $(m_{app}^2 = m^2 = 0)$ and in that case it is

$$P_1 = \frac{\int_{-\infty}^{\hat{m}_{app}^2/\Delta} dx\, e^{-x^2/2}}{\int_{-\infty}^{\infty} dx\, e^{-x^2/2}} = 0.036\,. \tag{63}$$

For $m_{app}^2 > 0$ the probability is even smaller. Furthermore the requirement $m_{app}^2 \geq 0$ is just a necessary condition for identifying it with the physical neutrino's squared mass. Thus our answer to question (a): *there is at most a 3.6% probability that the working hypothesis is correct.*

It is somewhat controversial how to set bounds on an observable when the experimental results lie outside the physical region, and more than one answer to our question (b) is possible:
- (b1) The first approach we consider is similar in spirit to that just presented. We can determine an upper bound P_2 on the probability that the result is equal to or smaller than $\hat{m}_{app}^2$ if the apparent

squared mass exceeds a value m_0^2:

$$P_2 = \frac{\int_{-\infty}^{(\hat{m}_{\text{app}}^2 - m_0^2)/\Delta} \mathrm{d}x \, e^{-x^2/2}}{\int_{-\infty}^{\infty} \mathrm{d}x \, e^{-x^2/2}} \, . \tag{64}$$

Conversely, by fixing a confidence level C.L.$= 1 - P_2$, we can determine the corresponding value of m_0^2 such that the above equation holds. For instance, if we choose $P_2 = 1\%$, we find that *at the 99% C.L. the apparent neutrino's squared mass is less than 15.8 eV^2.*
The interpretation of this limit is the following: to answer question (a) we used the fact that only positive values are physical. Now, if we have some additional information telling us that $m^2 > 15.8 \, \text{eV}^2$, then there is at most a 1% chance that the working hypothesis is correct.
Note that the identification $m_{\text{app}}^2 = m^2$ is not necessary a priori and actually it is one of the hypothesis being tested. Also, to reach our conclusion we needed only the probability distribution function (p.d.f.), $f(\hat{\alpha}|\alpha)$, giving the probability of observing an experimental result $\hat{\alpha}$ if the true value is α.
We remark that f is different from the distribution defining the probability that, given an experimental result $\hat{\alpha}$, the true value is α. This latter p.d.f., which we denote by $g(\alpha|\hat{\alpha})$, is the one we are going to use in a second approach to question (b), the so-called Bayesian approach to confidence limits, described extensively in Ref. [61] and references therein.
- (b2) Here one assumes that the working hypothesis is correct and one seeks information on the mass m from the knowledge of experimental result $\hat{m}^2$. To be precise, we list the assumptions:
  (i) the measured quantity can be identified with the physical neutrino mass, $m_{\text{app}}^2 = m^2$.
  (ii) Bayes' theorem holds:

$$g(m^2|\hat{m}^2) = \frac{f(\hat{m}^2|m^2) \, \pi(m^2)}{\int f(\hat{m}^2|m^2) \, \pi(m^2) \, \mathrm{d}m^2} \, , \tag{65}$$

where $\pi(m^2)$ is the a priori p.d.f of the neutrino squared mass, which we define as

$$\pi(m^2) = \begin{cases} 1 & \text{if } m^2 > 0 \, , \\ 0 & \text{otherwise} \, . \end{cases} \tag{66}$$

As we have chosen f to be Gaussian, $g(m^2|\hat{m}^2)$ is also Gaussian, but its m^2 domain is restricted to the positive axis. For a confidence level $1 - P_3$, the upper limit m_0^2 to the neutrino squared mass is now given by

$$P_3 = \frac{\int_{-\infty}^{(\hat{m}^2 - m_0^2)/\Delta} \mathrm{d}x \, e^{-x^2/2}}{\int_{0}^{\infty} \mathrm{d}x \, e^{-x^2/2}} \, . \tag{67}$$

For instance, if we choose $P_3 = 1\%$, this time we find $m_0^2 = 47.4 \, \text{eV}^2$ and we can say that *at the 99% confidence level the neutrino's squared mass is less than 47.4 eV^2.*
In the present context, for the same m_0^2 one has

$$P_2 = P_1 \cdot P_3 \, . \tag{68}$$

Thus P_2 is always smaller than P_3, and correspondingly the bound on the mass found with the second approach is always weaker than the first one.

We may say in conclusion that the two approaches answer two different questions:

- (b1) assuming that the physical mass squared is larger than some value m_0^2, what is the chance that the interpretation of experiments is correct and that the result does not exceed $-54\,\mathrm{eV}^2$?
- (b2) Assuming that the interpretation is correct, what is the probability that the physical mass squared is larger than m_0^2 and that experimental result does not exceed $-54\,\mathrm{eV}^2$?

Correspondingly, at a given confidence level, one associates two different bounds on the squared neutrino mass, which correspond to two different physical assumptions and attitudes: the first case (b1) is essentially a way of testing the interpretation of the experiment, if one is confident in a minimal value for neutrino mass; the second one (b2), is a way of testing a theoretical prediction on neutrino mass, if one believes in the interpretation of the experiment.

2.7.2. Statistics and the solar neutrino problem

The analogy with the previous case should be clear now. In the language of the previous section, the right-hand sides of Eqs. (55) define four apparent neutrino fluxes $\Phi_{\mathrm{p}}^{\mathrm{app}}$, $\Phi_{\mathrm{Be}}^{\mathrm{app}}$, $\Phi_{\mathrm{B}}^{\mathrm{app}}$, and $\Phi_{\mathrm{CNO}}^{\mathrm{app}}$, which can be identified with the physical fluxes *assuming* standard neutrinos.

Different attitudes are possible and correspondingly different questions can be raised. If one wants to test the chance of standard neutrinos with minimal assumptions about solar physics, then the relevant question is:

- (a) what is the probability that all the apparent fluxes are nonnegative?

If one is confident in some solar models, yielding definite predictions/lower bounds on the fluxes, $\Phi_{\mathrm{L},i}$, then again as a test of standard neutrinos the question is:

- (b1) what is the probability that neutrinos are standard if the true fluxes are at least $\Phi_{\mathrm{L},i}$, in face of the available results?

On the other hand, one who believes in standard neutrinos and wants to test solar models will be interested in upper bounds $\Phi_{\mathrm{U},i}$ on the fluxes. His question is now:

- (b2) assuming standard neutrinos, what is the probability that the true fluxes do not exceed $\Phi_{\mathrm{U},i}$, in view of the experimental results?

As compared to the β decay, the only complication is that we deal now with several variables (fluxes) instead of just one (the neutrino squared mass).

For this reason we resorted to Monte Carlo techniques. We generated a large ensemble of sets of four simulated signals (gallium, chlorine, KAMIOKANDE and the solar luminosity); each simulated signal was extracted by a Gaussian distribution with mean and width equal to its actual experimental central value and error. When appropriate we only considered the subsets of three simulated signals where one of the neutrino experiments (gallium, chlorine and KAMIOKANDE) was in turn excluded. Given any set of four (or three) simulated signals out of the ensemble, we derived three apparent fluxes: Φ_{p}, Φ_{B} and either Φ_{Be} or Φ_{CNO} assuming the other one (Φ_{CNO} or Φ_{Be}) equal to zero. We have chosen not to derive from the simulated signals both Φ_{Be} and Φ_{CNO}, since the possibility of separating the two signals is critically dependent on the difference between the ratio of the average cross sections for Be and CNO neutrinos in the chlorine experiment and the same ratio in the gallium experiments. Moreover, the limit obtained by assuming either Φ_{Be} or Φ_{CNO} to be zero is more conservative. Note that when we assume $\Phi_{\mathrm{CNO}} = 0$, the upper limit on Φ_{Be} is in fact an upper limit for Φ_{Be} and for $\Phi_{\mathrm{Be+CNO}}$ being the cross section for CNO neutrinos larger than the one for Be neutrinos. In practice the system of equations giving the signals as functions of the fluxes was inverted with the techniques of singular value decomposition that automatically take care both

Table 9

Information on neutrino fluxes. Φ_{Be} and Φ_{CNO} (Φ_B) in units of $10^9\,\mathrm{cm^{-2}\,s^{-1}}$ ($10^6\,\mathrm{cm^{-2}\,s^{-1}}$). All bounds are at the 99.5% C.L. Direct information (exp.) is only available for ^8B neutrinos, from Ref. [3], the indicated error here corresponds to 3σ. The bounds in (b1) correspond to no prior knowledge on the unknown variables. In (b2) we assume a priori $\Phi_i \geq 0$. The results of SSMs are also shown (same notation as in Table 1)

	(Exp.) Ref. [3]	(b1)	(b2)	P94 Ref. [16]	RVCD96 Ref. [22]	RSM Ref. [15]	FRANEC96
Φ_B	2.73 ± 1.14			6.48	6.33	6.62	5.16
Φ_{Be+CNO}		≤0.7	≤2.0	6.38	5.9	6.31	5.47
Φ_{Be}		≤0.7	≤2.0	5.18	4.8	5.15	4.49
Φ_{CNO}		≤0.5	≤1.5	1.20	6.33	1.16	0.98

of the case of almost degenerate equations (if one decides not to combine the two gallium data) and of the case of an overdetermined system (when the apparent fluxes are less than the number of equations), giving in this last case effectively the best χ^2 fit. In summary, we have generated an ensemble of a million apparent fluxes from the ensemble of a million simulated experiments. If Φ_{Be} is positive in this ensemble 60000 times out of a million, we say that the probability of standard neutrinos is 6%. The other limits are derived similarly considering different experiments and/or fluxes.

Alternatively, one could reduce the problem to a single variable, by considering linear combinations of the form

$$\Phi(x) = x\Phi_{Be}^{app} + (1-x)\Phi_{CNO}^{app} . \tag{69}$$

For standard neutrinos and $0 \leq x \leq 1$ this combination should be positive. By requiring that the physical constraints are satisfied for any x one can determine the required probabilities/bounds. Both methods give the same results, which, taking into account the errors on neutrino cross sections, can be summarized as follows:

- (a) the probability P_1 for both Φ_{Be}^{app} and Φ_{CNO}^{app} to be positive is less than about 2%. Should we disregard arbitrarily one of the experiments, one still has $P_1 \leq 6\%, 7\%$ or 9% neglecting, respectively, the results of chlorine, gallium or KAMIOKANDE experiment. This indicates that standard neutrinos ($\Phi_{Be}^{app} > 0$ and $\Phi_{CNO}^{app} > 0$) are unlikely;
- (b1) to the 99.5% C.L., without any a priori knowledge, $\Phi_{Be}^{app} + \Phi_{CNO}^{app}$ should not exceed $0.7 \times 10^9\,\mathrm{cm^{-2}\,s^{-1}}$;
- (b2) to the same confidence level, if one assumes a priori standard neutrinos, the combined flux of Be and CNO neutrinos does not exceed $2 \times 10^9\,\mathrm{cm^{-2}\,s^{-1}}$.

Similar statements hold for ^7Be +CNO neutrino fluxes separately, see Table 9.

The main message can roughly be summarized by saying that *the probability of standard neutrinos are low, not much more than 2%. However, the precise magnitude of the probability should be taken with caution*, at least for the following reasons: (i) statistical and systematic errors have been combined together and (ii) the assumption of Gaussian fluctuations might underestimate the probability, especially considering that we are dealing with the tail of the distribution.

2.8. Experimental results and standard solar models

Let us insist on the hypothesis of standard neutrinos and compare experimental information with theoretical estimates.

We report in Fig. 7 the results of several recent solar model calculations [15–20, 22, 23, 56] together with the experimental results. Some of the models predict a ^{8}B neutrino flux close to the KAMIOKANDE value; however no model is capable of reproducing the low Be+CNO flux implied by the experiments.

In Table 9, we have considered *only standard solar models* [15,16,22,56]. For standard neutrinos, the experimental information is also presented in the same table. The discrepancy between theory and experiment is about a factor two for the boron flux. *The discrepancy on Φ_{Be+CNO}, where the predicted values exceed the experimental upper bounds* (99.5% *C.L.*) *by a factor three, appears more important to us.*

The problem is mostly with beryllium neutrinos and let us examine it in some detail. The extraction of Φ_{Be} from experimental data (with the requirement $\Phi_{CNO} \geq 0$) yields an unphysically negative Be flux. Without any prior knowledge, Φ_{Be} cannot exceed $\frac{1}{10}$ of the RSM prediction at the 99.5% C.L. If we a priori force it to be non-negative, then the upper bound is $\frac{1}{5}$ of the RSM at the 95% C.L.; a value as high as $\frac{1}{3}$ of the RSM prediction is only allowed at the 99.5% C.L. All this indicates that ^{7}Be neutrino suppression is much stronger than that of ^{8}B neutrinos.

2.9. The beryllium–boron relationship

Additional insight on neutrino fluxes can be obtained by considering the physical connections among them. The relationship between ^{7}Be and ^{8}B neutrinos, particularly emphasized by Berezinsky [62], is most interesting.

Both neutrinos are "daughters" of the ^{7}Be nuclei, see Fig. 8. For this nuclide, electron capture (rate λ_{e7}) is favoured over proton capture (rate λ_{17}), due to the absence of the Coulomb barrier.
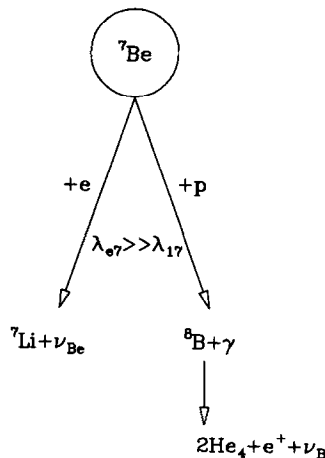

Fig. 8. The fate of ^{7}Be nuclei.

Thus the value of Φ_{Be} is a clear indicator of the parent ^{7}Be concentration, n_7:

$$n_7 \propto \Phi_{\text{Be}}/\lambda_{\text{e7}} \, . \tag{70}$$

Since Φ_{Be} comes out to be reduced by a (large) factor with respect to the SSM prediction, the same reduction has to occur for the ^{7}Be equilibrium abundance (λ_{e7} is weakly dependent on temperature, and it is essentially scaled from measurements in the laboratory [35]). The puzzle is thus with ^{8}B neutrinos, since:

$$\Phi_{\text{B}} \propto n_7 \lambda_{17} \, . \tag{71}$$

The observed (KAMIOKANDE) value of Φ_{B} being just a factor two below the SSM prediction, it looks that experiments are observing too high Φ_{B}! To put it in another way, one cannot kill the father/mother before the baby is conceived.

Should we insist on this approach, then we need to enhance $\lambda_{17}/\lambda_{\text{e7}}$. *Any attempt to reduce the discrepancy between the KAMIOKANDE and chlorine experiments with respect to SSM by lowering S_{17}* (the zero energy astrophysical factor for the p+^{7}Be $\rightarrow$ ^{8}B +γ reaction) *goes into the wrong direction.*

To make this argument more quantitative, let us define the reduction factors R_i with respect to the prediction of the reference solar model ($R_i = \Phi_i/\Phi_i^{\text{RSM}}$) [62]. From the chlorine and KAMIOKANDE data one gets

$$\frac{R_{\text{Be}}}{R_{\text{B}}} \leq -1 \pm 0.8 \tag{72}$$

which is another way of presenting the "inconsistency" between the chlorine and KAMIOKANDE data, see Section 2.3.

2.10. What if the sun were burning less now?

One might speculate that the *present* luminosity $L_\odot$ does not correspond to the *present* nuclear energy production rate L_{nuc} in the sun. Actually it takes about 8 min for neutrinos produced in the solar core to reach earth, whereas the time for electromagnetic energy to reach the solar surface is more than 10^4 yr, and one might imagine that L_{nuc} is different from $L_\odot$. Short time scale fluctuations in the nuclear energy production might not alter the photospheric temperature, the relevant time scale being of the order of 10^7 yr because of the enormous amount of gravitational energy stored in the solar structure. Although this hypothesis of a thermal instability is rather extreme, let us consider it as a way of exploiting the full potential of the "solar model independent" approach.

First of all, we remind that the result of combining chlorine and KAMIOKANDE experiments (see Section 2.3):

$$S_{\text{Cl},\,int} = -0.48 \pm 0.49 \, \text{SNU} \tag{73}$$

was independent of the solar luminosity constraint. The probability of finding $S_{\text{Cl},\,int}$ about 1σ below its physical limit is 16%. By exploiting the gallium result, we can find that the present situation is

even less probable. If we insist that the gallium result is consistent with the other experiments, then the signal originates essentially from p (=pp+pep) neutrinos:

$$\Phi_{\mathrm{p}} = \frac{S_{\mathrm{Ga}}}{\sigma_{\mathrm{Ga,p}}} = (60.2 \pm 6.5) \times 10^{9}\,\mathrm{cm}^{-2}\,\mathrm{s}^{-1}\,, \tag{74}$$

i.e. p neutrinos are essentially as many as calculated in standard solar models. From solar models we only assume $\Phi_{\mathrm{pep}}/\Phi_{\mathrm{p}} = \Phi_{\mathrm{pep}}^{\mathrm{RSM}}/\Phi_{\mathrm{p}}^{\mathrm{RSM}}$, i.e.: [16]

$$\Phi_{\mathrm{pep}} = 2.36 \times 10^{-3}\Phi_{\mathrm{p}}\,. \tag{75}$$

One can thus calculate the contribution of pep neutrinos to the chlorine signal:

$$S_{\mathrm{Cl,pep}} = \sigma_{\mathrm{Cl,pep}}\Phi_{\mathrm{pep}} = 0.23 \pm 0.025\,\mathrm{SNU}\,. \tag{76}$$

After subtracting this contribution from Eq. (73) we are left with

$$S_{\mathrm{Cl,Be+CNO}} = -0.71 \pm 0.49\,\mathrm{SNU}\,. \tag{77}$$

By requiring $S_{\mathrm{Cl,Be+CNO}} \geq 0$, one immediately derives that the probability of the present situation is at most 8%.

Essentially, the same argument can be presented in a more precise form. We abandon the luminosity constraint Eq. (43) or (54a) and still we have the three experimental signals, Eqs. (44)-(46) or Eqs. (54b)-(54d), in face of four unknowns: $\Phi_{\mathrm{p}}, \Phi_{\mathrm{Be}}, \Phi_{\mathrm{CNO}}$ and Φ_{B}. One can thus express one flux (e.g. Φ_{Be}) in terms of another flux (e.g. Φ_{CNO}) and of the experimental signals. In this way one finds

$$\begin{aligned}\Phi_{\mathrm{Be}} + 1.77\Phi_{\mathrm{CNO}} &= 4.59 S_{\mathrm{Cl}} - 1.29 \times 10^{-2}S_{\mathrm{Ga}} - 5.04\Phi_{\mathrm{B,Ka}} \\ &= -3.0 \pm 2.2\,,\end{aligned} \tag{78}$$

which is essentially equivalent to Eq. (77). This equation also shows *the relevance of direct ^{7}Be neutrino detection*. As an example, a measurement of Φ_{Be} in excess of $3.3 \times (10^{9}\,\mathrm{cm}^{-2}\,\mathrm{s}^{-1})$ would imply $\Phi_{\mathrm{CNO}} < 0$ at 3σ level, and thus would be a proof of non-standard neutrinos, even *without* the stationary sun hypothesis.

2.11. Universal neutrino oscillations

In the case of neutrino oscillations, similar arguments can be used when the averaged survival probability ($\mathrm{P}_{\nu_e \rightarrow \nu_e}$) is the same for all the components (pp, pep, Be, ...) of the neutrino flux. This situation is realized for $\Delta m^2 > 10^{-3}\,\mathrm{eV}^2$ (in this case coherent matter effects are negligible at any point in the sun, for any component of the solar neutrino flux). It is important to observe that in this situation the cross sections σ_i averaged over the neutrino energy spectra are the same as for standard neutrinos.

Thus by interpreting again $\Phi_{\mathrm{Be}}, \Phi_{\mathrm{CNO}}$ and Φ_{B} as the electron neutrino fluxes at earth, the case of *sterile neutrinos* is exactly equivalent to the one just discussed in Section 2.10, and we get again

---

[16] We verified that ξ varies by 2% when $L_{\odot}$ is changed by 10%.

Eq. (78). This means that the probability of universal oscillations into sterile neutrinos is less than 8%.

We remark that we used really minimal information from solar models, essentially Eq. (75). Clearly any additional hypothesis on the sun (e.g. a minimal non-vanishing ^{7}Be flux) will essentially exclude this scenario, see also Refs. [63, 64].

2.12. Concluding remarks

- All in all, a solar model independent evidence for non-standard neutrinos exists. It is however not overwhelming: the probability of standard neutrinos is less than a few percent (see Section 2.7), i.e. the indication is at the 2σ level (we point out that this conclusion is reached when giving up all our understanding of stellar physics).
- If one insists on standard neutrinos, then the ^{7}Be neutrino flux has to be drastically suppressed with respect to the prediction of SSMs and this suppression is stronger than that for ^{8}B neutrinos. Non-standard solar models attempting to solve the solar neutrino puzzle have to account for *both* these reductions.
- All this does not imply that the ^{7}Be flux on earth has to be small. That conclusion holds for standard neutrinos only. There are neutrino oscillation schemes which can account for all available data and, at the same time, predict a ^{7}Be signal quite consistent with the SSM prediction. (These models exploit the possibility of deforming energy spectra and/or transforming ν_e into ν_μ, which are active in the KAMIOKANDE detector, see Ref. [65]). In conclusion *the direct detection of ^{7}Be neutrinos is crucial.*

In this respect, one has to avoid the temptations illustrated by the following story [66]: The owner of a villa in Rome was explaining the civilization level of ancient Romans: "They even had telegraphs or telephones. When digging in my garden, I discovered ancient copper wires". His friend immediately went digging in his own garden and returned with the comment "You were right about their incredible civilization. They even had wireless communication. Indeed I found no cables upon digging".

3. Non-standard solar models: why and how?

3.1. Introduction

For standard neutrinos, one finds that the fluxes of intermediate energy neutrinos (^{7}Be and CNO) are strongly reduced with respect to the SSM expectations, so that the nuclear energy production chain appears strongly shifted towards the pp-I termination.

The question addressed in the next sections is the following: is it possible to build *non-standard* solar models in agreement with available experimental data? In other words, if we insist on standard neutrinos, is the solar neutrino puzzle restricted to the results of SSMs, or is the problem more general?

In order to enhance the pp-I termination, it is necessary that the ratio between the rates for the ^{3}He $+^3$He and ^{3}He $+^4$He reactions,

$$R = \overline{\lambda_{34}}/\overline{\lambda_{33}} \qquad (79)$$

is drastically decreased with respect to the SSM prediction (here and in the following λ_{ij} is the fusion rate of two nuclides with mass numbers i and j and the average is meant over the energy production region). In the (realistic) approximation that the total flux is given by the sum of ^{7}Be and pp components, i.e. only pp-I and pp-II contribute, the first termination has probability $P = \overline{\lambda_{33}}/(\overline{\lambda_{33}}+\overline{\lambda_{34}})$ and of course the other one has $1 - P$. In pp-I two pp neutrinos are emitted, against one pp plus one ^{7}Be neutrino in pp-II, so that

$$\frac{\varPhi_{\text{Be}}}{\varPhi_{\text{pp}}} = \frac{R}{2+R}. \tag{80}$$

In the RSM one has $\varPhi_{\text{Be}}/\varPhi_{\text{pp}} = 0.09$ so that $R_{\text{RSM}} = 0.2$; if the ^{7}Be neutrino flux has to be reduced by, say, a factor three, then one needs $R \approx 0.07$.

One finds just two ways for decreasing R:

(a) Adjusting the parameters so as to lower the inner temperature.

(b) Adjusting the ^{3}He nuclear cross sections, so as to make the ^{3}He $+^3$He reaction even more favoured with respect to the ^{3}He $+^4$He reaction.

We note, by the way, that the p+^{7}Be $\rightarrow ^8$B $+\gamma$ cross section is not relevant for enhancing the pp-I branch.

In this section we begin the discussion of case (a), by identifying the parameters which could affect the inner solar temperature. Non-standard solar models with reduced central temperature will be explicitly presented in the next section, whereas the effect of varying the ^{3}He nuclear cross sections will be discussed in Section 5. As a way of characterizing the non-standard solar models which we shall discuss later, we introduce in the final part of this section some algorithms, essentially based on "homology" (scaling) concepts.

3.2. Cooler solar models: why and how?

By lowering the temperature and therefore the collision energies, the tunnelling probabilities are decreased for both the ^{3}He $+^3$He and ^{3}He$+^4$He branches, the latter being more suppressed as heavier nuclei are involved, see Eq. (3); in conclusion, the ^{3}He $+^3$He branch gets favoured.

How can one decrease the inner solar temperature? As we shall see, there are a few analogies between the solar core and the human body. For this latter the following statements clearly hold:

(i) the (absolute) temperature is fixed to the level of $\pm 1\%$;

(ii) alteration of the temperature is a symptom, and not an illness in itself;

(iii) once you measure the temperature somewhere, you know it everywhere.

As regards the inner solar temperature, a comparison of the results of various SSM calculations (see Table 1) immediately shows the first point. The stability of the internal temperature for any given input physics will be further analysed in Section 4.2. Point (iii) will be discussed more extensively at the end of this section. Let us now concentrate on (ii). It means that one cannot treat, in principle, the central temperature T_c as an independent parameter. In fact, T_c cannot be decoupled from the solar structure, since severe constraints arise from the stability criterion. One has thus to study how T_c is altered when physical/chemical parameters are varied, while the basic equilibrium conditions are still satisfied. In other words, one has to study "different-but-still-reasonable" suns, i.e. pseudo-solar structures where stellar matter behaves differently from the predictions of standard physics, the basic equations for stellar structure and evolution still being satisfied.

In order to reduce T_c one can resort to several manipulations, playing on the physical and chemical inputs which determine the structure of the star, see Section 1.2:

(a) *A larger pp cross section.*
Increasing S_{pp} (the astrophysical zero energy S-factor for the $p + p \rightarrow d + e^+ + \nu_e$ reaction) implies a lower central temperature, since fusion gets easier while the solar luminosity has to be kept constant. Although S_{pp} is theoretically well determined (see Section 4.2), one can introduce an artificial variation just to get cooler pseudo-suns. In the language of Section 1.2, one is essentially changing the energy production rate per unit mass.

(b) *A less opaque sun.*
This is another way to get a cooler solar interior, as a smaller temperature gradient enlarges the region of nuclear burning, with less energy needed from the innermost core. In practice, this can be accomplished by using different ad hoc assumptions:

(b1) the metal fraction Z/X is significantly smaller than that indicated by the photospheric and/or meteoritic composition;

(b2) the radiative opacity is smaller than that computed by several authors [38, 39, 67];

(b3) some new mechanism could contribute to energy transport through the sun. In this connection some years ago (see e.g. [68, 69]) the possibility of weakly interacting massive particles (WIMPS) captured by and trapped inside the sun was discussed. We do not consider this hypothesis in view of the negative results of direct searches for such particles and for the lack of any observational evidence in later stellar evolution [70].

According to Section 1.2, one could also study modification of the equation of state. We do not consider this possibility as in the region where neutrinos are produced the deviation from a perfect gas law, although relevant for a detailed evaluation of the solar structure, cannot deeply modify the present sun.

On the other hand, there is an additional, still hypothetical possibility:

(c) *A younger sun.*
Should the sun be younger, the hydrogen mass fraction in the center would be higher and the same nuclear energy output could be produced at lower temperatures.

3.3. Homology relationships

In the next sections we shall present many solar models, where some physical input X (solar age, chemical composition,...) is varied from the starting value used in the calculations, X^*, by a scale factor x:

$$x = X/X^*.\tag{81}$$

As a result, one finds profiles for the physical quantities Ω (e.g. pressure, temperature, density,...) which are different from the profiles Ω^* of the starting model, at any point in the solar interior.

As we shall see, we find that in many cases the distributions of physical quantities follow with a good accuracy an "homologous" scaling relation

$$\Omega(x, m) = f_\Omega(x)\Omega^*(m),\tag{82}$$

(where m represents the mass coordinate $m = M(r)/M_\odot$, and $M(r)$ is the mass within the current values of the radius r) i.e. for any physical quantity, the profile along the mass coordinate has the

same shape as in the starting model; the difference with respect to it is just in a scale factor, which depends on the amount x of the variation of the parameter X and which can be different for different physical quantities (however $f_\Omega = 1$ for any Ω and X, when $X = X^*$).

This is not in principle an unexpected behaviour, since we know from the theory of stellar structures that similar relations holds for "homologous" stellar model. To understand the point, let us recall that a stellar model is governed by a set of differential equations whose solutions give the correct distribution of the physical quantities Ω throughout the structure. According to the linear structure of differential relations, given one solution (e.g. the starting model) further solutions can be generated by a scaling transformation of the physical quantities, as in Eq. (82), the different scaling factors being related through algebraic constraints.

Eq. (82) is thus essentially a way of transforming solutions into solutions. Note however that not any solution is obtained just by these transformations, much in the same way that not all stars are homologous to each other. As an example, we shall see that homology is violated when considering huge solar age variations, as the age alters the profile of helium abundance.

More generally, bearing in mind that $R_\odot$ has to be matched by tuning the mixing length, one finds that non-standard structures tend to have an homologous internal structure, with a strong departure from homology just in the more external layers.

We recall that our main interest is in the resulting neutrino flux, so that two points have to be borne in mind:

(i) We are primarily concerned with the energy production region ($m \leq 0.3$ or $R/R_\odot \leq 0.2$).

(ii) We are mainly interested in the temperature profile, as neutrino production depends crucially on temperature.

All this means that we do not bother if Eq. (82) is badly violated outside the central core, and that for physical quantities other than T we shall be satisfied if Eq. (82) holds only to a fair approximation. What really does matter is the temperature profile in the energy production region.

Clearly, if Eq. (82) holds for the temperature profile,

$$T(x, m) = f_T(x)T^*(m),\tag{83}$$

then from the knowledge of the temperature at a point say the center, we are able to compute it at any other point, the only relevant parameter being the scaling factor:

$$\tau = T_c/T_c^*.\tag{84}$$

In other words, the test of homology for the temperature profiles correspond to check the third statement mentioned in the previous section.

It is useful to specify, in preparation for the next sections, the algorithms we use to test Eq. (82) and to extract the dependence of the physical quantities on the inputs which will be varied when building non-standard solar models.

If Eq. (82) holds for a physical quantity Ω, then the ratio

$$\omega = \frac{\Omega(x, m)}{\Omega^*(m)}\tag{85}$$

is independent of the mass coordinate m and is purely determined by the physical input which has been varied. Qualitatively, this can be seen by looking at a graph where ω is plotted versus m. For

quantitative statements, it is useful to compute the average value of ω over the cells of our solar model and its variance $\Delta\omega$

$$\overline{\omega} = \frac{1}{N_m}\sum_k \omega(m_k) \,, \tag{86}$$

$$(\Delta\omega)^2 = \frac{1}{N_m}\sum_k [\omega(m_k) - \overline{\omega}]^2 \,, \tag{87}$$

where we assume to divide (a portion of) the solar profile into N_m cells, the kth one being centered at $m = m_k$. By definition, for a perfect homology $\Delta\omega = 0$. The ratio

$$\delta_\Omega = \Delta\omega / \overline{\omega} \tag{88}$$

is an indicator of the validity of the homology relationship for the quantity Ω, and typically we consider two regions:

(a) the energy production region ($m \leq 0.3$ or $R/R_\odot \leq 0.2$) which is of primary interest to us, as already remarked.

(b) The full radiative interior, ($m \leq 0.98$ or $R/R_\odot \leq 0.7$). Although such an extended area is not important for neutrino production, nevertheless it is interesting to study the behaviour of physical quantities up to the bottom of the convective layer, where useful constraints arise from helioseismological measurements.

3.4. Scaling laws for the physical quantities

Once homology has been tested, one still has to study the function $f_\Omega(x)$, i.e. the dependence on the input parameter X which is being varied.

A natural parameterization, again reminiscent of those encountered in the study of the homology relationship is of the form

$$\Omega(x,m) = x^\alpha \Omega^*(m) \,. \tag{89}$$

The coefficient α depends on the physical quantity Ω (as well as on X). For simplicity of notation we will understand this dependence. Note that for $x \to 1$, $\Omega \to \Omega^*$.

From Eq. (89), the power law coefficient α is determined as

$$\alpha = \log(\Omega/\Omega^*) / \log x \,. \tag{90}$$

If we have built N_x models, labelled by an index j specifying the value of the input parameter $(x = x_j)$ and if each model contains N_m cells, labelled by an index k indicating the value of the mass coordinate $(m = m_k)$ then one has $N_x \times N_m$ independent determinations of the coefficient α:

$$\alpha_{jk} = \frac{\log \frac{\Omega(x_j, m_k)}{\Omega^*(m_k)}}{\log x_j} \,. \tag{91}$$

In order to extract a suitable average value for α, we proceed in the following way:

(a) for the jth model, we perform an average over the cells

$$\overline{\alpha_j} = \frac{1}{N_m}\sum_k \alpha_{jk} \tag{92}$$

and evaluate the corresponding variance $\Delta\alpha_j$ from

$$(\Delta\alpha_j)^2 = \frac{1}{N_m}\sum_k (\alpha_{jk} - \overline{\alpha_j})^2 . \tag{93}$$

(b) We take then a weighted average over the different models, using $1/(\Delta\alpha_j)^2$ as a weighting factor:

$$\alpha = \frac{\sum_j \overline{\alpha_j}/(\Delta\alpha_j)^2}{\sum_j 1/(\Delta\alpha_j)^2} . \tag{94}$$

We remind that homology is well verified when $\Delta\alpha_j/\alpha_j$ is small, and this provides a justification for the choice of the weighting factor.

(c) We can also define a variance $\Delta\alpha$, specifying in some sense the global uncertainty on the coefficient just determined:

$$(\Delta\alpha)^2 = \frac{1}{N_x}\sum_j (\alpha_j - \alpha)^2 . \tag{95}$$

Note that $\Delta\alpha/\alpha$ essentially estimates the accuracy of the power law approximation (whereas $\Delta\alpha_j/\alpha_j$ indicates the accuracy of the homology relationships).

Generally we consider two kinds of variations of the input parameter, for the calculation of the power law coefficients α and of their variances:

(i) small variations: $| x - 1 | \leq 10\%$. This procedure, which was pioneered in [13], is useful to study the effect of changing an input parameter of the SSM within its estimated uncertainty (which is generally of the order of few percent, see Section 4).

(ii) Large variations: typically by an order of magnitude, i.e. for x well outside the range allowed for the SSMs. It is in this way that one is really building and testing non-standard solar models. Such models are actually called for if one wants to effectively suppress [7]Be neutrinos.

Clearly the coefficients found in (i) and (ii) should be equal – within numerical uncertainties – if the power laws were exact. Actually there is no deep reason for these laws to hold. They are just parameterizations of data and one should not be astonished to get different numbers for cases (i) and (ii). It is more of a surprise if the values are found to be close, indicating that the same simple parameterization holds over a wide range for the input parameter.

3.5. Scaling laws for neutrino fluxes

We assume again a power-law behaviour:

$$\Phi_i = x^{\alpha_i} \cdot \Phi_i^* . \tag{96}$$

In order to determine the coefficients α_i, we use algorithms similar to those of the previous section. As the fluxes are already summed over the cells we can skip point (a) of the previous section and we construct directly the average over the models. Again omitting for simplicity the index specifying the flux component, one has:

$$\alpha = \frac{1}{N_x}\sum_j \frac{\log[\Phi(x_j)/\Phi^*]}{\log(x_j)} \tag{97}$$

and the corresponding variance:

$$(\Delta\alpha)^2 = \frac{1}{N_x} \sum_j \left[\frac{\log[\Phi(x_j)/\Phi^*]}{\log(x_j)} - \alpha \right]^2 . \tag{98}$$

Since all pseudo-suns have the same luminosity, they will give (approximately) the same total neutrino flux:

$$\sum_i Q_i \Phi_i(x) = \text{const.} = \sum_i Q_i \Phi_i^* , \tag{99}$$

so that equations of the form of Eq. (96) cannot hold exactly for all the components of the neutrino flux and for arbitrary variations of the parameters. For small variations one gets, by differentiating Eq. (99) with respect to x, the constraint:

$$\sum_i \alpha_i Q_i \Phi_i^* = 0 \tag{100}$$

which can be used as a check of the calculations. For the case of large variations it is convenient to use Eq. (99) as a way of expressing one of the fluxes in terms of the others, so as to maintain the luminosity constraint. This is best done for the case of pp+pep neutrinos, as these are the least sensitive to variations of the physical inputs. For these latter, thus, instead of Eq. (96) we will generally use the expression:

$$\Phi_p = \Phi_p^* - \frac{Q_{Be}}{Q_p}(\Phi_{Be} - \Phi_{Be}^*) - \frac{Q_{CNO}}{Q_p}(\Phi_{CNO} - \Phi_{CNO}^*) , \tag{101}$$

where Φ_{Be} and Φ_{CNO} are given by Eq. (96).

3.6. Dependence on the central temperature

All in all, we are mainly interested in the change of neutrino fluxes (and other physical quantities characterizing the stellar interior) on the inner solar temperature, when some input parameter is varied.

This question can be easily answered on the basis of the above discussion, if we find – and we shall – that the temperature profiles satisfy the homology relationship:

$$T(x,m) = \frac{T_c(x)}{T_c^*} \cdot T^*(m) . \tag{102}$$

Neutrino fluxes, as well as the other quantities, can then be parameterized in terms of the scale factor T_c/T_c^*, see Eq. (84):

$$\begin{aligned} \Phi_i &= \Phi_i^* \cdot (T_c/T_c^*)^{\beta_i} \\ \Omega_i &= \Omega_i^* \cdot (T_c/T_c^*)^{\beta_i} . \end{aligned} \tag{103}$$

The β_i coefficients can be determined directly from the calculated fluxes for several models with a procedure similar to that presented in the previous section (this is the way we shall use for neutrino

fluxes). Alternatively, one can profit from the previous results. If one has determined the dependence of the central temperature on the parameter x:

$$T_c = x^{\alpha_T} \cdot T_c^* \tag{104}$$

and the dependence of the fluxes on the same parameter, see Eq. (96), then one has

$$\beta_i = \frac{\alpha_i}{\alpha_T} \ . \tag{105}$$

For neutrino fluxes, the most interesting comparison will be that of the β_i values obtained by varying different physical inputs. In principle they do not need to be the same. If we find that they are close, no matter which parameter is varied, then this will be a confirmation of our expectation that T_c is the quantity controlling the neutrino fluxes, independently of how that particular value of T_c is achieved.

4. Low central temperature solar models

4.1. Introduction

Solar models builders claim that the central temperature of the sun is known with an accuracy of one percent or better. This claim is often questioned by other physicists, who feel such an accuracy as too high on a matter where no direct observational data are available. Independently of personal feelings, a few pertinent questions are the following:

- If we insist that a low temperature solar model yields a drastically (say, a factor three) reduced ^{7}Be neutrino flux, how much should the physical and/or chemical inputs of solar models be varied? Is it enough to go slightly beyond estimated uncertainties, or are wild changes actually needed?
- Is it possible to get fluxes of both ^{7}Be and ^{8}B neutrinos consistent with available experimental information?

Following the lines sketched in Section 3, we now construct and discuss low inner temperature solar models. As the temperature is not an independent variable, we shall construct our pseudo-suns by acting on different inputs of the solar model: the $p + p \rightarrow d + e^+ + \nu$ cross section, the metal content of the sun, the adopted values for the radiative opacity and the solar age.

These inputs will be varied well beyond their estimated uncertainty, so as to build non-standard solar models. Generally, we will attempt to vary the input parameters as long as we get a ^{7}Be neutrino flux reduced to one third of the RSM prediction.

To give and estimate of the sensitivity of central temperature to the chosen input parameter, we will define $x(0.1)$ as the value of the scaling factor such that the central temperature is reduced by 10%.

A few common features of all the computed models will be summarized in Section 4.6, namely:

  (i) the temperature profiles appear, to quite a good approximation, homologous among the different models, in the sense specified in the foregoing section:

$$T(m) = \frac{T_c}{T_c^*} \cdot T^*(m) \ ; \tag{106}$$

(ii) no matter how the temperature variation is obtained, the neutrino fluxes are essentially determined by the scale factor

$$\tau = T_c/T_c^* \ . \tag{107}$$

In the same section the temperature dependence of the main components of the neutrino fluxes, as obtained by numerical simulations, will be also demonstrated analytically.

In Section 4.7 we will speculate on the possibility of getting information on the central solar temperature through homology and of testing the homology relationship itself with next generation experiments, elaborating an observation by Bahcall [71, 72], see also Ref. [73]. The final section contains our answer to the questions raised at the beginning.

In this entire Section 4, we shall for clarity divide the neutrino flux into the four components already introduced, Φ_p, Φ_{Be}, Φ_{CNO} and Φ_B. In Appendix B we will briefly discuss the ratios Φ_{pep}/Φ_p and Φ_N/Φ_{CNO}, mainly for substantiating our assertion about the stability of these quantities, among standard and non-standard models.

Clearly our interest is on the changes of physical quantities with respect to the reference solar model, BP95, when some input parameters are varied.

Actually, following Refs. [73, 74] all through this section and Section 5 we report results obtained by modifying the inputs of a starting solar model (CDF94) described in Ref. [73]: the equation of state was taken from Ref. [75], internal opacity tables from Ref. [39], corresponding to the chemical composition of Ref. [76] and diffusion was neglected. [17]

All quantities corresponding to the CDF94 *model will be labelled with the index* (∗) *here and in* Section 5.

4.2. The $p + p \to d + e^+ + \nu$ reaction rate

The rate of the initial reaction in the pp chain is too low to be directly measured in the laboratory (even in the sun's center this rate is extremely slow, of the order of 10^{-10} yr^{-1} consistently with the solar age) and it can be determined only by using the theory of low energy weak interactions, together with the measured properties of both the proton proton scattering and the deuteron. In terms of the astrophysical factor, $S_{11}(E)$ what really matters is its zero energy value, which for brevity, and following the usual notation, will be indicated simply as S_{pp}. While we refer to Refs. [14, 77] for an updated review, we remark that the calculated values [77, 78] are all in the range (3.89–4.21)×10^{-25} MeV b, i.e. they differ from their mean by no more than 3%. Kamionkowski and Bahcall [77] give an useful parameterization, in terms of the three quantities of physical interest for the determination of S_{pp}: the squared overlap integral $\lambda^2(0)$, the ratio G_A/G_V of the axial to vector coupling constants and the fractional correction δ to the nuclear matrix element due to exchange currents

$$S_{pp}[10^{-25}\,\text{MeV b}] = 3.89[\lambda^2(0)/6.92][(G_A/G_V)/1.2573]^2[(1 + \delta)/1.01]^2 \ . \tag{108}$$

The most recent evaluation of $\lambda^2(0)$ is from [77], obtained by using improved data for pp scattering and for the deuteron wave function and also including the effect of vacuum polarization. The

---

[17] CDF94 cannot be considered anymore as a standard solar model, since it does not satisfy the helioseismological constraints (Eqs. (6) and (8)).
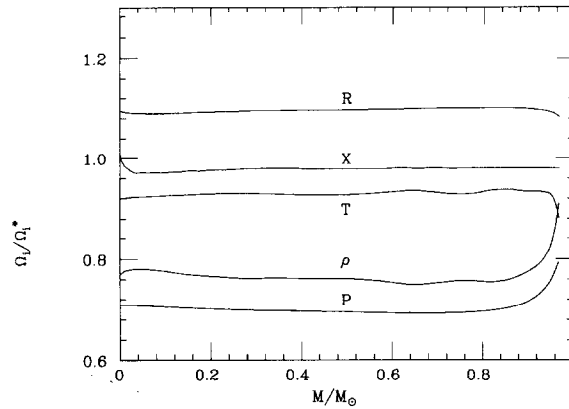
Fig. 9. For $x = S_{pp}/S_{pp}^* = 2$ the behaviour of several structure parameters, $\Omega_i(x,m)/\Omega_i(m)^*$, as a function of the mass coordinate in the whole internal radiative region. The considered structural parameters are: radius (R), density (ρ), temperature (T), pressure (P) and the hydrogen mass fraction (X).

estimated uncertainty is about $\pm 1\%$. The ratio G_A/G_V can be obtained with an accuracy of about 0.3% [61] from a weighted average of five precise modern experiments. The contribution of the exchange currents is $\delta \approx 1\%$, with a comparable uncertainty.

In summary, one has [77]

$$S_{pp} = 3.89 \times 10^{-25}(1 \pm 0.01)\,\mathrm{MeV\,b}\,. \tag{109}$$

Although some warning is in order as to the meaning of the quoted (1σ) error, one may conclude that well known physics determines S_{pp} to the level of few per cent or even better. Nevertheless, as explained in the previous section, the variation of S_{pp} well beyond its estimated uncertainty provides a good theoretical laboratory for investigating alternative solar-like structures.

In the RSM as well as in CDF94, S_{pp} corresponds to the central value of Eq. (109).

When varying $S_{pp}(S_{pp} \to s_{pp}S_{pp})$, we considered both the case of small variations (s_{pp} in the range 0.9–1.1) and large variations, up to $s_{pp} = 3.5$ which corresponds to a ^{7}Be neutrino flux reduced by a factor three. For drastically reductions of Φ_B, unreasonable variations of S_{pp} are needed, orders of magnitude larger than compatible with the estimated uncertainty. Briefly, we remark the following occurrences (see Ref. [79] for details):

(i) in the energy production region, temperature, density, pressure and radius all satisfy the homology relationship Eq. (88) to better than 1%, and the same holds throughout all the radiative interior (see Fig. 9). The same holds over the entire explored range in s_{pp}.

(ii) The hydrogen mass fraction, as a function of the mass coordinate, is essentially unchanged with respect to the CDF94 estimate, as it is constrained by the solar age.

(iii) For the power law coefficients α and β [see Eqs. (96) and (103)] of the quantities characterizing the physical interior we found the values in Table 10. The power laws look accurate ($\Delta\alpha/\alpha$ and $\Delta\beta/\beta$ being just a few percent) and the coefficients for small and large variation of S_{pp} are consistent, within their estimated uncertainties. In addition $s_{pp}(0.1){=}2.5$, i.e. one has to multiply S_{pp} by this huge factor to reduce the central temperature by 10%.

Table 10

Results of variations of S_{pp}, for quantities characterizing the solar interior and for the neutrino fluxes. We present the calculated values of α, see Eqs. (89) and (96), for the case of small and large variations. For this latter case, also the variances $\Delta\alpha$ are shown, Eq. (95). For the dependence on the central temperature, the corresponding β coefficients, Eq. (103), are also presented

S_{pp}/S_{pp}^* coefficient	0.9–1.1 α	1–3.5 $\alpha \pm \Delta\alpha$	0.9–1.1 β	1–3.5 $\beta \pm \Delta\beta$
T	−0.11	−0.11 ± 0.001	—	—
ρ	−0.37	−0.37 ± 0.01	+3.3	+3.3 ± 0.05
P	−0.49	−0.51 ± 0.01	+4.4	+4.6 ± 0.1
R	+0.12	+0.13 ± 0.003	−1.1	−1.1 ± 0.03
X	−0.01	−0.03 ± 0.004	+0.1	+0.3 ± 0.04
Φ_p	+0.11	+0.07 ± 0.01	−0.9	−0.6 ± 0.1
Φ_{Be}	−1.02	−1.1 ± 0.04	+8	+9 ± 0.3
Φ_{CNO}	−2.7	−2.2 ± 0.3	+21	+18 ± 2
Φ_B	−2.7	−2.7 ± 0.1	+21	+22 ± 1

(iv) The dependence of neutrino fluxes is also shown in Table 10. For the case of small variations, already investigated by Bahcall in Ref. [13, 24, 80], we essentially agree with his results. Even for large variations, power laws are very accurate for Φ_{Be} and Φ_B. For Φ_{pp} the accuracy is smaller, for the reasons outlined in Section 3.4. This holds for Φ_{CNO} as well, as this flux is the sum of two terms (Φ_N and Φ_O) which depend differently on temperature.

We stress that these features (points (iii) and (iv)) can be well understood analytically, assuming that the starting model and the pseudo-suns are connected by a homology transformation and that the hydrogen mass fraction profiles are the same, see Ref. [79].

4.3. Radiative opacity

An extensive and critical discussion of the uncertainties on radiative opacities is given in Ref. [14]. In the energy production region the typical difference between the outputs of the Livermore and the Los Alamos code is about (2–5)% [81]. At least half of the opacity in the central region is due to scattering on electrons and inverse bremsstrahlung in the field of H and He nuclei, processes which can be calculated with an accuracy of about 10%, or better. Bahcall and Pinsonneault [14] estimate a 1σ uncertainty of about 2.5%. On the other hand Turck-Chièze et al. [82] claim the uncertainty to exceed 5%, a point criticized in [14]. Recently Tsytovitch et al. [83] argued that some plasma physics effect have not been included in the calculations of the Livermore group, so that opacity at the solar center might be overestimated by 9%.

Although it is hard to make a definitive statement on such a complex matter, we shall conservatively take 5% as a 1σ uncertainty.

Since we aim to lower the internal temperatures, we investigated the effect of reducing the opacity. We scaled it uniformly along the solar profile by a factor *opa* with respect to CDF94. We consider *opa* as low as 0.6. This corresponds to a temperature reduction of 6% and $\Phi_{Be} \approx 0.5\Phi_{Be}^*$. For even
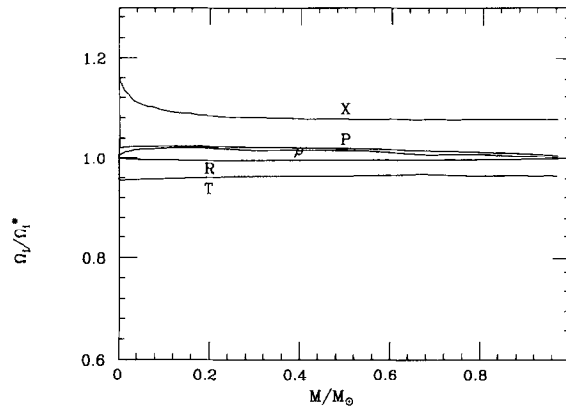
Fig. 10. Same as in Fig. 9, for $opa = 0.7$.

Table 11
Variations of opacity. Same notation as in Table 10

opa coefficient	0.9–1.1 α	0.6–1 $\alpha \pm \Delta\alpha$	0.9–1.1 β	0.6–1 $\beta \pm \Delta\beta$
T	+0.12	+0.12 ± 0.003	—	—
ρ	−0.06	−0.05 ± 0.006	−0.5	−0.4 ± 0.05
P	−0.08	−0.07 ± 0.003	−0.7	−0.6 ± 0.03
R	0	+0.01 ± 0.01	0	+0.1 ± 0.1
X	−0.28	−0.28 ± 0.01	−2.3	−2.3 ± 0.1
Φ_p	−0.11	−0.09 ± 0.01	−0.9	−0.68 ± 0.1
Φ_{Be}	+1.1	+1.2 ± 0.1	+8.5	+9.1 ± 1
Φ_{CNO}	+1.7	+1.7 ± 0.1	+13.4	+13 ± 1
Φ_B	+2.4	+2.6 ± 0.2	+19	+20.1 ± 1

smaller opacity, the resulting pseudo-sun would have an original helium abundance well below the cosmological value. By extrapolating, one finds $opa(0.1)=0.42$.

The following points are to be noted:

(i) The homology relationship is accurate to at least 1% for any variable characterizing the internal structure, over the entire radiative region, see Fig. 10.

(ii) Density, pressure and radius are essentially insensitive to opacity variations, see Table 11. On the other hand, when the opacity decreases the hydrogen mass fraction increases. This can be understood by observing that as the star gets less opaque, the interior becomes cooler. At the lower temperature, the pressure gradient needed to sustain gravity is then maintained with a larger hydrogen abundance.

(iii) The dependence of neutrino fluxes on the opacity parameter and the connection with the central temperature are also shown in Table 11. Again our results for small variations are well in agreement with those of [13, 24, 80].
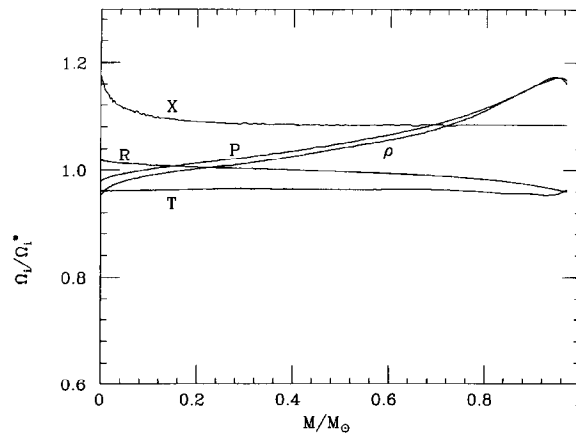
Fig. 11. Same as in Fig. 9, for $(Z/X)/(Z/X)^{SSM} = 0.5$.

4.4. The "metallicity" of the sun

Let us remind that the metallicity [18] is an input parameter constrained by photospheric observations. For a comprehensive review about the metal content of the solar interior we refer again to [15] and we mention just the main points: spectroscopic observations give the mass abundance (Z) of the heavy elements, relative to the hydrogen mass fraction (X), in the atmosphere of the present sun. About 75% of the heavy elements is accounted by carbon, nitrogen and oxygen. For these elements, the analysis of vibration–rotation and pure rotation lines of molecules as CO, CH, OH, NH in the infrared, from space experiments [76,84,85] provide accurate information. The abundance of elements heavier than oxygen is usually determined by absorption lines in the optical range; these clearly show the predominance of iron. The relative distribution of these elements can be usefully tested to the distribution of CI carbonaceous chondrite meteorites, which should keep the composition of these not volatile elements in the original solar nebula [45, 46]. It is important to note that the recent photospheric iron abundances [45] agree now well with the meteoritic values.

According to the most recent evaluations [45], one has for the photosphere of the present sun:

$$(Z/X)_{photo} = 0.0245 \tag{110}$$

with an accuracy better than 10%.

We remark that, due to diffusion towards the solar center, the original heavy elements abundance in the sun should be higher, by 10–15%.

When building solar models, this time we keep $z = (Z/X)/(Z/X)^*$ as a free variable. We considered small variations ($z = 0.9$–1.1) and large variations, with z as small as 0.1. With such a small value, the central temperature is decreased by about 10% and Φ_{Be} is about $\frac{1}{3}$ of the initial prediction. In this case $z(0.1) = 0.17$. While we refer for details to [73, 74], we summarize here the main results, see Fig. 11.

   (i) The temperature profile satisfies the homology relationship with an accuracy better than 1% throughout the entire radiative interior. Homology holds also for $R(m)$, but with less accuracy. On

---

[18] According to the astrophysical jargon, any element heavier than He is termed "metal" or "heavy element".

Table 12
Variations of Z/X. Same notation as in Table 10

$(Z/X)/(Z/X)^*$ coefficient	0.9–1.1 α	0.1–1 $\alpha \pm \Delta\alpha$	0.9–1.1 β	0.1–1 $\beta \pm \Delta\beta$
T	+0.06	+0.05 ± 0.005	—	—
ρ	+0.03	+0.02 ± 0.003	+0.5	+0.4 ± 0.06
P	+0.006	+0.001± 0.001	+0.1	+0.02 ± 0.02
R	−0.04	−0.01 ± 0.004	−0.7	−0.2 ± 0.1
X	−0.2	−0.13 ± 0.01	−3	−2.6 ± 0.2
Φ_p	−0.06	−0.04 ± 0.01	−0.9	−0.7 ± 0.1
Φ_{Be}	+0.62	+0.54 ± 0.03	9.9	+10.6 ± 0.4
Φ_{CNO}	+2	+1.7 ± 0.1	+31	+33 ± 2
Φ_B	+1.3	+1.1 ± 0.1	+21	+21 ± 1

the other hand, even in the energy production region, homology is only a fair approximation for pressure and density: for large variation of Z/X even in this restricted region $\delta\omega/\omega \approx 5\%$.

(ii) The picture is somehow similar to that of the opacity variations: R remains essentially unchanged on the average, whereas X grows as metallicity is diminished, see Table 12.

(iii) This similarity also reflects on the neutrino fluxes, the temperature dependence of these latter are essentially the same as in the previous subsection a part from Φ_{CNO}, see below.

As already mentioned, the similarity with the variations of the opacity can be readily understood since metallicity affects mainly the stellar opacity.

4.5. Rejuvenated suns

Unlike the other parameters used to constrain the SSM, the age of the sun is not an observable. It is inferred from the dating of the oldest meteorites, provided that a connection between the formation time of the meteorites and the birth of the sun (i.e. the ignition of H burning) is achieved. A recent discussion is provided by Wasserburg in [15]. On this basis Bahcall and Pinsonneault estimate (at 1σ) [15]

$$t_\odot = 4.57 \pm 0.01 \,\text{Gyr} . \tag{111}$$

Since the main difficulty is in establishing the evolution phase of the sun at the formation time of meteorites, we shall take as a conservative estimate of the uncertainty the duration of the pre-main sequence phase, $\Delta t_\odot \approx 30 \,\text{Myr}$.

The solar luminosity and age fix the amount of H which is burned into He in the solar core. In younger suns more H is available, so that fusion reactions are more likely and the observed luminosity can be reached at smaller T_c.

Correspondingly, a younger sun has a different composition in the energy production region, this difference becoming more and more marked as $t_\odot$ is shortened, and this drives the structure progressively away from homology (see Fig. 12).

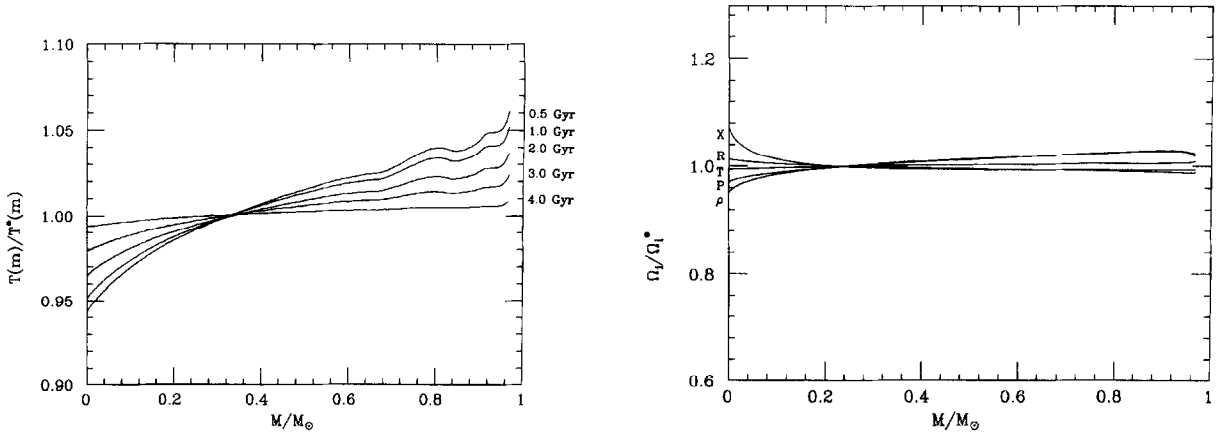In CDF94 we started with $t_\odot^* = 4.6 \,\text{Gyr}$.

Fig. 12. The temperature profiles $T(m)$ normalized to $T(m)^*$ for models with the indicated values of the solar age.

Fig. 13. Same as in Fig. 9, for the model with $t_\odot = 4$ Gyr.

Table 13
Variations of solar age. Same notation as in Table 10

$t_\odot/t_\odot^*$ coefficient	0.9–1.1 α	0.1–1 $\alpha \pm \Delta\alpha$	0.9–1.1 β	0.1–1 $\beta \pm \Delta\beta$
T	+0.03	+0.02 ± 0.007	—	—
ρ	+0.18	+0.11 ± 0.04	+6	+5.5 ± 2
P	+0.12	+0.08 ± 0.03	+4	+4 ± 2
R	−0.08	−0.05 ± 0.01	−3	−2.5 ± 0.5
X	−0.2	−0.13 ± 0.05	−7	−6.5 ± 2.5
Φ_p	−0.08	−0.04 ± 0.01	−1.4	−0.8 ± 0.1
Φ_{Be}	+0.57	+0.5 ± 0.1	+10	+11 ± 1
Φ_{CNO}	+0.9	+0.5 ± 0.2	+16	+12 ± 3
Φ_B	+1.	+0.8 ± 0.2	+18	+20 ± 1

We reduced the solar age down to $t_\odot = 0.1t_\odot^*$, this extreme corresponding to a central temperature reduction of about 6% and $\Phi_{Be} \approx 1/2\,\Phi_{Be}^*$. For even shorter ages, the structure of the pseudo-sun would be deeply modified by the occurrence of a central (^{3}He driven) convective core. We found the following results:

   (i) homology is now just a fair approximation (see Fig. 13). Even restricting oneself only to the energy production region, the accuracy in temperature is about 2% or less; that in density and pressure about 10% and for the hydrogen abundance it is merely about 25%.

   (ii) Correspondingly, the power laws for the variables characterizing the interior are only rather approximate ($\Delta\beta/\beta \approx 20\%$, see Table 13).

   (iii) As regards neutrino fluxes, we are in fair agreement with the results given in [13, 24, 80] for small variations. The dependences on temperature are in any case similar to those previously found.
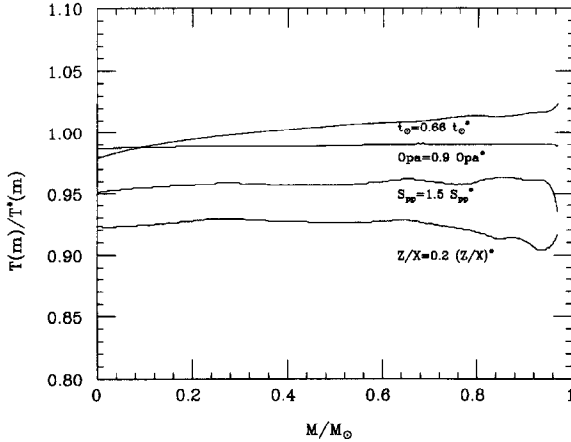
Fig. 14. The temperature profiles $T(m)$ normalized to $T^{SSM}(m)$ for a few representative non-standard solar models, from [73].
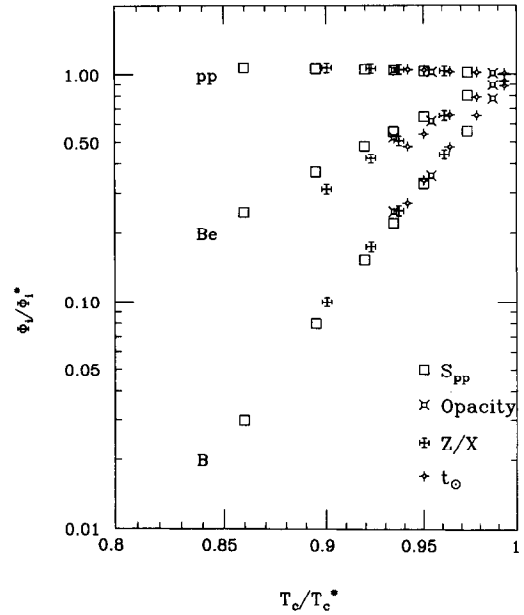
Fig. 15. The behaviour of Φ_{pp}, Φ_{Be}, and Φ_B as a function of the central temperature T_c when varying S_{pp}, opacity, Z/X and age, from [73].

4.6. Low temperature models and neutrino fluxes: summary and explanation

An important general feature of the models discussed above is the approximate homology of the temperature profiles

$$T(m) = \tau T^*(m) \,, \tag{112}$$

where $m = M/M_\odot$ is the mass coordinate, and the factor τ depends on the parameter which is varied but does not on m.

We have verified that Eq. (112) holds to an accuracy better than 1% in the entire radiative zone ($M/M_\odot \leq 0.98$ or $R/R_\odot \leq 0.7$) for all the models considered, except for huge (and really unreasonable) variations of $t_\odot$ (see Fig. 14). It is worth noting that $T(m)/T^*(m)$ stays constant throughout a region where $T(m)$ change by a factor five. The scaling factor τ may be taken as the ratio of the central temperature T_c to that of the starting model:

$$\tau = T_c/T_c^* \,. \tag{113}$$

The coefficients β_i for the power laws of neutrino fluxes versus temperature

$$\Phi_i = \Phi_i^* \left(\frac{T_c}{T_c^*}\right)^{\beta_i} \,. \tag{114}$$

are collected in Table 15, where we include for completeness all flux components.

Table 14
The power law coefficients for the reaction rates as a function of temperature, Eq. (118), calculated for $T = 15.6 \times 10^6$ K

Reaction	$\gamma = \dfrac{d \ln \langle \sigma v \rangle}{d \ln T}$
p+p	4
$^3\text{He} + ^3\text{He}$	16
$^3\text{He} + ^4\text{He}$	16
p+^{7}Be	13
e+^{7}Be	−0.5
p+^{14}N	20

One notes that β_p, β_{Be}, and β_B are largely independent of the parameter which is being varied (see also Fig. 15). In other words, *these fluxes are mainly determined by the central temperature, almost independently of the way the temperature variation is imposed.*

The dependences of the fluxes can be understood semi-quantitatively by simple analytical arguments. As a zeroth order approximation, let us assume that energy production occurs entirely through the pp-I termination, and that the chain is fully equilibrated. Requiring that the rate of ^{3}He burning $(n_3^2 \langle \sigma v \rangle_{33})$ corresponds to the fusion rate $(n_1^2 \langle \sigma v \rangle_{11}/2)$ at each point in the stellar core, the equilibrium ^{3}He density n_3 is given by [79]

$$n_3^2 = \frac{1}{2} n_1^2 \frac{\langle \sigma v \rangle_{11}}{\langle \sigma v \rangle_{33}} = \frac{2\varepsilon\rho}{Q_{pp}\langle \sigma v \rangle_{33}}, \qquad (115)$$

where ε is the energy production rate per unit mass.

The production of ^{7}Be nuclei, and consequently of ^{7}Be neutrinos, can be treated as a perturbation to the pp-I termination. Practically, every ^{7}Be nucleus produced is destroyed through electron capture, with emission of a ^{7}Be neutrino. The production rate per unit mass of the latter, w_{Be}^7, is thus equal to the production rate of ^{7}Be nuclei, again per unit mass:

$$w_{7_{Be}} = n_3 n_4 \langle \sigma v \rangle_{34}/\rho . \qquad (116)$$

With Eq. (115) and $n_4 = \rho Y N_A$ one gets

$$w_{7_{Be}} = \frac{N_A \sqrt{2}}{4\sqrt{Q_{pp}}} \frac{\langle \sigma v \rangle_{34}}{\sqrt{\langle \sigma v \rangle_{33}}} Y \sqrt{\varepsilon\rho} . \qquad (117)$$

The nuclear reaction rates $\langle \sigma v \rangle_{ij}$ are strongly temperature dependent. This dependence is usually parameterized by power laws [35]:

$$\langle \sigma v \rangle_{ij} \propto T^{\gamma_{ij}} \qquad (118)$$

and the coefficients γ_{ij} are given in Table 14.

Clearly quantities like Y, ε and ρ are also connected with temperature, but the dependence is much weaker than for the reaction rates; as a further approximation, we assume they are the same as in the starting model. On the other hand, we use homology for the temperature profiles. In this

way, from Eq. (117), the neutrino production at any mass coordinate m is related to that of the starting model:

$$w_{7_{Be}}(m) = w_{7*_{Be}}(m)\tau^{\gamma_{34}-(\gamma_{33}/2)} \, . \tag{119}$$

The same equation obviously holds for the fluxes on earth, $\Phi_i = (1/4\pi R_{ES}^2) \int dm\, w_i(m)$:

$$\Phi_{Be} = \Phi_{Be}^* \tau^{\gamma_{34}-\gamma_{33}/2} = \Phi_{Be}^* \tau^8 \, . \tag{120}$$

One can study the production of ^{8}B neutrinos similarly. Their production rate per unit mass is

$$w_{8_B} = n_1 n_7 \langle \sigma v \rangle_{17} / \rho \, , \tag{121}$$

whereas for ^{7}Be neutrinos one has

$$w_{7_{Be}} = n_e n_7 \langle \sigma v \rangle_{e7} / \rho \, . \tag{122}$$

By eliminating the equilibrium ^{7}Be nuclei density n_7 one has:

$$w_{8_B} = \frac{\langle \sigma v \rangle_{17}}{\langle \sigma v \rangle_{e7}} \frac{n_1}{n_e} w_{7Be} \tag{123}$$

Again assuming n_1/n_e to be essentially that of the starting model, one obtains after integrating over the mass coordinate:

$$\Phi_B = \Phi_B^* \tau^{\gamma_{17}+\gamma_{34}-(\gamma_{33}/2)-\gamma_{e7}} = \Phi_B^* \tau^{21.5} \, . \tag{124}$$

We are now also able to estimate the temperature dependence of Φ_p. We recall that the two main components are Φ_p and Φ_{Be}, and that their sum is fixed by the luminosity constraint. By differentiating with respect to T_c, this implies approximatively:

$$\beta_p = -\beta_{Be}(\Phi_{Be}^*/\Phi_p^*) = -0.6 \, . \tag{125}$$

The values we find are in agreement with the numerical estimates of Table 15. It is not surprising that the analytical values are quite close to the coefficients obtained by varying S_{pp}, since scaling works best in this case.

Let us remark a few relevant points:

- the temperature dependences of Φ_p, Φ_{Be} and Φ_B are well under control. One sees from the foregoing discussion that they are essentially determined by the behaviour of $\langle \sigma v \rangle_{ij}$ as a function of temperature; the latter behaviour is fixed mainly by the Coulomb barrier [35]. Solar physics only enters through the homology relationships of the temperature profiles.
- The flux Φ_{Be} can be determined independently of the value of the ^{7}Be lifetime. No matter what the value of this latter is, practically all ^{7}Be nuclei produced will emit a ^{7}Be neutrino.
- The ratio of Φ_B to Φ_{Be} is essentially governed by nuclear physics, its temperature dependence being that of $\langle \sigma v \rangle_{17}/\langle \sigma v \rangle_{e7}$.
- For any temperature one has

$$\frac{\Phi_B}{\Phi_B^*} \approx \left(\frac{\Phi_{Be}}{\Phi_{Be}^*}\right)^2 \tag{126}$$

Table 15

The β coefficients connecting the neutrino fluxes with the temperature, Eq. (103). The components of neutrino flux are indicated in the first column. The values presented are the best fit to the numerical calculations performed when each input parameter is varied in the range specified in the second row

Parameter scaling factor	S_{pp} 1–3.5	Opacity 0.6–1	Z/X 0.1–1	$t_\odot$ 0.1–1
Φ_{pp}	−0.6	−0.7	−0.7	−0.8
Φ_{pep}	2.2	−2.3	−1.7	0.5
$\Phi_p = \Phi_{pp+pcp}$	−0.6	−0.7	−0.7	−0.8
Φ_{Be}	9	9	11	11
Φ_N	15	12	31	9
Φ_O	24	15	36	18
$\Phi_{CNO} = \Phi_N + \Phi_O$	18	13	33	12
Φ_B	22	21	20	20

i.e. *the suppression/enhancement of Φ_B is much stronger than that of Φ_{Be}. A reduction of Φ_{Be} to 1/3 of the RSM prediction implies a reduction of Φ_B by an order of magnitude. This essentially illustrates the failure of low temperature models when compared with experimental data.*

The CNO flux appears sensitive not only to the temperature, but also to other parameters characterizing the solar interior. The drastically different exponents, found when varying the metallicity, can be understood by noting that the efficiency of the CN cycle is affected not only by temperature but also by the number densities of nuclei which act as catalyzers of the chain.

4.7. More about homology: additional consequences and a possible test

One generally thinks that the neutrino production zone is so well hidden below the solar surface that it can hardly be studied experimentally other than with neutrinos.

Actually, the accurate homology of temperature profiles, valid up to the border of the radiative interior, indicates a strict connection between the properties of the energy production region and of more external layers of the sun. If one is confident in homology, then a measurement of temperature at, say, the bottom of the convective zone immediately gives the temperature of the solar center.

A new generation of experiments is being planned for detecting monochromatic neutrinos produced in electron capture (^{7}Be $+e^- \rightarrow$ ^{7}Li$+\nu$) and in the pep ($p + e^- + p \rightarrow d + \nu$) reactions [10, 86, 87]. Bahcall [71, 72] has pointed out that one can, from measurements of the average energy difference between neutrinos emitted in solar and laboratory decay, infer the temperature of the production zone. The possibility of measuring inner solar temperatures through thermal effects on monochromatic neutrino lines is extremely fascinating (although remote). In this respect the homology relationship, Eq. (112), is particularly interesting, see Fig. 16. If homology holds, then a measurement of the solar temperature in the ^{7}Be production zone gives the value of T_c.

In addition, the homology relation itself is testable, in principle, by comparing the temperatures at two different points, as can be done by looking at the shapes of both the ν_{Be} and ν_{pep} lines. We remark that this would be a test of the energy transport mechanism in the inner sun.
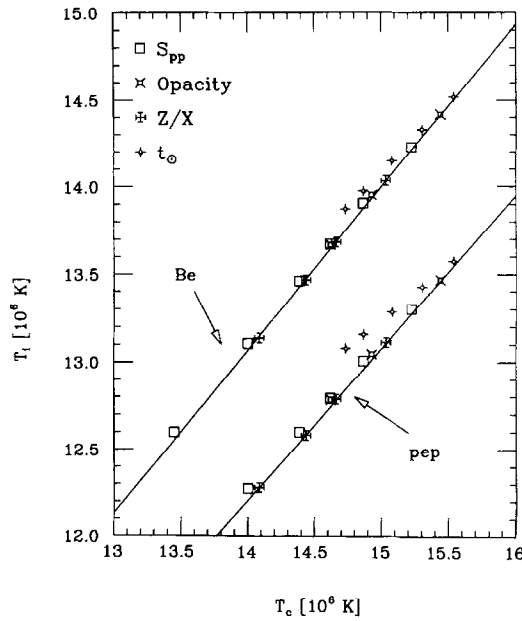
Fig. 16. Relations among the temperatures T at the ^{7}Be and pep peak production zones ($R/R_\odot = 0.06$ and $R/R_\odot = 0.09$, respectively) and the central temperature T_c in non-standard solar models. Data from numerical calculations are shown with the same symbols as in Fig. 15, while full lines show the scaling relations $T_i = T_c(T_i^*/T_c^*)$, from [73].

4.8. On the accuracy of the central solar temperature

A rough estimate of T_c can be obtained by equating the thermal energy of a hydrogen nucleus to its gravitational energy ($kT_c \approx GM_\odot m_p/R_\odot$). In this way one finds $T_c \approx 2 \times 10^7$ K, in good agreement with the much more refined SSM estimates (see Table 1). Different standard solar models give the same value of T_c within 1% and solar model builders claim that the present accuracy on T_c is of the same order.

From the preceding discussion, the reader can derive his own opinion about this claim. We have seen that the main regulators of the central solar temperature are S_{pp}, the metallicity, the solar age and the opacity of the solar interior. In terms of the uncertainties in these quantities, one has

$$\left(\frac{\Delta T_c}{T_c}\right)^2 = \left(\alpha_{T,S_{pp}}\frac{\Delta S_{pp}}{S_{pp}}\right)^2 + \left(\alpha_{T,Opa}\frac{\Delta Opa}{Opa}\right)^2 + \left(\alpha_{T,Z/X}\frac{\Delta(Z/X)}{(Z/X)}\right)^2 + \left(\alpha_{T,Age}\frac{\Delta Age}{Age}\right)^2. \qquad (127)$$

Using the power law coefficients $\alpha_{T,i}$ and the estimated uncertainties summarized in Table 16, one actually gets $\Delta T_c/T_c \approx 1\%$. One also sees that most of the error results from the uncertainties in opacity and in metallicity (note that with the uncertainties as estimated in [14, 15] the global uncertainty on T_c would be halved).

The next question is how the main parameters should be varied in order to get a solar model with drastically reduced ^{8}B and/or ^{7}Be neutrino fluxes. For instance if one requires $\Phi_B/\Phi_B^* \approx \frac{1}{2}$ a reduction of T_c by 3% is needed. Although this does not look terribly outside the allowed T_c range, really huge variations of the physical inputs are needed (see again Table 16, 4th column).

Table 16
Values of the coefficients $\alpha_{T,X}$ relating temperature to the input parameter, $T_c = T_c^*(X/X^*)^{\alpha_{T,X}}$ see Eq. (103), our estimated uncertainties of the input parameters $(\Delta X/X)$, and variations $(\delta X/X)$ required to reduce T_c by 3, 7 and 13%, respectively

X	$\alpha_{T,X}$	$\Delta X/X$ (%)	$\left.\frac{\delta X}{X}\right|_{-3\%}$ (%)	$\left.\frac{\delta X}{X}\right|_{-7\%}$ (%)	$\left.\frac{\delta X}{X}\right|_{-13\%}$ (%)
S_{pp}	−0.13	1	+25	+70	+190
Opacity	+0.13	5	−20	−40	−66
Z/X	+0.06	10	−40	−70	−90
$t_\odot$	+0.05	0.6	−45	−75	−94

The situation is even more desperate if one tries to reduce the ^{7}Be flux by a factor two (three). In this case temperature has to be reduced by at least 7% (13%), which requires the really unreasonable variations given in the last columns of Table 16. The input parameters are to be varied by an order of magnitude (or more) with respect to their estimated uncertainties. Even a 40% reduction of opacity can only reduce the ^{7}Be neutrino flux by at most a factor two. Last but not least, as is clear from Eq. (126), it is essentially impossible to account for the reductions of both Φ_{Be} and Φ_B.

One concludes that a solution to the solar neutrino problem cannot be found merely by reducing the central temperature.

5. Nuclear reactions in the sun

One may suspect that the solar neutrino problem is due to some inadequacy in our understanding of nuclear reactions in the solar interior. What could be wrong with the nuclear burning rates used in standard solar model calculations? There are (at least) three sides to this question, viz.:

- Nuclear physics: as repeatedly stated, the astrophysical S-factors used in stellar model calculations are generally obtained by extrapolating experimental data taken at energies higher than those relevant for the solar interior. Although the underlying theory is robust, one can be suspicious of extrapolations.
- Atomic/molecular physics: experiments in the laboratory use atomic or molecular targets. At the lowest measurable energies, electron screening is relevant and its effect has to be subtracted when deriving cross sections for bare nuclei. Indeed, the effect of electron screening has been detected [88], however, theory and experiments seem to disagree [88, 89].
- Plasma physics: the burning rates for bare nuclei are then to be corrected for the screening of nuclear charges by the solar plasma. In any calculation, the predicted effects are small; however, the theory is not completely satisfactory [90] and there are no direct experimental tests. The disagreement between theory and experiment for electron screening in atomic/molecular targets provides some warnings: although that is a different context, one has to keep an open mind about the possible effect of plasma screening on neutrino production.

As shown in Section 2, the main problem is with the ^{7}Be neutrinos, so that particular attention has to be given to the reactions in the pp chain preceding the formation of ^{7}Be nuclei; in other words, those reactions which determine the branching between the pp-I and pp-II chains (see Fig. 1). The rôle of the p+p cross section was already discussed in Section 4.2, as it is one of central temperature regulators. The value of the p+d $\rightarrow$ ^{3}He $+\gamma$ cross section is unimportant. It is orders of magnitude

Table 17
Estimates for $S_{33}(0)$ (MeV b)

CF88 [41]	5.57
PA91 [98]	5.0 ± 0.3
All data	5.3 ± 0.2
$E > 100\,\text{keV}$	5.2 ± 0.2
Adiabatic scr.	5.1 ± 0.2

larger than that of the weak interaction p+p→ d+e$^+$ + ν_e process, so that on a very short time scale equilibrium is reached and any practically pp reaction is followed by the production of one ^{3}He nucleus.

The cross sections for reactions between He isotopes,

$$^3\text{He} + ^3\text{He} \rightarrow ^4\text{He} + 2\text{p} \quad \text{and} \quad ^3\text{He} + ^4\text{He} \rightarrow ^7\text{Be} + \gamma, \tag{128}$$
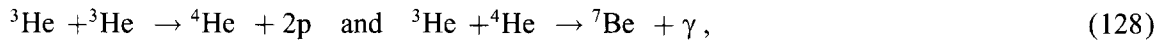
are clearly crucial and we shall pay particular attention to them. On the other hand, the proton capture by ^{7}Be:

$$\text{p} + ^7\text{Be} \rightarrow ^8\text{B} + \gamma \tag{129}$$

is of minor relevance for the flux of ^{7}Be neutrinos and governs essentially only the production of ^{8}B neutrinos, see Section 5.4. Similarly, the reaction:

$$\text{p} + ^{14}\text{N} \rightarrow ^{15}\text{O} + \gamma, \tag{130}$$

which will be briefly discussed in Section 5.5, essentially determines the production of CNO neutrinos only.

The goal of this section is to study the changes induced in neutrino fluxes when the nuclear burning rates are changed with respect to RSM inputs. The comparison of these results with neutrino experiments will be discussed in Section 6. As mentioned in Section 4, we recall that our starting standard solar model here is CDF94 [73, 74].

5.1. The status of $^3He + ^3He \rightarrow ^4He + 2p$ reaction

The relevant energy range is determined by the energy E_0 and the halfwidth, $\Delta/2$ of the Gamow peak.[19] For the central solar temperature one has $E_0 = 22\,\text{keV}$ and $\Delta = 12\,\text{keV}$. The available experimental data [91–97] are shown in Fig. 17. Data below 25 keV do not exist and at the lowest measured energies errors are of the order of 20% or greater, so that some extrapolation is necessary in order to reach the relevant energy range.

The astrophysical S-factors are usually parameterized with a Taylor expansion:

$$S_{ij}(E) = S_{ij}(0) + S'_{ij}(0)E + \tfrac{1}{2}S''_{ij}(0)E^2, \tag{131}$$

where mainly the coefficient $S_{ij}(0)$ matters for the sun, as E_0 is much smaller than the nuclear energy scale. In Table 17 we present some estimates of $S_{33}(0)$: the value used in the Caughlan and

---

[19] $E_0 = 1.22(Z_1^2 Z_2^2 \mu T_6^2)^{1/3}$ keV and $\Delta = 0.749(Z_1^2 Z_2^2 \mu T_6^5)^{1/6}$ keV, see e.g. [35].
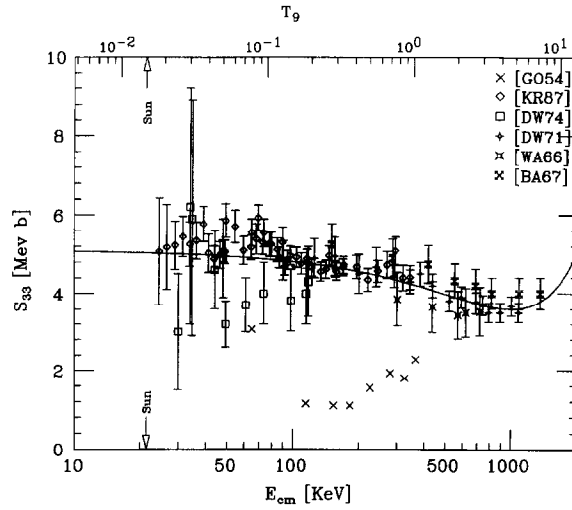
Fig. 17. The ^{3}He (^{3}He ,^{4}He)2p reaction. Experimental data for the S-factor as a function of CM energy (lower scale). The corresponding temperature $T_9 (= T \times 10^{-9})$, such that $E_0(T_9) = E_{cm}$, is also indicated (upper scale). The full curve corresponds to Eq. (132). The Gamow peak for the solar center is indicated by the arrows. The listed symbols corresponds to data in [91,96], from top to bottom.

Fowler compilation [41] corresponds to the experimental result of [92]: Parker and Rolfs [98] give a weighted average of several experimental results.

We derived a new estimate of $S_{33}(0)$ by reanalyzing all available data, except for those of the pioneer experiment by Good et al. [91] which is systematically a factor 2–3 below the others and carries no estimated error. A fit to the data using Eq. (131) gives $S(0) = (5.3 \pm 0.1)$ MeV b. The data at low energies are however affected by electron screening [35]. This effect is negligible at $E \geq 100$ keV and data above this threshold give the value of the 4th row in Table 17. A slightly smaller result is obtained if one considers all energies and corrects for electron screening effect in the adiabatic approximation [89], as shown in the last row. We consider this last value as the best estimate of $S_{33}(0)$ for bare nuclei. Correspondingly we find

$$S_{33}(E) = (5.1 \pm 0.2) + (-3.0 \pm 0.4)E + \tfrac{1}{2}(3.0 \pm 1.0)E^2 . \tag{132}$$

This expression (energies in MeV and S in MeV b) gives a good fit to all data ($\chi^2_{d.o.f.} = 0.8$).

At the Gamow peak near the solar center, one thus finds $S_{33} = 5.0$ MeV b, slightly higher than, but still consistent with the value used in the RSM, $S_{33} = 4.8$ MeV b. In CDF94 we used $S^*_{33} = 4.98$ MeV b.

5.2. The status of ^{3}He + ^{4}He → ^{7}Be + γ reaction

The range of relevant energies is essentially the same as above ($E_0 = 23$ keV, $\Delta = 12$ keV), whereas data are available only at $E > 100$ keV. Concerning the experimental results collected in Fig. 18, the following comments are needed: (i) the original data of [99] have been corrected, following the comment in [100]; (ii) data from [101] have been multiplied by a factor 1.4 according to [102]; (iii) errors quoted in [103] have been doubled so that fluctuations among data points
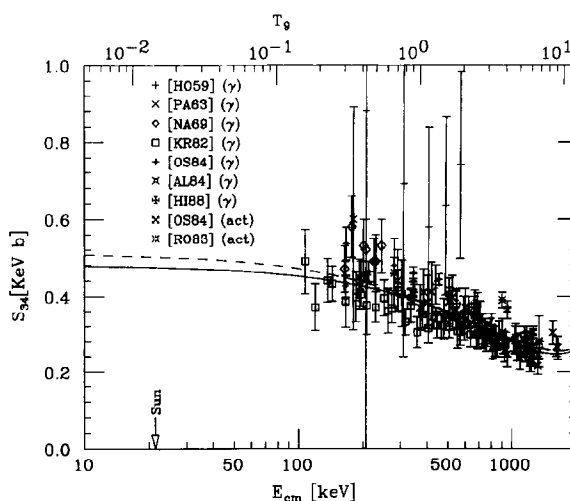
Fig. 18. The ^{3}He $(^4$He,$\gamma)^7$Be reaction. Experimental data for the S-factor as a function of CM energy (lower scale). The corresponding temperature T_9, such that $E_0(T_9) = E_{cm}$, is also indicated (upper scale). The full (dashed) curve corresponds to Eq. (133) (Eq. (134)). The listed symbols correspond to data in [105,99–101,106,102,103,107], from top to bottom.

Table 18
Estimates for $S_{34}(0)$ (keV b)

CF88 [41]	0.54
PA91 [98]	0.533 ± 0.017
Quadratic	0.48 ± 0.01
Exponential	0.51 ± 0.01

become statistically consistent; (iv) at all the energies where data are available electron screening is irrelevant.

Again what matters is the astrophysical S-factor at zero energy. In Table 18 we report some different determinations of this quantity. The value used in [41] coincides with that of the review paper [104], which was obtained as a weighted average of the extrapolations provided by different experiments. A similar, more recent analysis [98] gave a slightly smaller value. It has however to be remarked that the extrapolations were performed using different theoretical models, so that combination of extrapolated values is dubious. We performed a new analysis of all experimental data [99–103, 105–108]. For a quadratic expansion of the astrophysical S-factor we find

$$S_{34}(E) = [(4.8 \pm 0.1) + (-2.9 \pm 0.2)E + (0.9 \pm 0.1)E^2] \times 10^{-4} \tag{133}$$

(again E in MeV and S in MeV b). Alternatively, by using an exponential parameterization, as frequently adopted in the literature and supported by theoretical models (see e.g. [109]), we get

$$S_{34}(E) = (5.1 \pm 0.1) \times 10^{-4} \exp[(-0.83 \pm 0.07)E + (0.25 \pm 0.03)E^2]. \tag{134}$$

By using these two parametrizations, at the Gamow peak near the solar center one finds respectively $S_{34}(E_0) = 4.74$ and 5.01 in 10^{-4} MeV b. One sees that uncertainties due to the extrapolation

procedure are at least comparable to the quoted statistical error, so that the global error is about $\pm 2 \times 10^{-5}$ MeV b.

The value of $S_{34}(E_0)$ used in the RSM is based on [98], after introducing a 1.6% decrease due to the vacuum polarization effect [110], yielding $S_{34}(E_0) = 5.17 \times 10^{-4}$ MeV b, slightly larger than that given by our preferred expression Eq. (134), but still consistent with it within uncertainties. In CDF94 we had $S_{34}^*(E_0) = 5.26 \times 10^{-4}$ MeV b.

5.3. Neutrino fluxes and helium reactions

In order to estimate the dependence of ^{7}Be and ^{8}B neutrino fluxes on the nuclear cross sections, essentially we repeat here the argument of Section 4.6. Let us first consider the local equilibrium concentration of the parent ^{7}Be nuclei, n_7. ^{7}Be is created in the ^{3}He $+\,^4$He reaction and destroyed, essentially via electron capture, with a lifetime τ_{e7}. Thus, at equilibrium

$$n_7 = \tau_{e7} n_3 n_4 \langle \sigma v \rangle_{34} \, , \tag{135}$$

where n_i is the number density of the nuclei with mass number equal to i. The ^{3}He equilibrium density is obtained by equating its creation rate (i.e. the rate of the p+d $\to\,^3$He $+\gamma$ reaction, which equals the rate of p+p $\to$ d $+ e^+ + \nu_e$) to the burning rate, which is dominated by the ^{3}He $+\,^3$He reaction. With this approximation, one gets:

$$n_3^2 = \tfrac{1}{2} n_1^2 \langle \sigma v \rangle_{11} / \langle \sigma v \rangle_{33} \, . \tag{136}$$

By using the above equations one can derive:

$$n_7 = (1/\sqrt{2}) \tau_{e7} n_1 n_4 \sqrt{\langle \sigma v \rangle_{11}} \langle \sigma v \rangle_{34} \Big/ \sqrt{\langle \sigma v \rangle_{33}} \, . \tag{137}$$

If the rates $\langle \sigma v \rangle_{33}$ and $\langle \sigma v \rangle_{34}$ differ from the starting inputs, one expects that only the probabilities of the pp terminations are varied whereas the densities n_1, n_4 and the temperature are essentially unchanged with respect to the starting predictions, since the hydrogen burning rate and the helium abundance in the solar interior are determined by the present luminosity and the present age of the sun. This expectation is confirmed by numerical experiments, see for example Fig. 19. One thus gets that only the following combination of $\langle \sigma v \rangle_{33}$ and $\langle \sigma v \rangle_{34}$ matters:

$$\chi = \langle \sigma v \rangle_{34} \Big/ \sqrt{\langle \sigma v \rangle_{33}} \, . \tag{138}$$

In terms of χ one has

$$n_7 = n_7^* \chi / \chi^* \, . \tag{139}$$

We remark that Eq. (139) holds at each point in the solar interior.

Assuming for the moment that there are no resonances in the energy range of interest and that the low-energy astrophysical S-factors differ from those used in the starting model by a constant factor s_{ij} ($S_{ij}(E) = s_{ij} S_{ij}^*(E)$), then at any point in the sun:
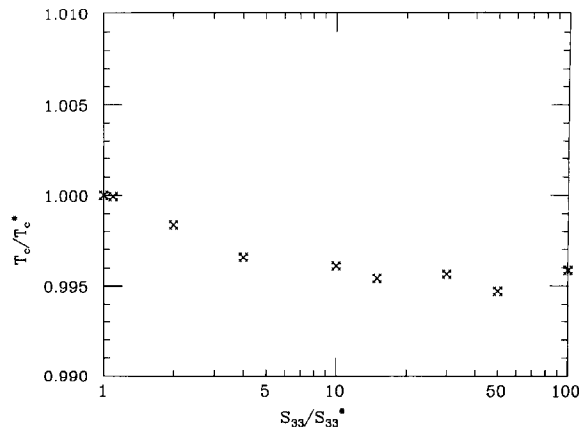
$$\chi / \chi^* = s_{34} / \sqrt{s_{33}} \tag{140}$$

Fig. 19. The central temperature T_c as a function of S_{33}.

Table 19

Variation of $\chi = S_{34}/\sqrt{S_{33}}$. We present the coefficients α_i for the parameterization $\Phi_i = \Phi_i^*(\chi/\chi^*)^{\alpha_i}$, for χ in the range indicated in the first row. In the second column the values of Ref. [24] are shown. For the case of large variations, the variances $\pm\Delta\alpha$ are also presented

χ/χ^* Reference	0.9–1.1 [24]	0.9–1.1 This work	0.1–1 This work
Φ_p	−0.06	−0.05	−0.05 ± 0.01
Φ_{Be}	+0.86	+0.86	+0.92 ± 0.02
Φ_{CNO}	−0.05	−0.04	−0.02 ± 0.01
Φ_B	+0.80	+0.92	0.91 ± 0.02

and, consequently,

$$n_7 = n_7^{SSM} S_{34}/\sqrt{S_{33}} .$$ (141)

The ^{7}Be and ^{8}B neutrino fluxes, which are obviously both proportional to n_7, scale then in the same way

$$\Phi_{Be} = \Phi_{Be}^* s_{34} s_{33}^{-0.5} ; \qquad \Phi_B = \Phi_B^* s_{34} s_{33}^{-0.5} .$$ (142)

The p (= pp+pep) neutrino flux can be best derived by the luminosity constraint, Eq. (43).

Numerical experiments confirm these analytical estimates. In Fig. 20 one sees that for each component the flux is actually determined by the variable χ and that Eq. (142) provides a good approximation. In Table 19 we show the power law coefficients for the main components of the neutrino flux. Our results for small variations agree with those which can be derived from [24]. The last column presents the case of large variations. One notes that the numerical values are well in agreement with the analytical estimates presented above.

Note also that pp+pep and CNO neutrinos are essentially insensitive to variations of χ as expected since the temperature is unchanged.
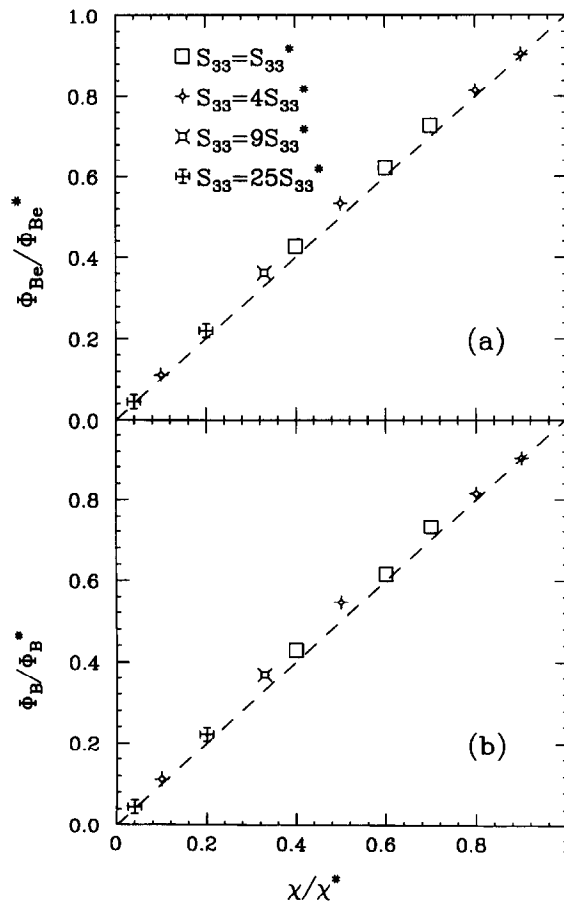
Fig. 20. The flux of (a) ^{7}Be neutrinos and (b) ^{8}B neutrinos as a function of $\chi = S_{34}/S_{33}^{1/2}$ for several values of S_{33}, as calculated by using the FRANEC code. The dashed line corresponds to Eq. (142), from [112].

Large variations are really necessary if one wants a reduction of ^{8}B and ^{7}Be neutrino flux by a factor 2–3. As an example, if S_{33} is kept fixed then S_{34} has to be reduced by a factor 2–3, or S_{33} has to be enhanced by a factor 4–9 if S_{34} is unchanged. This is clearly in conflict with the experimental situation discussed in the previous sections.

The only way out, a desperate one, is to invoke a resonance [111] in the ^{3}He $+^3$He reaction, the resonance energy E_r being below the experimentally explored region, i.e. $E_r \leq 25$ keV. Such a resonance is not predicted theoretically; furthermore experimental searches for excited ^{6}Be states in reactions like ^{6}Li(p,n)^{6}Be and others failed [35]. One can however not definitely exclude this possibility [35].

A resonance would affect the various components of the neutrino flux differently. Qualitatively, a very low energy resonance will be more effective in the more external (cooler) solar regions, so that the ^{7}Be neutrino flux can be more suppressed than the ^{8}B flux. The converse is true for a higher energy resonance, the border between the two regimes being provided by the Gamow energy for the ^{3}He $+^3$He reaction, about 22 keV near the solar center.

Table 20
Different determinations of $S(0)_{17}$, from [120

Ref.	$S(0)_{17}$ [eV b]
[114]	15 ± 6
[115]	27 ± 4
[116]	25.2 ± 2.4
[117]	19.4 ± 2.8
[118]	41.5 ± 9.3
[119]	20.2 ± 2.4

The best case for our purpose [112] is that of $E_r = 0$ which corresponds, for a strong resonance, to

$$\frac{\Phi_{Be}/\Phi_{Be}^*}{\Phi_B/\Phi_B^*} = 0.75 . \tag{143}$$

In practice, the effect of such a zero energy resonance can be mimicked by introducing a resonance S-factor, S_{res} and parameterizing the fluxes as:

$$\Phi_{Be} = \Phi_{Be}^* (1 + \tfrac{16}{9} S_{res}/S_{33}^*)^{-1/2}, \tag{144}$$

$$\Phi_B = \Phi_B^* (1 + (S_{res}/S_{33}^*))^{-1/2}. \tag{145}$$

All other fluxes are unchanged, except for the pp+pep flux which can be derived by the luminosity constraint, Eq. (43). In Section 6 we compare the results of solar models with such a hypothetical resonance with experiments.

Before concluding this section, we remark that, in principle, also a narrow resonance below threshold (i.e. $E_r < 0$) could work, since again it is more efficient in the ^{7}Be production region than in the solar center, where ^{8}B is produced. Note however that the resonance has to be very close to the threshold, otherwise it is uninfluential.

The experimental situation on such hypothetical resonances should be clarified by the ongoing LUNA experiment [113] at the underground Gran Sasso National Laboratory.

5.4. The $p + {}^7Be \rightarrow {}^8B + \gamma$ reaction

The determination of S_{17}, the astrophysical factor for the p+^{7}Be $\rightarrow$ ^{8}B +γ reaction, involves several complications: (i) extrapolations are needed to reach the relevant energies in the solar interior ($E_0 = 19$ keV) as measurements have been performed only at $E_{CM} > 100$ keV [114–119], see Johnson et al. [120] for a detailed discussion about the extrapolation procedure; (ii) the number of ^{7}Be nuclei present in the target is most accurately determined by monitoring the build-up of ^{7}Li (the ^{7}Be decay product) as a function of time, using the ^{7}Li(d,p)^{8}Li reaction, see [121]. For this technique to be useful, the cross section for this latter reaction must be known and there has been considerable work on this point since 1978, resulting in a determination with an accuracy of 6% [121]. Note that in the past different values of this normalization cross section have been used by different authors.

The available data from different experiments, all normalized to the same value $\sigma_{dp} = 157 \pm 10$ mb and extrapolated according to [120], are summarized in Table 20. For deriving an average value,
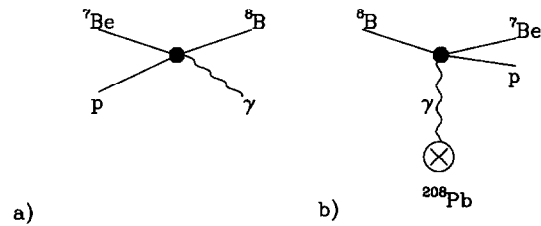
Fig. 21. Proton capture (a) and Coulomb dissociation (b) reactions.

the experimental results of [116] and [119] are particularly important since they correspond to measurements performed over a wide energy interval, reaching the lowest energies. One has to remark that, at each energy, the values of [119] are systematically lower than those of [116]. Keeping into account this uncertainty, Johnson et al. derived:[20]

$$S_{17}(0) = 22.4 \pm 2.1 \text{ eV b} .$$ (146)

This is the value adopted in the reference solar model (Table 28).

The Coulomb dissociation process has recently attracted a great deal of attention as an alternative method to study radiative capture reactions of astrophysical interest at low energies. The process can be treated as the absorption of a virtual photon, essentially the inverse of the radioactive capture process, see Fig. 21. The cross section for Coulomb dissociation of ^8B – the $^{208}Pb(^8B , ^7Be \; p)^{208}P$ reaction – was measured with a radioactive ^8B beam at RIKEN [124] and a preliminary value $S_{17}(0) = 16.7 \pm 3.2$ eV b was deduced from the data. A theoretical analysis of the same data by Langanke and Shoppa [125] yielded an even smaller value, $S_{17}(0) = 12 \pm 3$ eV b, which was however criticized in [126].

All in all, this indirect approach looks very nice, but the extraction of S_{17} is experimentally difficult and theoretically complex, and we agree with the authors of Ref. [125] that *"The recently developed technique of Coulomb dissociation might prove itself as a very useful tool in nuclear astrophysics ... The ^8B Coulomb dissociation experiment at RIKEN takes a first step in this direction and should be continued and refined. However a reliable determination of the astrophysically important cross section for the $^7Be \; (p, \gamma)^8B$ reaction from ^8B Coulomb dissociation experiments has to wait until improved data become available"* [127].

We thus consider Eq. (146) as our reference value, and we will study the effects of varying S_{17}. It is clear that acting on a very minor termination of the fusion chain, the properties of the solar interior (profiles of temperature, density, ...) will be unchanged. This expectation is confirmed by numerical experiments, see for instance Fig. 22. Thus, only the relative intensity of the pp-II and pp-III terminations are affected, and consequently only the ^7Be and ^8B neutrino fluxes will change, their sum being fixed at the SSM value. If the astrophysical factor is scaled by an amount s_{17}, one has

$$\Phi_B/\Phi_{Be} = s_{17}\Phi_B^*/\Phi_{Be}^* , \qquad \Phi_B + \Phi_{Be} = \Phi_B^* + \Phi_{Be}^* .$$ (147)

---

[20] Recently, the value $\sigma_{dp} = 146$ mb has been recommended in Ref. [122]. A reanalysis of all data by Greife and Junker within the NACRE collaboration yields $S_{17}(0) = 19.9$ eV b [123].
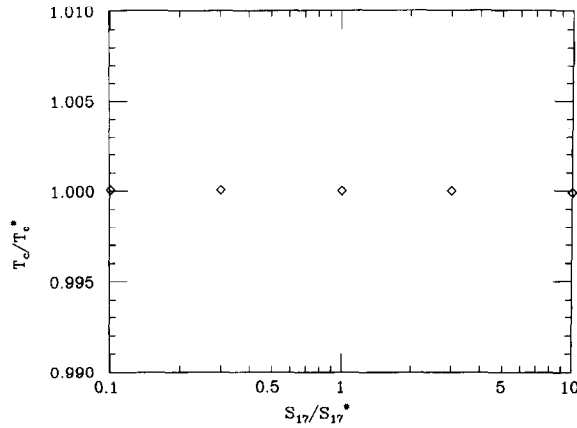
Fig. 22. The central temperature T_c as a function of S_{17}.

Table 21
Power law coefficients for variations of S_{17}. Same notation as in Table 10

S_{17}/S_{17}^*	0.1–10
Φ_p	$(+1.1 \pm 0.4)10^{-4}$
Φ_{Be}	$(-2.5 \pm 2.0)10^{-3}$
Φ_{CNO}	$(-1.7 \pm 0.7)10^{-4}$
Φ_B	(0.996 ± 0.003)

This clearly implies:

$$\Phi_B = \Phi_B^{SSM} \, s_{17} \, \frac{1 + \Phi_B^*/\Phi_{Be}^*}{1 + s_{17}\Phi_B^*/\Phi_{Be}^*}, \qquad \Phi_{Be} = \Phi_{Be}^{SSM} \, \frac{1 + \Phi_B^*/\Phi_{Be}^*}{1 + s_{17}\Phi_B^*/\Phi_{Be}^*}. \qquad (148)$$

We remind that the pp-III termination is very disfavored with respect to the pp-II, so that, to a very good approximation:

$$\Phi_B = s_{17} \, \Phi_B^*, \qquad \Phi_{Be} = \Phi_{Be}^*. \qquad (149)$$

These analytical estimates are (obviously) confirmed by numerical experiments, see Table 21. Note that the slight dependences of Φ_{pp} and Φ_{CNO} are not significant, being at the level of the numerical accuracy.

In conclusion, only the flux of ^8B neutrinos is significantly affected when S_{17} is changed, the dependence being linear to a very good approximation. Clearly, playing with S_{17} cannot be the solution of the solar neutrino puzzle, as the production of intermediate energy neutrinos is unchanged.

5.5. The $p+^{14}N \rightarrow ^{15}O + \gamma$ reaction

We will briefly review the status of this reaction since it is the slowest process in the main CN cycle, and thus it controls the production of CNO neutrinos.

The Gamow peak in the solar center corresponds to $E_0 = 27$ keV, whereas laboratory measurements have been performed at energy in excess of 100 keV, so that extrapolations are necessary.

The data of earlier investigations [128–133] were extrapolated by various groups, yielding different values for $S_{1,14}(0)$ ranging from about 2 to 10keVb [35]. This discrepancy illustrates the difficulty in determining absolute cross sections. Fowler et al. in 1975 [134] recommended $S_{1,14}(0)=3.32$ keV b, by means of some unspecified, judicious treatment of experimental data and/or theoretical input. Schröder et al. [135] performed a comprehensive experimental study, the only one covering continuously the energy range $E = 200$–3600 keV and measuring absolute cross sections, γ-ray angular distribution and excitation functions. This work removed most of the appearent discrepancies among previous experiments. The extrapolated result, $S_{1,14}(0) = 3.20 \pm 0.54$ keV b, is *"essentially identical with the previously recommended value of* 3.32 keV b" [98, 135]. In his latest compilation Fowler [41] adopted the value found by Schröder et al. On the other hand, Bahcall and Pinsonneault [14] quoted:

$$S_{1,14}(0) = 3.32 \pm 0.40 \text{ keV b} \tag{150}$$

and later reduced the central value by 1%, after including the effect of vacuum polarization [15].

Concerning solar neutrinos, the CNO neutrino flux scales linearly with $s_{1,14}$:

$$\Phi_{\text{CNO}} = \Phi_{\text{CNO}}^* s_{1,14} . \tag{151}$$

In order to keep the same luminosity, also pp and pep neutrino fluxes are slightly changed:

$$\Phi_{\text{p}} = \Phi_{\text{p}}^* s_{1,14}^{-0.02} , \tag{152}$$

all other components being essentially unsensitive to $s_{1,14}$.

5.6. Plasma screening of nuclear charges

5.6.1. The results of different models

The burning rates of bare nuclei derived from experiments need to be corrected to take into account the screening provided by the stellar plasma. The study of screened nuclear reaction rates was started with the pioneer work of Salpeter [136]; it has been addressed by several authors, see e.g. [137–140], and recently reviewed in [90,141]. In the sun the screening effects are small, however different calculations yield relatively different nuclear reaction rates.

As a starting point let us neglect any screening effect, i.e. reactions take place for bare ions with rates λ_{NOS}. The results of the corresponding solar model are shown in Table 22 (NOS). Due to the screening, the actual rates λ will be larger:

$$\lambda = \lambda_{\text{NOS}} f , \tag{153}$$

where the enhancement factors f depend on the reaction and on the plasma properties. Various approaches have been developed for evaluating these factors.

In the weak-screening approximation (WES), originally introduced by Salpeter [136], one has for a Debye plasma wherein partial electron degeneracy is included:

$$\ln f^{\text{WES}} = Z_1 Z_2 e^2 / (R_{\text{D}} kT) , \tag{154}$$

Table 22
Comparison among solar models with different screening predictions: NOS = no screening, WES = weak screening [136], MIT = Mitler [14], GDGC = Graboske et al. [138] and CSK=Carraro et al. [139]. We show the central temperature $T_c[10^7 \text{ K}]$, the helium abundance in mass Y, the metal fraction Z, the values of each component of the neutrino flux $(10^9 \text{ cm}^{-2} \text{ s}^{-1})$, the calculated signals for the chlorine (Cl) and the gallium (Ga) experiments (SNU), from [90]

	NOS	WES	MIT	GDGC	CSK
T_c	1.573	1.566	1.566	1.564	1.567
Y	0.288	0.289	0.289	0.289	0.289
Z $(\times 10^2)$	1.85	1.85	1.84	1.84	1.85
pp	60.0	59.6	59.7	60.0	59.7
pep	0.146	0.142	0.142	0.143	0.143
^{7}Be	4.82	4.97	4.93	4.79	4.94
^{8}B $(\times 10^3)$	5.51	6.36	6.13	5.59	6.21
^{13}N	0.46	0.55	0.52	0.47	0.54
^{15}O	0.39	0.48	0.45	0.40	0.47
Cl	7.7	8.8	8.5	7.8	8.6
Ga	130	134	133	130	134

where $Z_{1,2}$ are the charges of the reacting nuclei, T is the temperature and R_D is the Debye radius, see Ref. [142]. In this scheme, the reacting particles are assumed to move slowly in comparison to the plasma particles (adiabatic approximation). Also modifications of the Coulomb potential are assumed to be sufficiently weak so that the linear approximation holds (see [120] for a more extensive discussion about the validity of this approach). In the sun, the weak-screening approximation is justified (to some extent) for the pp-reaction, whereas the other nuclear reactions occur in the so-called intermediate screening regime.

Graboske et al. [138] (GDGC) used Eq. (154) when $f^{WES} < 1.1$; for larger values (up to 2) they derived the enhancement factors by using general thermodynamic arguments and interpolation of Monte Carlo calculations. The explicit expressions can be found in Ref. [138].

Mitler [140] (MIT) developed an analytical method which goes beyond the linearized approach and which correctly reproduces both the limits of weak and strong screening. Neglecting the small effects of a radial dependence in the effective potential, see [141], the enhancement factors are given then by

$$\ln f^{MIT} = -\frac{8}{5}(\pi e n_e)^2 R_D^5 [(\zeta_1 + \zeta_2 + 1)^{5/3} - (\zeta_1 + 1)^{5/3} - (\zeta_2 + 1)^{5/3}]/(kT), \qquad (155)$$

where $\zeta_{1,2} = 3Z_{1,2}/(4\pi n_e R_D^3)$ and n_e is the average electron density.

In the Salpeter approach one assumes the reacting nuclei to be so slow that the plasma can fully rearrange itself while the nuclei are moving (as in the Born–Oppenheimer approximation used in molecular physics) and dynamical effects (corrections to the Born–Oppenheimer approximation) are completely neglected. Carraro et al. [139] (CSK) observed that the reacting nuclei actually move faster than most of the plasma ions (the Gamow peak energy is generally larger than thermal energy), so that ionic screening plays a smaller rôle under this condition. They calculated the dynamic response of the plasma in the framework of the linearized theory. The resulting enhancement factors
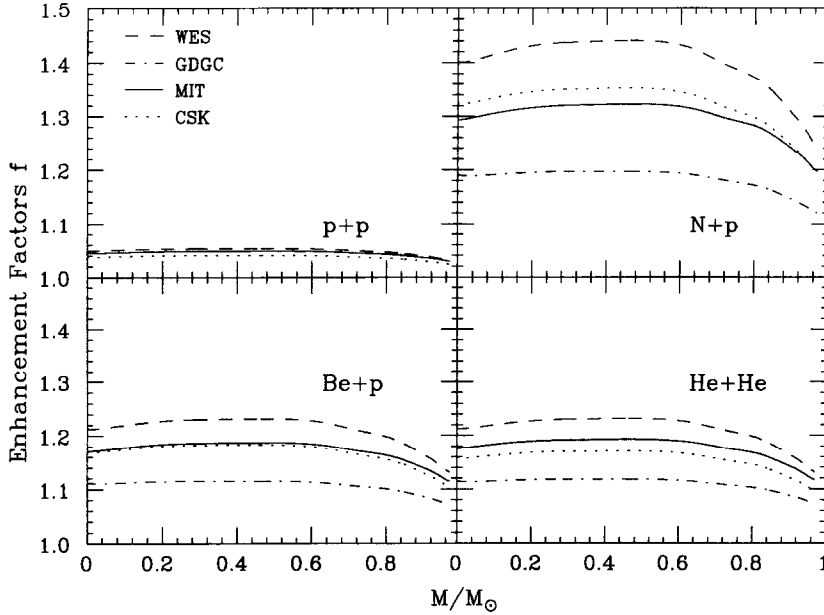
Fig. 23. Enhancement factors along the solar profile. The results of weak screening [136] (dashed curves), Graboske et al. [138] (dot-dashed curves), Mitler [139] (solid curves) and Carraro et al. [139] (dotted curves) are shown, from [90].

are expressed in terms of those of the weak screening:

$$\ln f^{\text{CSK}} = C \ln f^{\text{WES}} .$$ (156)

The coefficients C essentially specify the corrections to the adiabatic limit, which obviously corresponds to $C = 1$. At the center of the sun the correction factors are [139]: $C_{p+p} = 0.76$, $C_{^3He+^3He} = 0.75$, $C_{^3He+^4He} = 0.76$, $C_{p+^7Be} = 0.80$, $C_{p+^{14}N} = 0.82$. Note that the isotopic dependence is rather weak (in all previous models there was no isotopic dependence).

We shall not discuss the strong screening limit which is definitely too far from solar conditions (see e.g. [142]).

From Table 22, where we report the results of solar models corresponding to the different approaches, one notes the following features:

(i) The largest differences arise between the no screening model and the weak screening model. Φ_B can vary by at most 15%, the chlorine signal is stable to within 13% and the gallium signal at the level of 3%.

(ii) The GDGC model, extensively used in stellar evolution codes, yields values very close to the no screening model; the difference between the two is at the level of 1% for Φ_{Be} and Φ_B, as well as for the chlorine and gallium signals.

In Fig.23 we show the enhancement factors along the solar profile, calculated by using the different prescriptions outlined above, for the reactions relevant to hydrogen burning in the sun; as concerns the CN cycle, we pay attention only to the slowest reaction: $p + {}^{14}N \rightarrow {}^{15}O + \gamma$. All the enhancement factors depend very weakly on the mass coordinate, at least in the energy production region ($M/M_\odot < 0.3$). This is clear in the weak screening regime, since the dependence on the solar structure parameters

Table 23
Enhancement factors for different screening prescriptions, calculated in central solar conditions. Same notations of Table 22, from [90]

	WES	MIT	GDGC	CSK
p+p	1.049	1.045	1.049	1.038
He+He	1.213	1.176	1.115	1.158
^{7}Be+p	1.213	1.171	1.112	1.169
^{14}N+p	1.403	1.293	1.192	1.324

is just of the form ρ/T^3 (see Eq. (154) and remind $R_D \propto \sqrt{T/\rho}$) and this quantity is approximately constant along the solar profile. The same holds in the strong regime [142], and thus the approximate constancy in the intermediate regime is not a surprise. For these reasons, in the following we shall concentrate on the enhancement factors calculated at the solar center (see Table 23).

The weak-screening approximation, Eq. (154), always yields the largest enhancement factors, as it is physically clear since electrons and ions are assumed to be free and capable of following the reacting nuclei and in addition the electron cloud is allowed to strongly condense around the nuclei (in the linear approximation the electron density becomes infinite at the nuclear site). By using the Mitler model, where electron density at the nuclear site is fixed at n_e, one obtains smaller enhancement factors. The same holds for the model where the limited mobility of ions and thus their partial screening capability is taken into account. The GDGC enhancement factors are systematically smaller than the others (except for the pp reactions where, by definition, they are equal to the weak screening prescription). It is thus clear that the corresponding neutrino fluxes and experimental signals are the closest ones to those of the no-screening models. One notes that the enhancement factors for He+He and p+^{7}Be are very close: actually, in the weak screening approximation only the product of nuclear charges enters.

All in all, the enhancement factors are relatively close to unity, however none of the approaches to screening discussed above is completely satisfactory. The weak screening approximation is not justified for reactions other than the pp, since $Z_1 Z_2 e^2/(R_D kT)$ is not small. The GDGC results stems from an interpolation of numerical computations and the prescription of the authors yields an unphysical discontinuity at the border between the weak and intermediate regimes [141]. The CSK result, which incorporates dynamic effects of finite nuclear velocity, is however derived in the framework of a linear theory, i.e. the weak screening approximation. The Mitler approach goes beyond the weak screening approximation; on the other hand, the partial mobility of ions due to ion-interaction effects and/or to the finite thermal velocity is not taken into account. Also, the value of the electron density at the nucleus is somehow artificially kept equal to the average electron density n_e.

5.6.2. A model independent analysis

The role of screening on solar neutrinos can be investigated, more generally, in a model independent way [90]. In the previous section we saw that a few features are common to any screening model:

(i) the enhancement factors f can be taken constant in the energy production region, so that one needs to specify the values at the solar center only.

(ii) They are almost insensitive to isotopic effects, i.e. approximately

$$f_{^3\mathrm{He}+^3\mathrm{He}} \simeq f_{^3\mathrm{He}+^4\mathrm{He}} \tag{157}$$

and we will refer generically to an enhancement factor for helium–helium reactions, $f_{\mathrm{He}+\mathrm{He}}$.

(iii) To a good approximation, the enhancement factor is determined by the product of the electric charges of the reacting nuclei, so that we can take

$$f_{\mathrm{p}+^7\mathrm{Be}} = f_{\mathrm{He}+\mathrm{He}} \ . \tag{158}$$

In this case one is left with just three numbers, $f_{\mathrm{p}+\mathrm{p}}$, $f_{\mathrm{He}+\mathrm{He}}$ and $f_{\mathrm{p}+^{14}\mathrm{N}}$, *which we shall consider as free parameters.* We recall that $f \geq 1$ since in the plasma the Coulomb repulsion between the reacting nuclei is diminished.

The introduction of (spatially constant) enhancement factors is equivalent to an overall change of the astrophysical S-factors:

$$S_{ij} \rightarrow S_{ij} f_{i+j} \tag{159}$$

and we can exploit the results for the variations of the astrophysical S-factors presented previously.

Concerning the role of $f_{\mathrm{p}+\mathrm{p}}$, we recall that an increase of S_{pp} immediately implies a reduction of the central temperature T_{c}. From Table 10,

$$T_{\mathrm{c}}/T_{\mathrm{c}}^{\mathrm{NOS}} = (f_{\mathrm{p}+\mathrm{p}})^{-1/9} \ , \tag{160}$$

where the superscript NOS refers to the no-screening solar model. From the same table, by using the dependence of neutrino fluxes on S_{pp}, one immediately gets the effect of the screening factor:

$$\Phi_{\mathrm{Be}} = \Phi_{\mathrm{Be}}^{\mathrm{NOS}} (f_{\mathrm{p}+\mathrm{p}})^{-1.1} \ , \tag{161}$$

$$\Phi_{\mathrm{B}} = \Phi_{\mathrm{B}}^{\mathrm{NOS}} (f_{\mathrm{p}+\mathrm{p}})^{-2.7} \ , \tag{162}$$

$$\Phi_{\mathrm{CNO}} = \Phi_{\mathrm{CNO}}^{\mathrm{NOS}} (f_{\mathrm{p}+\mathrm{p}})^{-2.2} \ . \tag{163}$$

Concerning the $^3\mathrm{He} +^3\mathrm{He}$ and $^3\mathrm{He} +^4\mathrm{He}$ reactions, we recall from the foregoing section that the $^7\mathrm{Be}$ equilibrium concentration scales as

$$n_7 \propto S_{34}/\sqrt{S_{33}} \propto \sqrt{f_{\mathrm{He}+\mathrm{He}}} \ . \tag{164}$$

This is clearly the dependence of $^7\mathrm{Be}$ neutrino flux; for Φ_{B} one has to remind that it is proportional to S_{17} and thus an extra power of $f_{\mathrm{He}+\mathrm{He}}$ occurs:

$$\Phi_{\mathrm{Be}} = \Phi_{\mathrm{Be}}^{\mathrm{NOS}} (f_{\mathrm{He}+\mathrm{He}})^{1/2} \ , \tag{165}$$

$$\Phi_{\mathrm{B}} = \Phi_{\mathrm{B}}^{\mathrm{NOS}} (f_{\mathrm{He}+\mathrm{He}})^{3/2} \ . \tag{166}$$

The enhancement factor for $\mathrm{p}+^{14}\mathrm{N}$ only matters for the CN cycle:

$$\Phi_{\mathrm{CNO}} = \Phi_{\mathrm{CNO}}^{\mathrm{NOS}} f_{\mathrm{p}+^{14}\mathrm{N}} \ . \tag{167}$$

We can put together all the previous results in the following way:

$$\Phi_{\mathrm{Be}} = \Phi_{\mathrm{Be}}^{\mathrm{NOS}} (f_{\mathrm{He}+\mathrm{He}})^{1/2} (f_{\mathrm{p}+\mathrm{p}})^{-1.1} \ , \tag{168}$$

$$\Phi_B = \Phi_B^{NOS}(f_{He+He})^{3/2}(f_{p+p})^{-2.7} , \tag{169}$$

$$\Phi_{CNO} = \Phi_{CNO}^{NOS} f_{p+^{14}N}(f_{p+p})^{-2.2} . \tag{170}$$

The behaviour of pp-neutrinos, as usual, can be best derived by using the conservation of luminosity.

By using the above equations with the enhancement factors given in Table 23, one can quantitatively reproduce, to a large extent, the numerical results presented in Table 22. Furthermore, we have verified that these analytical results are quite accurate for a wide range of the f factors, by using our stellar evolution code.

Note also that although ^{3}He $+^3$He and ^{3}He $+^4$He have the same enhancement factor, the equilibrium concentration of ^{7}Be, and thus Φ_{Be} and Φ_B, are changed when screening is introduced.

6. Non-standard solar models and experimental results

6.1. Introduction

We compare now the predictions of non-standard solar models with the experimental results on solar neutrinos. The basic questions are:

- Is there a solar model that accounts for all available results, *assuming standard neutrinos*?
- What would change if one of the experiments were wrong?
- If – as it happens – no model is successful, what is the reason of the failure?

For this purpose, we consider solar models characterized by three parameters:

(1) the central solar temperature, T_c, which accounts for (most of) the effect of changing the astrophysical factor S_{pp} for the $p+p \to ^2H + e^+ + \nu_e$ cross section, the solar opacity or the age of the sun; neutrino fluxes are determined essentially by T_c, independently of the way in which that particular temperature is achieved (see Fig. 15 and Refs. [73, 143, 144]);

(2) the astrophysical factor S_{33}, which can be used as an effective parameter controlling both cross sections for the He+He reactions: by varying S_{33}, at fixed S_{34}, one can tune the parameter $\chi = S_{34}/\sqrt{S_{33}}$, which determines the neutrino fluxes when the cross sections for the ^{4}He $+ ^3$He and/or ^{3}He $+ ^3$He channels are altered (see Section 5.3);

(3) the astrophysical factor S_{17} for the $p+^7$Be $\to ^8$B $+ \gamma$ reaction.

These three parameters are really independent of each other; we recall that T_c is essentially unaffected by variations of S_{33} and/or S_{17}.

Possible variations of screening factors will not be discussed extensively since, as shown in the previous section, they can be rephrased in terms of variations of astrophysical S-factors (see however Ref. [90]).

The dependence of the neutrino fluxes on the three parameters is shown in Fig. 24. For T_c we use the exponents corresponding to (large) variations of S_{pp} (see Table 10). For the dependence on the cross sections of the two He+He reactions, we explicitly consider the case of a zero-energy resonance in the ^{3}He $+ ^3$He channel, as given by Eqs. (144) and (145) and use the resonant contribution S_{33}^{res} as a free parameter. This possibility has the best chance of producing agreement with the data, since it suppresses more strongly Φ_{Be} than Φ_B: a non-resonant variation is even less effective [111,112,73]. The pp-neutrino flux, Φ_{pp}, is determined by imposing the luminosity constraint, see Eq. (101). Note

$$\Phi_{Be} = \Phi_{Be}^{RSM} \left(\frac{T_c}{T_c^{RSM}}\right)^9 \left(1 + \frac{16}{9}\frac{S_{33}^{res}}{S_{33}^{RSM}}\right)^{-0.5}$$

$$\Phi_{B} = \Phi_{B}^{RSM} \left(\frac{T_c}{T_c^{RSM}}\right)^{22} \left(1 + \frac{S_{33}^{res}}{S_{33}^{RSM}}\right)^{-0.5} \left(\frac{S_{17}}{S_{17}^{RSM}}\right)$$

$$\Phi_{N} = \Phi_{N}^{RSM} \left(\frac{T_c}{T_c^{RSM}}\right)^{15}$$

$$\Phi_{O} = \Phi_{O}^{RSM} \left(\frac{T_c}{T_c^{RSM}}\right)^{24}$$

$$\Phi_{pep} = \Phi_{pep}^{RSM} \left(\frac{T_c}{T_c^{RSM}}\right)^{2.2}$$

$$\Phi_{pp} = \Phi_{pp}^{RSM} - \sum_i \frac{Q_i}{Q_{pp}}(\Phi_i - \Phi_i^{RSM}) \qquad i = Be, B, N, O, pep$$

Fig. 24. Dependence of the main solar fluxes on T_c, S_{17} and S_{33} (this latter parameterized by its zero-energy resonant contribution S_{33}^{res}). The coefficients Q_i are defined in Eq. (34).

that S_{17} affects only the ^8B neutrino flux significantly. As reference fluxes Φ_i^{RSM}, we use the ones of the reference standard model (RSM) of Bahcall and Pinsonneault ("best model with diffusion"), which are given in Table 3 [15].

We remark that the precise values of the exponents and coefficients in Fig. 24 are not important for our discussion; somewhat different exponents could origin, if the change in T_c was induced by means other than changing the astrophysical factor S_{pp}, or if these power laws were fitted on different ranges of parameters. Such different choices do not affect the essence of our conclusions.

In the following sections, we first vary one single parameter at a time, and then analyze all possible combined variations. In addition, we repeat the analysis after having arbitrarily discarded any one of the experiments and, finally, we discuss the reasons of the failure of all our attempts. This section updates and extends the analyses of Refs. [73, 74, 145–147].

6.2. Fitting all experimental results

Let us consider the ensemble of solar models originating fluxes Φ_i as parameterized in Fig. 24. We performed a χ^2 analysis to establish quantitatively how well these models compare with experimental data. A given solar model predicts theoretical signals S_X^{th} (X = gallium, chlorine and KAMIOKANDE) according to the formula

$$S_X^{th} = \sum_i \sigma_{X,i}\,\Phi_i\,, \tag{171}$$

with the averaged neutrino cross sections $\sigma_{X,i}$ given in Table 5. These theoretical signals are to be compared with the experimental signals S_X^{ex} reported in Table 6. GALLEX and SAGE results have been combined into a single gallium signal as in Eq. (26). As usual, we define the likelihood function as

$$\chi^2(T_c, S_{33}^{res}, S_{17}) = \sum_{XY}(S_X^{ex} - S_X^{th})V_{XY}^{-1}(S_Y^{ex} - S_Y^{th})\,. \tag{172}$$

The covariance matrix V_{XY} takes into account both experimental and theoretical uncertainties. These latter always include the errors on the averaged neutrino cross sections $\sigma_{X,i}$. Theoretical uncertainties on neutrino fluxes reflect uncertainties on T_c, S_{33}^{res} and S_{17}. When some of these variables are used as

Table 24

Best fits to the combined experimental results obtained by varying the seven possible combinations of the parameters T_c, S_{33}^{res} and S_{17}. For comparison, the first two rows also show the experimental and RSM results. The first column reports the χ^2/d.o.f. (just the χ^2 when the number of parameters is greater or equal to the number of data). The second column reports the best-fit values of the parameters in units of the RSM, and the last three columns the corresponding signals for the gallium, chlorine and KAMIOKANDE experiments

	χ^2/d.o.f.	Best-fit values	S_{Ga} (SNU)	S_{Cl} (SNU)	Φ_B^{Ka} 10^6 cm^{-2} s^{-1}
Experiment			74 ± 8	2.55 ± 0.25	2.73 ± 0.38
RSM	58.5/3		137.0	9.3	6.62
S_{17}	50.7/2	0.28	125	4.00	1.85
T_c	22.0/2	0.936	103	2.71	1.54
S_{33}^{res}	18.1/2	13.9	99	2.90	1.72
T_c S_{33}^{res}	16.1/1	0.973 4	97	2.68	1.66
S_{33}^{res} S_{17}	13.9[a]/1	200 4.2	96	3.03	1.96
T_c S_{17}	10.7[a]/1	0.879 5.0	94	2.74	1.94
T_c S_{33}^{res} S_{17}	7.4[a]	0.929 9 5.0	90	2.76	2.07

[a] Indicates that the value is not a local minimum, but it is the lowest value within the explored region ($S_{17} \leq 5S_{17}^{RSM}$ and $S_{33}^{res} \leq 200S_{33}^{RSM}$).

free parameters only the uncertainties corresponding to the remaining ones are included. The propagation of these latter uncertainties to the fluxes is established by means of power laws similar to those of Fig. 24, optimized for the case of small variations. The matrix V_{XY} is not diagonal because the same parameter can affect more than one flux and the same flux contributes in general to more than one signal. The use of the full covariance matrix is really necessary, since otherwise apparently good fits can be achieved in an unphysical way [73, 144, 148, 149]. Error correlation means, for instance, that we cannot use the uncertainty in Φ_B to strongly reduce its contribution to the Davis experiment, while having at the same time a smaller reduction in the KAMIOKANDE experiment. More details on the calculation of the covariance matrix can be found in Ref. [73].

We explored a wide region for the three parameters: T_c down to 8% of the RSM value, S_{17} from zero up to five times the RSM value and S_{33}^{res} from zero up to 200 times the value of S_{33}^{RSM}. With three experimental results, one has two degrees of freedom (d.o.f.) when the three parameters are varied one at the time, and no d.o.f. when all three are varied simultaneously. The results of this analysis are summarized in Table 24 which needs the following comments.

(1) None of the attempts succeeds in giving an acceptable χ^2 even when we use as many parameters as the experimental data.

(2) The smallest χ^2, obviously obtained when all parameters are left free, corresponds anyhow to quite unphysical variations: T_c comes out 7% smaller than the RSM value and the S_{17} astrophysical factor is five times larger.

Table 25
The best fits when just two experimental results are included. Same notations as in Table 24

	Ga + Ka		Cl + Ga		Cl + Ka	
	χ^2/d.o.f.	Best	χ^2/d.o.f.	Best	χ^2/d.o.f.	Best
RSM	39.6/2		50.2/2		41.9/2	
S_{17}	35.0/1	0.50	30.5/1	0.12	22.8/1	0.21
T_c	18.6/1	0.950	10.9/1	0.929	9.4/1	0.939
S_{33}^{res}	13.3/1	6.8	8.18/1	22.2	8.87/1	13
T_c S_{33}^{res}	12.9	0.987 4	7.3	0.975 6	7.5	0.972 3
S_{33}^{res} S_{17}	8.2[a]	150 5.0	6.4[a]	200 3.3	7.2	198 4.1
T_c S_{17}	7.8[a]	0.890 5.0	5.3[a]	0.874 5.0	4.8[a]	0.880 5.0
T_c S_{33}^{res} S_{17}	4.9[a]	0.936 8 5.0	3.4[a]	0.928 11 5.0	3.6[a]	0.922 6 5.0

(3) All the best fits give too high signals for the gallium and chlorine experiments and too low a ^{8}B flux as compared to KAMIOKANDE; in other words, *the KAMIOKANDE signal looks too high for an astrophysical solution.*

(4) When varying only one parameter at a time, a resonant increase of the ^{3}He + ^{3}He cross section is the most effective way, as it allows a higher suppression of ^{7}Be relative to ^{8}B neutrino flux. The central temperature is less effective, since it gives a too large suppression of the ^{8}B neutrino flux. S_{17} only affects the ^{8}B neutrino flux and it is totally useless for the present solar neutrino problem, *which is mostly a problem of the intermediate energy neutrinos.*

(5) A significantly reduced χ^2 is obtained by changing S_{17} together with T_c or S_{33}. Note, however, that the smallest χ^2 is obtained at the border of the parameter space, i.e. in an extremely unphysical region. On the other hand, there is no significant gain when varying at the same time T_c and S_{33}^{res} as they both mainly shift the balance towards the pp-I chain.

6.3. What if one experiment were wrong?

There is no rational reason for doubting any of the experimental data. Nevertheless in the same spirit as discussed in Section 2, we have repeated the analysis of the previous section excluding in turn the KAMIOKANDE, chlorine and gallium result. (Note that, excluding the gallium result, we are giving up two experiments, GALLEX and SAGE.)

The results of this exercise, reported in Table 25, show that the situation is essentially unchanged:

(1) Again none of the attempts succeeds in giving an acceptable χ^2, even when we use more parameters than experimental data.

(2) As previously, the best fit corresponds anyhow to extremely unphysical values of the input parameters.

(3) The smallest χ^2 are obtained disregarding either the KAMIOKANDE or gallium data. In other words, these two results taken together are the hardest to reconcile with astrophysics. *The point is that Gallium result implies that only the* pp-I *chain is effective, whereas KAMIOKANDE shows that* pp-III, *and hence* pp-II, *are operational.*

6.4. What went wrong with solar models?

Tables 24 and 25 present the quantitative evidence that any solar model (which we are able to parametrize) cannot account for the experimental data, even when one of these data is arbitrarily removed. In this section we discuss the physical motivations of such failure, giving through Figs. 25–27 a graphical illustration of the results of Tables 24 and 25.
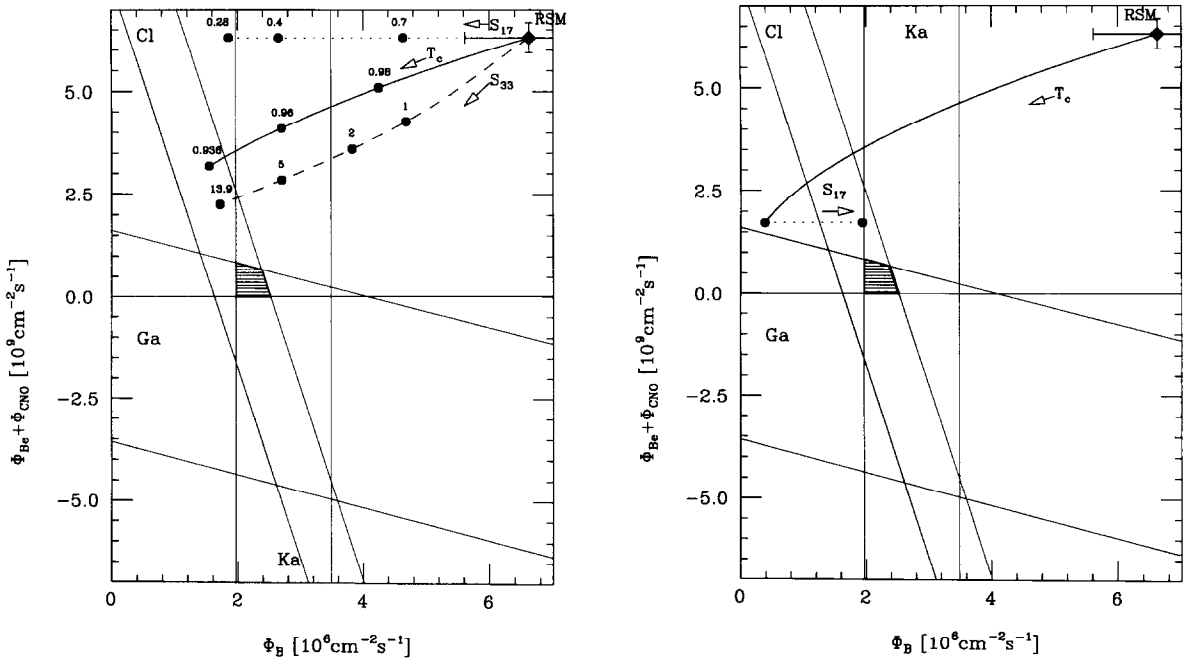

Fig. 25. ^{7}Be plus CNO neutrino fluxes versus ^{8}B neutrino flux. The three stripes, labeled Ga, Cl and Ka, confine the regions allowed at the 2σ level by the three current experimental data (GALLEX + SAGE, chlorine, and KAMIOKANDE) with the constraint due to the luminosity sum rule. The hatched area emphasizes the interception of the three regions. The diamond shows the RSM prediction. The solid (dashed, dotted) line shows the effect of decreasing T_c (increasing the resonant part of S_{33}, decreasing S_{17}). Dots indicate the fluxes at specific values of the parameters shown by the label in units of their RSM values.

Fig. 26. Similar to Fig. 25, but this time two parameters are changed in the same model. The temperature is decreased down to $T_c = 0.88$ (solid curve) and, then, S_{17} is increased up to five times its RSM value (dotted line).
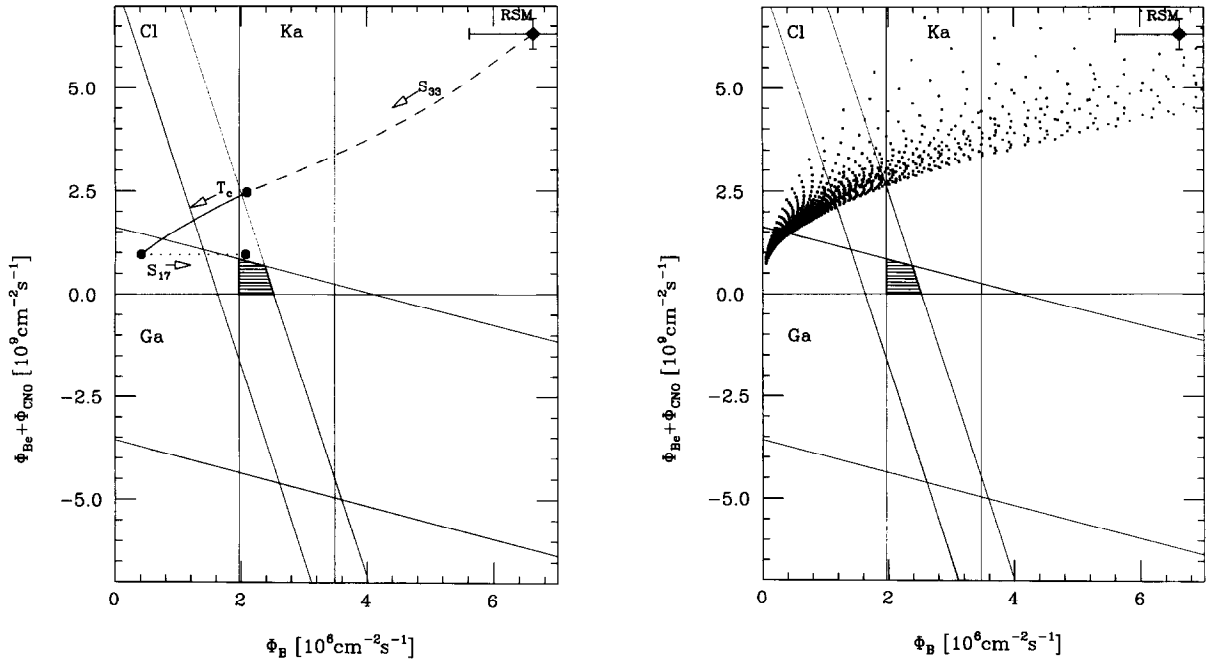
Fig. 27. Similar to Fig. 25, but this time all three parameters are changed in the same model. First S_{33}^{res} is increased from zero up to nine times the RSM value of S_{33} (dashed curve), then T_c is decreased down to 0.929 (solid curve) and, finally, S_{17} is increased up to five times its RSM value (dotted line). The order of the transformations is obviously inconsequential.

Fig. 28. The dotted area shows the result of arbitrarily varying the enhancement factors f_{p+p}, f_{He+He} and $f_{p+^{14}N}$ up to $f = 6$. We recall that in standard solar model calculations $f \lesssim 1.2$, see Section 5.

The starting point is that any combination of two experimental data requires, with respect to the RSM, a strong suppression of the intermediate-energy–neutrino flux (^{7}Be and CNO), much stronger than that of the ^{8}B flux, as was extensively discussed in Section 2.

In the (Φ_B, Φ_{Be+CNO}) plane, assuming standard neutrinos, the regions allowed at the 2σ level by each experiment and their intersection are indicated in Fig. 25.

The aim of non-standard solar models is to push the predictions close to this area allowed by experiments.

In Fig. 25 we show the effect of changing one of the three parameters in turn. A reduction of S_{17} only affects the ^{8}B flux and we are left with a much too high Φ_{Be+CNO}. Reducing the temperature decreases both Φ_B and Φ_{Be}, however Φ_B is suppressed more strongly than Φ_{Be} contrary to experimental evidence. The resonant increase of the ^{3}He + ^{3}He cross section succeeds in reducing Φ_{Be} almost to zero while leaving part of Φ_B; however, Φ_{Be+CNO} is still too high since $\Phi_{CNO} = \Phi_{CNO}^{RSM}$ is by itself sufficient to spoil the agreement with the data.

In Fig. 26 we show the effect of changing two parameters at the same time. The best case is when T_c and S_{17} are changed. In fact, only T_c is able to cut both Φ_{Be} and Φ_{CNO}, and S_{17} helps to bring Φ_B back up. We stopped at $T_c = 0.88$ and $S_{17} = 5S_{17}^{RSM}$ (which are already completely unphysical

values!) and yet have not reached the allowed region (which of course could be attained by even smaller T_c together with larger S_{17}).

Finally, we show the effect of changing all three parameters in Fig. 27. This case does not differ from the previous one; the main difference is that since we use S_{33}^{res} to cut Φ_{Be} and use T_c mostly to cut Φ_{CNO} we can reach even a lower value of Φ_{Be+CNO} with a relatively higher temperature. However, within the framework of present physical knowledge, one cannot find a justification to accept a non-standard solar model with the required decrease of temperature (7%).

For the same reasons, playing with screening factors does not help; see Fig. 28 where the three screening factors f_{p+p}, f_{He+He} and $f_{p+^{14}N}$ (see Section 5.6.2) are arbitrarily varied by huge amounts with respect to the RSM estimates. Again the suppression of intermediate energy neutrinos is too weak in comparison with experimental results.

All in all, the fits we found are not acceptable, i.e. the chances of an astrophysical solution look very weak even if we are extremely generous on the region spanned by the physical inputs. In Section 2 we found that the probability of standard neutrinos is at most 2% when all fluxes are left as absolutely free parameters. It is thus not a surprise to reach an even stronger conclusion when some astrophysical input is used.

7. The never ending story?

The sun or the neutrino, who is at fault? To express our opinion on such a matter, let us summarize the main points of this review.

Assuming standard neutrinos:

- the available experimental results appear mutually inconsistent, even if some of the four experiments were wrong. This is a solar-model independent evidence for non-standard neutrinos. This evidence, however, is not an overwhelming one, since there is still a few percent (at most) probability of neutrinos being standard, i.e. we have a "2-σ level effect" (see Section 2). We remark that this conclusion is reached at the cost of giving up all our understanding of stellar physics.
- Even neglecting these inconsistencies, the flux of intermediate energy neutrinos (^{7}Be + CNO), as derived from experiments, is significantly smaller than the predictions of SSMs. The main puzzle is with ^{7}Be neutrinos, for which the theoretical predictions are really robust. If one insists on standard neutrinos, one has definitely to abandon standard solar models, all predicting a much too high ^{7}Be neutrino flux.
- In addition, the suppression of ^{7}Be neutrinos is much stronger than that of ^{8}B neutrinos. Non-standard solar models fail to account for *both* these reductions.
- Even extremely non-standard models cannot account for data, even when one of the experimental data is arbitrarily omitted. All the fits that we attempted are unacceptable (see Section 6), i.e. the chances of a nuclear or astrophysical solution appear to us very weak, although we have been extremely generous in the region spanned by the physical inputs. Since we have found that the probability of standard neutrinos is about 2% or less when all fluxes are left as free parameters, it is not a surprise to reach an even stronger limit when some astrophysical input is used.

Let us wait (and hope) for future experiments, bringing *direct*, decisive evidence of some non-standard neutrino property.

Acknowledgements

Appendix A. Our standard solar model

We present the solar model resulting from an updated version of FRANEC[21] (Frascati Raphson Newton Evolutionary Code), where the diffusion helium and heavy elements is included and the OPAL equation of state (EOS) [36, 150] is used. The EOS is consistent with the adopted opacity tables, i.e. the most recent evaluation from the same Livermore group [151] and this should further enhance the reliability of the model. In addition, updated values of the relevant nuclear cross sections are used and more refined values of the solar constant and age are adopted.

We discuss the effects of each of these improvements, showing that they are essential in order to get agreement with the helioseismological information about the bottom of the convective zone. We also calculate neutrino fluxes and the expected signals in ongoing experiments.

FRANEC has been described in previous papers (e.g. see Ref. [152, 153]). Recent determinations of the solar luminosity ($L_\odot = 3.844 \times 10^{33}$ erg s^{-1}) and of the solar age ($t_\odot = 4.57 \times 10^9$ yr) are used [15]. The present ratio of the solar metallicity to solar hydrogen abundance by mass corresponds to the most recent value of Ref. [45]: $(Z/X)_{photo} = 0.0245$.

Following the standard procedure, for each set of assumed physical inputs, the initial Y, Z and the mixing length parameter α were varied until the radius, luminosity and $(Z/X)_{photo}$ at the solar age matched the observed values within a tenth of percent or better. We considered the following steps:

(a) As a starting point we used the Straniero equation of state [75], the OPAL opacity tables which were available in 1993 [39, 40] for the solar metallicity ratio of Ref. [45], combined with the molecular opacities of Ref. [154]; diffusion was ignored. This model may be useful for a comparison with the Bahcall and Pinsonneault model without diffusion, described in Ref. [15], as the chemical composition is the same, although it is not the most updated one.

(b) Next, we introduced the OPAL equation of state. With respect to other commonly used EOS, this one avoids an ad hoc treatment of the pressure ionization and it provides a systematic expansion in the Coulomb coupling parameter that includes various quantum effects generally not included in other computations (see Refs. [36, 150] for more details).

---

[21] Based on the work of Ciacio et al. [56].

Table 26
Comparison among solar models obtained with different versions of the FRANEC code. The labels (a)–(e) corresponds to the models defined in the Appendix A. Our best standard solar model is (e). The last column shows the helioseismological results

	(a)	(b)	(c)	(d)	(e) Our best	Helioseism.
$t_\odot$ (Gyr)	4.57	4.57	4.57	4.57	4.57	
$L_\odot$ (10^{33} erg cm^{-2} s^{-1})	3.846	3.843	3.844	3.843	3.844	
$R_\odot$ (10^{10} cm)	6.961	6.963	6.959	6.959	6.960	
$(Z/X)_{photo}$	0.0245	0.0245	0.0245	0.0245	0.0245	
α	2.023	1.774	1.786	1.904	1.901	
X_{in}	0.699	0.718	0.722	0.711	0.711	
Y_{in}	0.284	0.265	0.261	0.269	0.269	
Z_{in}	0.0171	0.0176	0.0177	0.0198	0.0198	
X_{photo}	0.699	0.718	0.722	0.743	0.744	
Y_{photo}	0.284	0.265	0.261	0.238	0.238	0.233–0.268
Z_{photo}	0.0171	0.0176	0.0177	0.0182	0.0182	
$R_b/R_\odot$	0.738	0.726	0.728	0.716	0.716	0.710–0.716
T_b (10^6 K)	1.99	2.10	2.08	2.17	2.17	
c_b (10^7 cm s^{-1})	2.11	2.16	2.16	2.22	2.22	2.21–2.25
T_c (10^7 K)	1.555	1.545	1.542	1.569	1.569	
ρ_c (100 g cm^{-3})	1.524	1.472	1.470	1.514	1.518	
Y_c	0.63	0.61	0.61	0.63	0.63	

(c) We used the latest OPAL opacity tables [151], solar metallicity ratio as in [45] and again the molecular opacities of Ref. [154] for temperature below 10^4 K. With respect to Ref. [40] the new OPAL tables include the effects on the opacity of seven additional elements and some minor physics changes; moreover the temperature grid has been made denser.

(d) We included the diffusion of helium and heavy elements. The diffusion coefficients have been calculated using the subroutine developed by Thoul, see Ref. [51]. The diffusion equations were integrated numerically. At any time step, after updating the physical and chemical quantities as usually done in FRANEC, we took into account the effect of diffusion. Our time steps are about 3×10^7 yr. The variations of the abundance of H, He, C, N, O and Fe are followed; all these elements are treated as fully ionized. According to Ref. [51] all other elements are assumed to diffuse at the same rate as the fully ionized iron. To account for the effect of heavy element diffusion on the opacity coefficients, we calculated the total heavy elements abundance in each spherical shell in which the solar model is divided and we interpolated (by a cubic spline interpolation) between opacity tables with different total metallicity ($Z = 0.01, 0.02, 0.03, 0.04$).

(e) Finally, we investigated the effect of updating the nuclear cross sections for ^{3}He+^{3}He and ^{3}He+^{4}He reactions, following a recent new analysis of all available data, described in Section 5. For S_{34}, we used the exponential parametrization of Eq. (134).

The resulting solar models are summarized in Table 26 and deserve the following comments.

Table 27
Neutrino fluxes and signals obtained with different versions of the FRANEC code. Labels (a)–(e) correspond to the models defined in Appendix A. Our best prediction is (e)

	(a)	(b)	(c)	(d)	(e) our best
Φ_{pp} ($10^9\,\mathrm{cm^{-2}\,s^{-1}}$)	60.17	60.37	60.66	59.76	59.92
Φ_{pep} ($10^9\,\mathrm{cm^{-2}\,s^{-1}}$)	0.14	0.14	0.14	0.14	0.14
Φ_{Be} ($10^9\,\mathrm{cm^{-2}\,s^{-1}}$)	4.58	4.22	4.09	4.71	4.49
Φ_{N} ($10^9\,\mathrm{cm^{-2}\,s^{-1}}$)	0.39	0.36	0.35	0.52	0.53
Φ_{O} ($10^9\,\mathrm{cm^{-2}\,s^{-1}}$)	0.33	0.30	0.29	0.45	0.45
Φ_{B} ($10^6\,\mathrm{cm^{-2}\,s^{-1}}$)	4.73	4.18	3.95	5.37	5.16
S_{Ga} (SNU)	126	121	120	130	128
S_{Cl} (SNU)	6.9	6.2	5.9	7.7	7.4

(a → b): The introduction of the new OPAL EOS reduces appreciably the initial helium abundance. The Straniero [75] EOS underestimates the Coulomb effects neglecting the contribution due to the electrons, which are considered as completely degenerate, whereas the OPAL EOS includes corrections for Coulomb forces which are correctly treated. The models with Straniero EOS have a higher central pressure and a higher central temperature, and correspondingly a higher initial helium abundance. The effect of an underestimated Coulomb correction was discussed in Ref. [17]. Note that the transition between radiative and convective regions is not correctly predicted by the model, the convective region being definitely too shallow.

(b → c): The updating of the radiative opacity coefficients has minor effects. The convective zone is again too shallow.

(c → d): This step shows the effects of diffusion. Helium and heavy elements sink relative to hydrogen in the radiative interior of the star because of the combined effect of gravitational settling and of thermal diffusion. This increases the molecular weight in the core and thus the central temperature raises. The surface abundances of hydrogen, helium and heavy elements are appreciably affected by diffusion. For example, the initial value $Y_{in} = 0.269$ is reduced to the present photospheric value $Y_{photo} = 0.238$. The predicted depth of the convective zone and the sound speed are now in good agreement with helioseismological values. It is natural that when diffusion is included the radiative region reduces its size. With respect to models without diffusion, in the external regions the present helium fraction is reduced while the metal fraction stays at the observed photospheric value. Thus the opacity increases and convection starts deeper in the sun.

(d → e): The modifications of our solar model arising from the new values of the nuclear cross sections are negligible with respect to the other improvements just presented.

The predicted neutrino fluxes and signals are summarized in Table 27 for our models. All in all, the results are quite stable with respect to the changes we have introduced as long as diffusion is neglected. On the other hand, due to the higher central temperature, model (d) has significantly higher ^8B and CNO neutrino fluxes. It is essentially the increase of Φ_B which enhances the predicted Chlorine signal. The slight change in the nuclear cross sections weakly affect neutrino fluxes and signals. The ^7Be and ^8B fluxes are reduced by about 5% as a consequence of the correspondingly

Table 28

Astrophysical S-factors (MeV barn) and their derivatives with respect to energies S' (barn) for the RSM [15] and for our models

	RSM	Models (a)–(d)	Model (e) our best
$S(0)_{11}$	3.89×10^{-25}	3.89×10^{-25}	3.89×10^{-25}
$S'(0)_{11}$	4.52×10^{-24}	4.52×10^{-24}	4.52×10^{-24}
$S(0)_{33}$	4.99	5.00	5.1
$S'(0)_{33}$	-0.9	-0.9	3.0
$S(0)_{34}$	5.24×10^{-4}	5.33×10^{-4}	5.1×10^{-4}
$S'(0)_{34}$	-3.1×10^{-4}	-3.10×10^{-4}	-4.23×10^{-4}
$S(0)_{17}$	2.24×10^{-5}	2.24×10^{-5}	2.24×10^{-5}
$S'(0)_{17}$	-3.00×10^{-5}	-3.00×10^{-5}	-3.00×10^{-5}
$S(0)_{12C+p}$	1.45×10^{-3}	1.40×10^{-3}	1.40×10^{-3}
$S'(0)_{12C+p}$	2.45×10^{-4}	4.24×10^{-3}	4.24×10^{-3}
$S(0)_{13C+p}$	5.50×10^{-3}	5.50×10^{-3}	5.50×10^{-3}
$S'(0)_{13C+p}$	1.34×10^{-2}	1.34×10^{-2}	1.34×10^{-2}
$S(0)_{14N+p}$	3.29×10^{-3}	3.32×10^{-3}	3.32×10^{-3}
$S'(0)_{14N+p}$	-5.91×10^{-3}	-5.91×10^{-3}	-5.91×10^{-3}
$S(0)_{15N(p,\gamma)^{16}O}$	6.40×10^{-2}	6.40×10^{-2}	6.40×10^{-2}
$S'(0)_{15N(p,\gamma)^{16}O}$	3.00×10^{-2}	3.00×10^{-2}	3.00×10^{-2}
$S(0)_{15N(p,\alpha)^{12}C}$	7.80×10	7.04×10	7.04×10
$S'(0)_{15N(p,\alpha)^{12}C}$	3.51×10^{2}	4.21×10^{2}	4.21×10^{2}
$S(0)_{16O+p}$	9.40×10^{-3}	9.40×10^{-3}	9.40×10^{-3}
$S'(0)_{16O+p}$	-2.30×10^{-2}	-2.30×10^{-2}	-2.30×10^{-2}

smaller value of S_{34} (see Table 28). Should we use the polynomial expansion of Eq. (133) one would get a further 5% decrease.

Appendix B. The stability of pep and CNO neutrino fluxes

We already compared the predictions of standard solar models by different authors in Section 4, see also Table 3. We discuss here the stability of the ratios $\xi = \Phi_{pep}/(\Phi_{pp} + \Phi_{pep})$ and $\eta = \Phi_N/(\Phi_N + \Phi_O)$ among the non-standard solar models which we have built in Section 4.

Figs. 29 and 30 show the situations as some input parameter $(S_{pp}, Z/X, \ldots)$ is varied by a scaling factor X/X^*. In all the presented models, the central temperatures differ by that of the starting solar model by no more than 5%. The following features are to be remarked:

(i) variations of ξ with respect to the starting model prediction do not exceed 10%;

(ii) η is stable to within 20% level or better;

(iii) as in all models we considered that the central temperature is smaller or equal to that of the starting solar model, the rate of the key reaction $p + {}^{14}N \rightarrow \gamma + {}^{15}O$ is reduced and the CN chain is less equilibrated, resulting in a smaller ${}^{15}O$ neutrino production, which accounts for $\eta > \eta^*$ systematically. On the other hand the behaviour of ξ looks erratical: it may increase as well as decrease when the
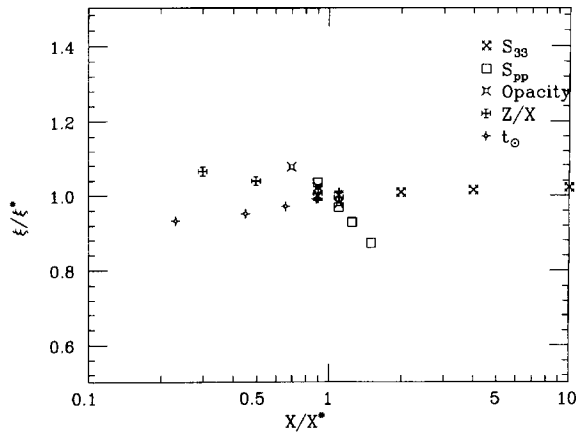
Fig. 29. The behaviour of $\xi = \Phi_{pep}/(\Phi_{pp} + \Phi_{pep})$ as one of the input parameters is varied by a scaling factor X/X^*.

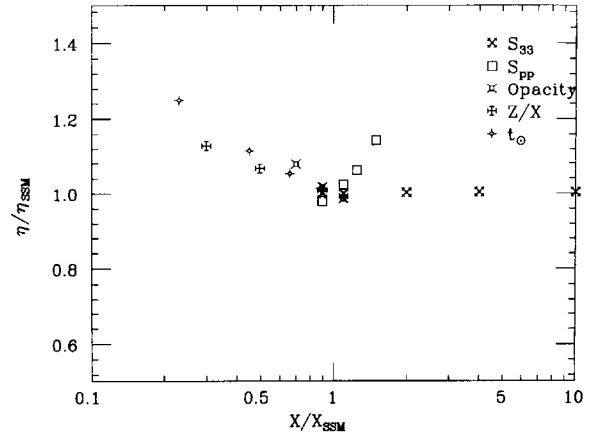Fig. 30. The behaviour of $\eta = \Phi_N/(\Phi_N + \Phi_O)$ as one of the input parameters is varied by a scaling factor X/X^*.

central temperature is reduced, presumably since ξ is sensitive to the electron density more than to the temperature.

References

[1] B. Pontecorvo, Chalk River Report, PD 205 (1946).
[2] R. Davis Jr., D.S. Harmer and K.C. Hoffman, Phys. Rev. Lett. 20 (1968) 1205; B.T. Cleveland et al., Nucl. Phys. B (Proc. Suppl.) 38 (1995) 47 and references therein.
[3] K.S. Hirata et al., Phys. Rev. Lett. 63 (1989) 16; T. Kajita, ICRR-Report, 332-94-27 (December 1994), and references therein.
[4] J.N. Bahcall and H.A. Bethe, Phys. Rev. Lett. 65 (1990) 2233.
[5] GALLEX collaboration, P. Anselmann et al., Phys. Lett. B 327 (1994) 377; 357 (1995) 237, and references therein.
[6] A.I. Abazov et al., Phys. Rev. Lett. 67 (1991) 3332; SAGE collaboration, J.N. Abdurashitiv et al., Nucl. Phys. B (Proc. Suppl.) 48 (1996) 299, and references therein.
[7] GALLEX Collaboration, P. Anselmann, Phys. Lett. B 342 (1995) 440.
[8] SAGE Collaboration, S.R. Elliott et al., Nucl. Phys. B (Proc. Suppl.) 48 (1996) 370.
[9] M. Takita, in: Frontiers of Neutrino Astrophysics, eds. Y. Suzuki and K. Nakamura (Universal Academy Press, Tokyo, 1993) p. 135.
[10] C. Arpesella et al., Borexino at Gran Sasso: proposal for a real time detector for low energy solar neutrinos, internal report INFN, Milano (1992); C. Arpesella et al., Nucl. Phys. B (Proc. Suppl.) 48 (1996) 375.
[11] G.T. Ewan, in: Frontiers of Neutrino Astrophysics, eds. Y. Suzuki and K. Nakamura (Universal Academy Press, Tokyo, 1993) p. 147.
[12] J. Seguinot, T. Ypsilantis, G. Bonvicini, P. Giusti, G. Laurenti and A. Zichichi, College de France preprint LPC/95-08 (1995).
[13] J.N. Bahcall and R. Ulrich, Rev. Mod. Phys. 60 (1988) 297.
[14] J.N. Bahcall and M.H. Pinsonneault, Rev. Mod. Phys. 64 (1992) 885.
[15] J.N. Bahcall and M.H. Pinsonneault, Rev. Mod. Phys. 67 (1995) 781.
[16] C.R. Proffitt, Astrophys. J. 425 (1994) 849.
[17] S. Turck-Chièze and I. Lopes, Astrophys. J. 408 (1993) 347.

[18] C. Charbonnel and Y. Lebreton, Astron. Astrophys. 380 (1993) 666.

[19] I.J. Sackmann, A.J. Boothroyd and W.A. Fowler, Astrophys. J. 360 (1990) 727.

[20] G. Berthomieu, J. Provost, P. Morel and Y. Lebreton, Astron. Astrophys. 268 (1993) 775.

[21] J. Christensen-Dalsgaard, C.R. Proffitt and M.J. Thompson, Astrophys. J. 403 (1993) L75; S. Basu, J. Christensen-Dalsgaard, J. Schou, M.J. Thompson and S. Tomczyk, Astrophys. J. (1996) to appear.

[22] O. Richard, S. Vauclair, C. Charbonnel and W.A. Dziembowski, preprint e-archive astro-ph/9601136; Astron. Astrophys. (1996) in press.

[23] A. Dar and G. Shaviv, Astrophys. J. 468 (1996) 933.

[24] J.N. Bahcall, Neutrino Astrophysics (Cambridge University Press, Cambridge, 1989).

[25] M. Koshiba, Phys. Rep. 220 (1992) 229.

[26] S. Turck-Chièze et al., Phys. Rep. 230 (1993) 57.

[27] Solar Neutrinos, the first thirty years, eds. J.N. Bahcall, R. Davis Jr., P. Parker, A. Smirnov and R. Ulrich (Addison-Wesley, New York, 1995).

[28] S.A. Eddington, Nature 106 (1920) 14.

[29] G. Gamow, Z. Phys. 51 (1928) 204.

[30] E.U. Condon and R.W. Gurney, Phys. Rev. 33 (1929) 127.

[31] R.d'E. Atkinson and F.G. Houtermans, Z. Phys. 54 (1929) 656.

[32] C.F. von Weizsäcker, Phys. Z. 38 (1937) 176.

[33] H.A. Bethe and C.L. Critchfield, Phys. Rev. 54 (1938) 248 and 862.

[34] H.A. Bethe, Phys. Rev. 55 (1939) 434.

[35] C.E. Rolfs and W.S. Rodney, Cauldrons in the Cosmos (The University of Chicago Press, Chicago, 1988).

[36] F.J. Rogers, IAU Colloquium 147, in: The Equation of State in Astrophysics, eds. F.J. Rogers and E.L. Schatzman (Cambridge University Press, Cambridge, 1994).

[37] A.N. Cox and R.T. Giuli, Principles of Stellar Structure (Gordon and Breach, New York, 1968).

[38] C.P. Iglesias, F.J. Rogers and B.G. Wilson, Astrophys. J. 360 (1990) 221.

[39] C.P. Iglesias, F.J. Rogers and B.G. Wilson, Astrophys. J. 397 (1992) 717.

[40] F.J. Rogers and C.P. Iglesias, Astrophys. J. Suppl. 79 (1992) 507.

[41] G.R. Caughlan and W.A. Fowler, Atomic Data and Nuclear Data Tables, 40 (1988) 284.

[42] M. Stix, 'The Sun' (Springer, Berlin, 1989).

[43] Astronomical Almanac for the year 1994 (US Government Printing Office, Washington and Her Majesty's Stationery Office, London, 1993).

[44] C.W. Allen, Astrophysical Quantities (The Athlone Press, University of London, London, 1976).

[45] N. Grevesse and A. Noels, in: Origin and Evolution of the Elements, eds. N. Prantzos, E. Vangioni Flam and M. Cassè (Cambridge University Press, Cambridge) p. 15, N. Grevesse and A. Noels, Phys. Scripta T 47 (1993) 133.

[46] E. Anders and N. Grevesse, Geochim. Cosmochim. Acta 53 (1989) 197.

[47] P.D. Noerdlinger, Astron. Astrophys. 57 (1977) 407.

[48] A.N. Cox, J.A. Guzik and R.B. Kidman, Astrophys. J. 342 (1989) 1187; J.A. Guzik and A.N. Cox, Astrophys. J. 411 (1993) 394.

[49] J.N. Bahcall and A. Loeb, Astrophys. J. 360 (1990) 267.

[50] C.R. Proffitt and G. Michaud, Astrophys. J. 371 (1991) 584; C.R. Proffitt and G. Michaud, Astrophys. J. 380 (1991) 238; G. Michaud and C.R. Proffitt, IAU colloquium 137, Inside the Stars, eds. W.W. Weiss and A. Baglin (Astronomical Society of the Pacific, San Francisco, 1993).

[51] A.A. Thoul, J.N. Bahcall and A. Loeb, Astrophys. J. 421 (1994) 828.

[52] A. Kovetz and G. Shaviv, Astrophys. J. 426 (1994) 787.

[53] J. Christensen-Dalsgaard, Nature 376 (1995) 641.

[54] J. Christensen-Dalsgaard, D.O. Gough and M.J. Thompson, Astrophys. J. 378 (1991) 413.

[55] B. Ricci, preprint INFNFE-09-96 (1996); Astropart. Phys. 6 (1997) in press.

[56] F. Ciacio, S. Degl'Innocenti and B. Ricci, preprint (1996); Astron. Astrophys., submitted.

[57] J.N. Bahcall et al., preprint IASSNS-AST 95/47, Phys. Rev. C (1996) to appear.

[58] J.N. Bahcall and P.I. Krastev, Phys. Rev. D 53 (1996) 4211.

[59] J.N. Bahcall, B.T. Cleveland, R. Davis Jr. and J. Rowley, Astrophys. J. 292 (1985) L79.

[60] E. Bellotti et al., Proposal for a permanent Gallium neutrino observatory (GNO) at Laboratori nazionali del Gran Sasso, preprint (1996).

[61] Review of particle properties, Phys. Rev. D 50 (1994) 1173.

[62] V. Berezinsky, Comm. Nucl. Part. Phys. 21 (1994) 249.

[63] P.I. Krastev and S.T. Petcov, preprint IASSNS-AST 95/40; Phys. Rev. D. (1995) submitted; S.T. Petcov, Nucl. Phys. B (Proc. Suppl.) 43 (1995) 12.

[64] G. Fiorentini et al. (1996) in preparation.

[65] E. Calabresu, N. Ferrari, G. Fiorentini and M. Lissia, Astropart. Phys. 4 (1995) 159.

[66] V. Telegdi, private communication.

[67] W.F. Huebner, A.L. Merts, N.H. Magee and M.F. Argo, Los Alamos Scientific Report LA-6760 M (1977); W.F. Huebner, in: Physics of the Sun, eds. P.A. Sturrock, T.E. Holzer, D.M. Mihalas and R.K. Ulrich (Reidel, Dordrecht, 1986).

[68] D.N. Spergel and W.H. Press, Astrophys. J. 294 (1985) 663.

[69] J. Kaplan et al., Astrophys. J. 378 (1991) 315.

[70] S. Degl'Innocenti, A. Weiss and L. Leone, preprint (1996); Astron. Astrophys., submitted; D. Dearburn, G. Raffelt, P. Salati, J. Silk and A. Bouchet, Astrophys. J. 354 (1990) 568.

[71] J.N. Bahcall, Phys. Rev. Lett. 71 (1993) 2369.

[72] J.N. Bahcall, Phys. Rev. D 49 (1994) 3923.

[73] V. Castellani, S. Degl'Innocenti, G. Fiorentini, M. Lissia and B. Ricci, Phys. Rev. D 50 (1994) 4749.

[74] Castellani, S. Degl'Innocenti, G. Fiorentini, M. Lissia and B. Ricci, Phys. Lett. B 324 (1994) 425; and addendum Phys. Lett. B 329 (1994) 525.

[75] O. Straniero, Astron. Astrophys. Suppl. 76 (1988) 157.

[76] N. Grevesse, in: Evolution of stars: the photospheric abundance connection, eds. G. Michaud and A. Tutukov (International Astronomical Union, 1991) p. 63.

[77] M. Kamionkowski and J.N. Bahcall, Astrophys. J. 420 (1994) 884.

[78] R.J. Gould and N. Guessoum, Astrophys. J. 359 (1990) L67.

[79] V. Castellani, S. Degl'Innocenti and G. Fiorentini, Phys. Lett. B 303 (1993) 70.

[80] J.N. Bahcall and A. Ulmer, Phys. Rev. D 53 (1996) to appear.

[81] F.J. Roger and C.P. Iglesias, Astrophys. J. 371 (1991) 408.

[82] S. Turck-Chièze et al., Astrophys. J. 335 (1988) 415.

[83] V.N. Tsytovich, R. Bingham, U. de Angelis, A. Forlani and M. Occorsio, Astropart. Phys. 5 (1996) 197.

[84] N. Grevesse et al., Astron. Astrophys. 242 (1991) 488.

[85] E. Biemont et al., Astrophys. J. 375 (1991) 818.

[86] A. Alessandrello et al., Report No. INFN/AE-92/28 (1992).

[87] R.S. Raghavan et al., Report No. AT&T Bell Laboratories Technical Memorandum 11121-930824-27TM (1993).

[88] H.J. Assenbaum, K. Langanke and C. Rolfs, Z. Phys. A 327 (1987) 461; S. Engstler, G. Raimann, C. Angulo, U. Greife, C. Rolfs, U. Schröder, E. Somorjai, B. Kirch and K.Z. Langanke, Physica A 342 (1992) 471.

[89] L. Bracci, G. Fiorentini, V.S. Melezhik, G. Mezzorani and P. Quarati, Nucl. Phys. A 513 (1990) 316; L. Bracci, G. Fiorentini and G. Mezzorani, Proc. of TAUP 1989, eds. A. Bottino and P. Monacelli (Edition Frontières, Gif sur Yvette, 1989).

[90] B. Ricci, S. Degl'Innocenti and G. Fiorentini, Phys. Rev. C 52 (1995) 1095.

[91] W. Good, W.E. Kunz and C.D. Moak, Phys. Rev. 94 (1954) 97.

[92] A. Krauss, H.W. Becker, H.P. Trautvetter and C. Rolfs, Nucl. Phys. A 476 (1987) 273.

[93] M.R. Dwarakanath, Phys. Rev. C 9 (1974) 805.

[94] M.R. Dwarakanath and H. Winkler, Phys. Rev. C 4 (1   ) 1532.

[95] N. Wang, V. Novatskii, G. Osetinskii, N. Chien and I. hepurcenko, Soviet Nucl. Phys. 3 (1966) 777.

[96] A.D. Bacher, T.A. Tombrello, in: Nuclear research with   w-Energy Accelerators, eds. J.B. Marion and D.M. Van Patter (Academic Press, New York, 1967) p. 195.

[97] R.E. Brown, F.D. Correll, P.M. Hegland, J.A. Koepke   C.H. Poppe, Phys. Rev. C 35 (1987) 383.

[98] P.D. Parker and C. Rolfs, in: The solar interior and atr osphere, A. Cox, W. Livingston and M.S. Mattews, eds. (University of Arizona, Tucson, 1991) p. 31.

[99] P.D. Parker and R.W. Kavanagh, Phys. Rev. 131 (1963 2578.

[100] K. Nagatani, M. Dwarakanath and D. Ashery, Nucl. Phys. A 128 (1969) 325.
[101] H. Kräwinkel, H. Becker, L. Buchmann, J. Gorres, K. Kettner, W. Kieser, R. Santo, P. Schmalbrock, H. Trauttvetter, A. Vielks, C. Rolfs, J. Hammer, R. Azuma and W. Rodney, Z. Phys. A 304 (1982) 307.
[102] M. Hilgmeier, H. Becker, C. Rolfs, H. Trautvetter and J. Hammer, Z. Phys. A 329 (1988) 243.
[103] J. Osborne, C. Barnes, R. Kavanagh, M. Kremer, G. Mathews, J. Zyskind, P. Parker and A. Howard, Phys. Rev. Lett. 48 (1982) 1664; J. Osborne, C. Barnes, R. Kavanagh, R. Kremer, G. Mathews, J. Zyskind, P. Parker and A. Howard, Nucl. Phys. A 419 (1984) 115.
[104] P.D. Parker, in: Physics of the Sun, ed. P.A. Sturrock (Reidel, Dordrecht, 1985) p. 15.
[105] H.D. Holmgren and R.L. Johnston, Phys. Rev. 113 (1959) 2556.
[106] T. Alexander, G. Ball, W. Lennard, H. Geissel and H. Mak, Nucl. Phys. A 427 (1984) 526.
[107] H. Robertson, P. Dyer, T. Bowles, R. Brown, N. Jarmie, C. Maggiore and S. Austin, Phys. Rev. C 27 (1983) 11.
[108] H. Volk, H. Kräwinkel, R. Santo and L. Wallek, Z. Phys. 310 (1983) 91.
[109] R. Williams and S. Koonin, Phys. Rev. C 23 (1981) 2773.
[110] M. Kamionkowski and J.N. Bahcall, Phys. Rev. C 49 (1994) 545.
[111] W.A. Fowler, Nature 238 (1972) 24.
[112] V. Castellani, S. Degl'Innocenti and G. Fiorentini, Astron. Astrophys. 271 (1993) 601.
[113] C. Arpesella et al., Nuclear Astrophysics at Gran Sasso Laboratory (proposal for a pilot project with a 30 keV accelerator), Report No. LNGS 91-18 (1991).
[114] R.W. Kavanagh, Nucl. Phys. 15 (1960) 411.
[115] P.D. Parker, Phys. Rev. 150 (1966) 851; Astrophys. J. 153 (1968) C85.
[116] R.W. Kavanagh, T.A. Tombrello, J.M. Mosher and D.R. Goosman, Bull. Am. Phys. Soc. 14 (1969) 1209.
[117] F.J. Vaughn, R.A. Chalmers, D. Kohler and L.F. Chase, Phys. Rev. C 2 (1970) 1657.
[118] C. Wiezorek, H. Kräwinkel, R. Santo and L. Wallek, Z. Phys. A 283 (1977) 121.
[119] B.W. Filippone, A.J. Elwyn, C.N. Davids and D.D. Koetke, Phys. Rev. C 28 (1983) 2222.
[120] C.W. Johnson, E. Kolbe, S.E. Koonin and K. Lankanke, Astrophys. J. 392 (1992) 320.
[121] B.W. Filippone, Ann. Rev. Nucl. Part. Sc. 36 (1986) 717.
[122] F. Strieder et al., Z. Phys. A (1996) to appear.
[123] U. Greife and M. Junker, internal report of NACRE collaboration (1996).
[124] T. Motobayashi et al., Phys. Rev. Lett. 20 (1994) 2680; J. Phys. Soc. Japan 65 (1996) to appear.
[125] K. Langanke and T. D Shoppa, Phys. Rev. C 49 (1994) 1771; Errata Phys. Rev. C 51 (1995) 2844.
[126] M. Gai and C.A. Bertulani, Phys. Rev. C 52 (1995) 1706.
[127] K. Langanke and T. D Shoppa, Phys. Rev. C 52 (1995) 1709.
[128] E.J. Woodbury, R.N. Hall and W.A. Fowler, Phys. Rev. 75 (1949) 1462.
[129] D.B. Duncan and J.E. Perry, Phys. Rev. 82 (1951) 809.
[130] W.A.S. Lamb and R. Hester, Phys. Rev. 107 (1957) 550 and 108 (1957) 1304.
[131] R.E. Pixley, Ph.D. Thesis, California Institute of Technology, 1957.
[132] G.M. Bailey and D.F. Hebbard, Nucl. Phys. 46 (1963) 529; 49 (1963) 666.
[133] D.C. Hensley, Astrophys. J. 147 (1967) 818.
[134] W.A. Fowler, G.R. Caughlan and B.A. Zimmerman, Ann. Rev. Astron. Astrophys. 13 (1975) 113.
[135] U. Schröder et al., Nucl. Phys. A 467 (1987) 240.
[136] E.E. Salpeter, Australian J. Phys. 7 (1954) 373.
[137] E.E. Salpeter and H.M. Van Horn, Astrophys. J. 155 (1969) 183.
[138] H.C. Graboske, H.E. DeWitt, A.S. Grossman and M.S. Cooper, Astrophys. J. 181 (1973) 457.
[139] C. Carraro, A. Schäfer and S.E. Koonin, Astrophys. J. 331 (1988) 565.
[140] H.E. Mitler, Astrophys. J. 212 (1977) 513.
[141] H. Dzitko, S. Turck-Chièze, P. Delbourgo-Salvador and Ch. Lagrange, Astrophys. J. 447 (1995) 428.
[142] D.D. Clayton, Principles of Stellar Evolution and Nucleosynthesis (McGraw-Hill, New York, 1968).
[143] S.A. Bludman, N. Hata, D.C. Kennedy and P. Langacker, Phys. Rev. D 47 (1993) 2220.
[144] N. Hata and P. Langacker, Phys. Rev. D 50 (1994) 632.
[145] S. Degl'Innocenti, G. Fiorentini and M. Lissia, physics e-print hep-ph/9408386; Nucl. Phys. B (Proc. Suppl.) 43 (1995) 66.
[146] V. Berezinsky, G. Fiorentini and M. Lissia, Phys. Lett. B 341 (1994) 38.

[147] V. Berezinsky, G. Fiorentini and M. Lissia, Phys. Lett. B 365 (1996) 185.
[148] G.L. Fogli and E. Lisi, Astrophys. Phys. 2 (1994) 91; 3 (1995) 185.
[149] E. Gates, L.M. Krauss and M. White, Phys. Rev. D 51 (1995) 2631.
[150] F.J. Rogers, F.J. Swenson and C.A. Iglesias, Astrophys. J. 456 (1996) 902.
[151] F.J. Rogers and C.A. Iglesias, in: Astrophysical application of powerful new database, eds. S.J. Adelman and W.L. Wiesse, ASP Conference series, Vol. 78, 1995, p. 31.
[152] A. Chieffi and O. Straniero, Astrophys. J. Suppl. 71 (1989) 47.
[153] V. Castellani, A. Chieffi and O. Straniero, Astrophys. J. Suppl. 78 (1992) 517.
[154] D.R. Alexander and J.W. Ferguson, Astrophys. J. 437 (1994) 879.
[155] W.A. Dziembowski, A.A. Pamyatnykh and R. Sienkiewicz, Mon. Not. R. Astron. Soc. 249 (1991) 602.
[156] A.N. Cox and J.N. Steward, Astrophys. J. Suppl. 19 (1970) 243.
[157] D. Mihalas, W. Dappen and D.G. Hummer, Astrophys. J. 331 (1088) 815.
[158] P.P. Eggleton, J. Faulkner and B.P. Flannery, Astron. Astrophys. 23 (1973) 235.
[159] J. Christensen-Dalsgaard and W. Dappen, Astron. Astrophys. Rev. 4 (1992) 267.
[160] W. Dappen, D.O. Gough and M.J. Thompson, in: Seismology of the Sun and Sun-like Stars, ed. E.J. Rolfe (ESTEC, Noordwijk, 1988) in Ref. [155].
[161] W. Dappen, D.O. Gough, A.G. Kosovichev and M.J. Thompson, in: Challenges to the Theories of the Structure of Moderate-mass Stars, eds. D.O. Gough and J. Toomre (Springer, Heidelberg, 1991) in Ref. [155].
[162] S.V. Vorontsov, V.A. Baturin and A.A. Pamyatnykh, Nature 349 (1991) 49.
[163] W.A. Dziembowski, P.R. Goode, A.A. Pamyatnykh and R. Sienkiewicz, Astrophys. J. 432 (1994) 417.
[164] F.P. Hernandez and J. Christensen-Dalsgaard, Mon. Not. R. Astron. Soc. 269 (1994) 475.
[165] M.B. Aufderheide et al., Phys. Rev. C 49 (1994) 678.